PROCESSING HIGHLY POROUS CALCIUM PHOSPHATE CERAMICS FOR USE IN BIOREACTOR CORES FOR CULTURING HUMAN LIVER CELLS IN-VITRO

by

Anthony Finoli

B. S. in Materials Science and Engineering, University of Pittsburgh, 2008

Submitted to the Graduate Faculty of

The Swanson School of Engineering in partial fulfillment

of the requirements for the degree of

Doctor of Philosophy in Materials Science and Engineering

University of Pittsburgh

2013

UNIVERSITY OF PITTSBURGH

SWANSON SCHOOL OF ENGINEERING

This dissertation was presented

by

Anthony Finoli

It was defended on

July 12, 2013

and approved by

John Barnard, PhD, Professor
Department of Mechanical Engineering and Materials Science

Jung-Kun Lee, PhD, Associate Professor
Department of Mechanical Engineering and Materials Science

Ipsita Banerjee, PhD, Assistant Professor
Department of Chemical and Petroleum Engineering

Dissertation Director: Ian Nettleship, PhD, Associate Professor
Department of Mechanical Engineering and Materials Science

PROCESSING HIGHLY POROUS CALCIUM PHOSPHATE CERAMICS FOR USE IN BIOREACTOR CORES FOR CULTURING HUMAN LIVER CELLS IN-VITRO

Anthony Finoli, PhD

University of Pittsburgh, 2013

Chronic liver disease is the 11th highest cause of death in the United States claiming over 30,000 lives in 2009. The current treatment for chronic liver failure is liver transplantation but the availability of tissue is far less than the number of patients in need. To develop human liver tissue in the lab a 3D culturing environment must be created to support the growth of a complex tissue. Hydroxyapatite (HAp) has been chosen as a scaffold material because of its biocompatibility in the body and the ability to create a bioresorbable scaffold. By using a ceramic material, it is possible to create a three dimensional, protective environment in which tissue can grow.

The first part of this study is to examine the behavior of adult human liver cells grown on composites of HAp and different biocompatible hydrogels. Porous HAp has been created using an emulsion foaming technique and cells are injected into the structure after being suspended in a hydrogel and are kept in culture for up to 28 days. Functional assays, gene expression and fluorescent microscopy will be used to examine these cultures. The second part of this study will be to develop a processing technique to create a resorbable scaffold that incorporates a vascular system template. Previous experiments have shown the high temperature decomposition of HAp

into resorbable calcium phosphates will be used to create a multiphase material. By controlling the amount of transformation product formed, it is proposed that the resorption of the scaffold can be tailored. To introduce a pore network to guide the growth of a vascular system, a positive-negative casting technique has also been developed. A positive polymer copy can be made of a natural vascular system and ceramic is foamed around the copy. During sintering, the polymer is pyrolyzed leaving a multiscale pore network in the ceramic. By combining these techniques, it is proposed that a calcium phosphate bioreactor core can be processed that is suitable for the culturing of human liver tissue.

TABLE OF CONTENTS

LIST OF TABLES

LIST OF FIGURES

PREFACE

I would like to acknowledge first my advisor Dr. Nettleship for all of his guidance over the last 6 years. I would also like to thank Dr. Gerlach and Dr. Schmelzer for guidance with all things related to biology and bioreactors; as well Dan Mckeel and Patrick Over for their help with cell culturing and the ceramic processing work of Dr. Chris Pekor, Nicole Ostrowski, Curtis Larimer Kelsey Finegan, Katie Beckwith, Claire Barrett, Ishan Jaidka, and Julie Fornaciari. I would finally like to thank my parents David and Vivian Finoli as well as my family and friends who have supported me throughout graduate school, especially Daniel Biondo who helped proofread this document.

1.0 INTRODUCTION

Chronic liver disease, the 11th highest cause of death in the United States, claimed over 30,000 lives in 2009. Currently the treatment for chronic liver failure is liver transplantation, but the amount of available tissue is far less than the number of patients in need [1]. Regenerative medicine techniques are currently being investigated to supplement the need for transplantable tissue. In the work of Lagasse and others, liver progenitor cells are injected into the body at different entry points, with varying degrees of success [2,3]. In Lagasse's case, they were able to form functional liver tissue in the lymphatic system of rats to reverse the symptoms of liver failure. In this technique, tissue or cells are grown in the body to supplement the function of the patient's dying liver [2]. Though the developments are promising, many aspects of the procedure must be examined before it is viable for clinical use. Chief among these is the need for a widely available supply of human liver tissue and cells, most likely grown in the lab (in-vitro).

Human hepatic (liver) cells can come from three main sources: adult hepatocytes, fetal liver derived progenitors and embryonic stem cells. Of the three, fetal liver derived cells are the most useful because of their higher expandability in comparison to the adult cells. Furthermore, fetal cells are easier to differentiate in to functional liver tissue than embryonic stem cells [4]. The growth of human fetal liver (HFL) cells in 2D and 3D cultures has been well documented in the literature [4-6]. HFL cells were used in preliminary experiments, however, in most cases

cells were not successfully cultured for any amount of time. While these cells show promise in future tissue engineering applications, adult liver cells will be used in this work due to the successful culturing of these cells in the lab.

To realistically grow liver tissue from adult liver cells, a 3D matrix is utilized to support the cells in a culture at a size suitable for clinical use. Commonly, hydrogels are used to culture the cells [6]. This scaffold structure must have a high porosity to facilitate cell seeding and fluid flow while being rigid enough to support the weight of the growing tissue. There is an additional option of templating a natural vascular system inside the scaffold to guide the cells in the formation of pathways for blood flow necessary for transplantation. The scaffold should also dissolve as the tissue begins to grow and remodel the structure. Biodegradable polymers are one option and have been used extensively in tissue engineering [7]. The low rigidity of biodegradable polymer foams and the difficulty in processing a vascular template, however, make these materials less than ideal. Metallic foams have also been used to grow cells and while magnesium alloys are biodegradable, gas evolution during degradation suggests that they will not make ideal scaffolds for tissue growth [8]. Ceramic foaming techniques have been developed to create highly porous, permeable structures. High sintering temperatures facilitates the use of a polymeric template of a vascular system that can be burnt out during heating. Biocompatible calcium phosphates, specifically hydroxyapatite (HAp), have successfully been used as scaffolds for culturing several different cell types including liver cells from both human and rat sources [9,10]. Calcium phosphate ceramics can also be made to be bioresorbable by taking advantage of a high temperature decomposition of hydroxyapatite to resorbable calcium phosphate phases, the most important being tricalcium phosphate [11-13].

Finally, a 3D environment must be created to culture the cells in-vitro. This can be accomplished through the use of bioreactors. A bioreactor is a vessel that provides a controlled environment to culture cells. Perfusion bioreactors possess a stationary core where nutrients and oxygen are perfused to cells and waste products are removed, mimicking physiologic conditions [4]. Culturing human fetal and adult liver cells in perfusion reactors have led to the spontaneous reorganization of the primary human liver cells to tissue-like structures [4,14]. Further, ceramic scaffolds have been placed in these reactors with human and rat liver cancer cells. These latter reactors have shown some positive liver cell function after being cultured in the reactor and subsequent implantation into the kidney of a rat [10]. While these results are promising, it is of great importance to develop a 3D system in which primary human liver cells can grow and form functioning tissue for implantation. The objective of this study is to create a hydroxyapatite/hydrogel structure suitable for the growth of human liver cells and eventual formation of functioning liver tissue. The high temperature phase transformation will be used to create a resorbable structure, and the hydrogels will be used to mimic the extracellular matrix for the cells in culture. Finally, polymeric templates will be used to create channels in the composite for the growth of a vascular system. The influence of different materials of the composite scaffold on the culture of human adult liver cells will be examined.

2.0 BACKGROUND

2.1 HYDROXYAPATITE STRUCTURE AND BIOCOMPATIBILITY

2.1.1 Structure

Hydroxyapatite (HAp) is the main mineral composition of bone [12,15] and has been widely used in the field of tissue engineering as a filler for bone defects [16]. Its chemical formula is $Ca_{10}(PO_4)_6(OH)_2$ and it exhibits two crystal structures: hexagonal with a space group of $P6_3/m$ [17] and more recent studies show a monoclinic structure with a space group of $P2_1/b$ [12]. Clinically, HAp is used in many bone related implants such as coatings on metal hip implants to promote bone ingrowth [18] and as discs in spinal fusion surgeries [19].

2.1.2 Biocompatibility

Hench describes a bioactive material as being non-toxic and biologically active. This combination of properties results in a material that forms an interfacial bond with tissue [15]. This principle is generally used in bone implants to create a strong bond between the existing bone and the surface of the hydroxyapatite implant, which then stimulates further bone growth into the porous ceramic structure. This principle is also useful in organ bioreactors; in that cells implanted into the bioreactor core can adhere to the surface of the ceramic, allowing for the

growth of tissue [15]. Toxicity studies have been completed showing that HAp has no cytotoxic effects in solution, outside the issue of small particles causing an immune response [15,20]. Also several different cell types have been shown to grow on HAp. These include bone [21,22], mesenchymal stem cells (repair cells of the body) [23] and liver cells [9,10], which will be discussed later.

2.2 DISSOLUTION/RESORPTION OF CALCIUM PHOSPHATES

2.2.1 Dissolution of calcium phosphates

During in-vitro tissue engineering, it is important that the scaffold resorbs as new tissue is formed. Hydroxyapatite has shown little to no resorption both in-vivo (in the body) [24] and in-vitro [13], however, many other calcium phosphates show substantial dissolution in many different fluids. The resorption of the ceramic is generally measured from the liberation of calcium and phosphate ions into solution and the reprecipitation of calcium phosphate (CaP) structures useful in bone cell applications. A study by Ducheyne et al examined the dissolution of multiple calcium phosphates [13]. Dissolution studies were performed in calcium and phosphate free tris buffered solutions. It was found that Tetracalcium phosphate (TeCP) released the most amount of Ca^{+2} ions into the solution, followed by the two prominent phases of tricalcium phosphate α-TCP, β-TCP, and finally HAp, of which only a minute amount of ions were released over the 1000 hour study (<5E-2 mM compared to 160E-2 mM for TeCP) [13]. Similar studies have been completed in-vivo using a subcutaneous (under skin) model, exhibiting similar results. HAp showed minimal weight loss over the course of the study, in contrast to

other phases, which dissolved significantly [25]. If HAp is to be used in a tissue remodeling application, the resorption must be greatly increased. In the literature, several methods have successfully increased HAp resorption. These usually include the use of dopants [26-33] and the mixing of HAp with more resorbable phases of calcium phosphates [25].

2.2.2 Dopant additions

The most common doped form of HAp is carbonate-substituted HAp (CHA), due to its composition being very close to natural bone. Because the carbonate ions can occupy one of two different lattice sites, there are two types of CHA. In type A, the carbonate substitutes for one of the hydroxyl ions whereas in B-Type, the carbonate substitutes for a phosphate ion. Achieving pure B-Type is difficult because the phosphate ion has greater charge than the carbonate creating an issue for charge balance by calcium. This is "solved" by adding sodium to the reaction, but that addition makes it difficult to achieve a pure final product. Natural bone, however, more closely mimics a form when the A-Type and B-Type are formed simultaneously creating AB-Type [26]. When testing CHA in fetal bovine serum, it was shown that Ca ions were liberated over the course of two hours while phase pure HAp only measurably released Ca ions into the serum for two minutes. There was no measurable difference in protein absorption from the serum onto the surface of either ceramic, which is a measure bioactivity of the material [27].

With the high dissolution rates observed for bioactive glasses [15], silicon-substituted HA (SiHA) has been studied extensively in the literature [28-30]. Silicate ions can be substituted easily into the PO_4-3 sites in the lattice. Studies have shown that the presence of silicon in amounts around 0.5 wt% have increased dissolution and bone cell growth during in-vivo tests. By implanting both SiHA and HAp powders in a femoral bone defect of both sheep and rabbits

for up to 12 weeks, the addition of Si to the lattice greatly improved the dissolution behavior of the material with no negative effects to the cells. Several groups found that SiHA showed improved dissolution at the grain boundaries of the material and that increased local Si ion concentration improved bone growth in the defect [29,30].

One recent study explored the use of several different elements in creating hydroxyapatite including magnesium, zinc, cadmium and yttrium. Because Mg, Zn and Cd all have the same charge as calcium, the Ca^{+2} was easily replaced in the lattice. The yttrium was more difficult because of the charge difference. Two Y atoms must replace three Ca atoms creating a vacancy for every two Y atoms. The first three substitutions went as planned but in the yttrium substitution; it was found that not all of the yttrium dissolved into the apatite creating a second phase that was not present in any other substitution [31]. Cd and Zn doped apatites exhibited little dissolution in fetal bovine serum, while Y doped apatite showed larger amounts of Ca^{+2} release and bone cell adhesion in culture than undoped HAp [32]. Magnesium substitutions show either slightly decreased dissolution and bio-activity, indicated by the decrease in attachment of bone cells as compared to HAp in culture [32,33], or has been seen to be toxic to cells when doped at a high concentration in a HAp/collagen 1 sponge due to large amounts of Mg ion release [33].

Doping of TCP has also been extensively examined with similar effects to HAp doping seen in dissolution behavior [34]. In this case the dissolution rate of TCP is much higher than that of HAp [13] and a decrease in Ca ion liberation from the structure is desired. Use of biphasic calcium phosphates (HAp/TCP mixtures) has been extensively studied in the form of powders [35] and their subsequent dissolution and biocompatibility behaviors [25]. By mixing the two phases, dissolution rates between the two pure materials have been achieved [13,25].

Dissolution experiments have also been conducted on dense biphasic materials to examine the mechanisms of the resorption process [36,37]. It was seen that more dense samples dissolved slower than samples that were not fully densified during sintering. This occurred because pitting was the only dissolution mechanism seen in dense samples. When the CaP was not fully dense, dissolution occurred from surface pitting and from the increased surface area. Another mechanism for dissolution was found if CaO was formed at the grain boundaries of the ceramic. This would degrade quickly opening up more surface area for CaP dissolution [37]. These materials are of great interest to the bone remodeling community because TCP dissolution rates are too high for adequate bone growth while HAp does not fully dissolve in the body.

2.3 HYDROXYAPATITE PHASE TRANSFORMATION AND EFFECT ON MICROSTRUCTURE

2.3.1 Decomposition

At high temperatures HAp undergoes decomposition to different phases of calcium phosphate. This is heavily dependent on environmental conditions, surface area and the exact chemistry of the HAp being studied, but in all cases the HAp first goes through a reversible reaction as follows. From 400°C to temperatures as high as 1000°C, the HAp undergoes the process of dehydroxylation to form oxyhydroxyapatite (OHA) [11,12]:

$$Ca_{10}(PO_4)_6(OH)_2 \rightarrow Ca_{10}(PO_4)_6(OH)_{2(1-x)} + xH_2O \ (0 < x < 1). \quad \textbf{2.1}$$

To a certain extent, this OHA will transform back upon cooling, however, this phase can be stable at room temperature [38]. At higher temperatures, the OHA will then further decompose

depending on the exact conditions. Many papers describe a transformation to tricalcium phosphate (TCP) and CaO at temperatures ranging from 800-1300°C [11] following this equation:

$$Ca_{10}(PO_4)_6(OH)_{2(1-x)} \rightarrow 3Ca_3(PO4)_2 + CaO + (1 - x)H_2O \ (0 < x < 1). \quad \textbf{2.2}$$

At temperatures below 1125°C the β form of TCP is created and at higher temperatures the phase is created and remains upon cooling [13]. At temperatures above 1350°C powders of OHA will further react to create tetracalcium phosphate (TeCP) following this equation [39]:

$$Ca_{10}(PO_4)_6(OH)_{2(1-x)} \rightarrow 2Ca_3(PO_4)_2 + Ca_4(PO_4)_2O + (1 - x)H_2O. \quad \textbf{2.3}$$

Several other phases have been reported during the decomposition of HAp including oxyapatite ($Ca_{10}O(PO_4)_6$) which would then transform to TeCP, α-TCP and calcium pyrophosphate ($Ca_2P_2O_7$) at temperatures above 1450°C [40].

This behavior has been shown to be affected by stoichiometry. Calcium deficient HAp will lead to TCP forming at higher temperatures than stoichiometric HAp [41]. Environmental conditions, such as high water vapor content, also have been shown to suppress the decomposition [39].

As seen above, these different phases of calcium phosphate can be used to tailor the resorption rate of the ceramic. HAp has a slow resorption rate in the body compared to TCP. Previous studies have taken advantage of this by using a mixture of the two phases to create a material with a median resorption rate that is attractive for tissue engineering [35,42]. A logical use of the high temperature decomposition of HAp would be to create a structure with multiple calcium phosphate phases.

Thermal decomposition of hydroxyapatite has been widely studied in powders [11,40] and dense pellets [11,43]. In general, the effect of the transformation to TCP is seen as negative because the transformation is disruptive and the consequent cracking decreases the mechanical

integrity in dense samples [43,44]. Furthermore, the decomposition products have exhibited different resorption behavior in physiological conditions [12,45]. In the first instance, the decomposition of HAp occurs at the surfaces of the ceramic, making the extent of transformation dependent on the surface-to volume ratio. For example, different phase transformation kinetics have been observed in powders compared to dense bulk pieces [11].

One area that is not specifically addressed in the literature is the effect of pores on the transformation kinetics of porous HAp. Many papers have examined processing techniques such as gel casting [46] and direct foaming of HAp [47,48], but they did not study the effect of the pore structure on the thermal decomposition at high sintering temperatures. The effect of two kinetic processes must be examined to understand the decomposition behavior in porous HAp ceramics derived from powders. The first process is sintering, which reduces the surface-to-volume ratio of the ceramic and for which the controlling diffusion distance is the interpore spacing. The second process is the decomposition of HAp for which the diffusion distance is half the thickness of the ceramic. This latter diffusion distance can obviously be quite different for a foam and a bulk ceramic. The effect of pore structure on thermal decomposition and microstructure of highly porous foams will be examined in this study.

2.4 PROCESSING OF CASTABLE POROUS CERAMICS

For the purpose of this proposal, an open pore network must be achieved in order to sustain the growth of cells in a bioreactor. This is comprised of a foam with open gates in between the pores to allow for uniform cell inoculation and fluid flow throughout the structure. In this specific case

we also need a flexible shaping operation so the foam can be castable to the required geometry. The literature concerning the processing castable porous ceramics will be examined.

2.4.1 Foam Physics

Before the creation of a solid foam can be discussed, principles of liquid foams must be examined to better understand its development. Foams can be described by the topological elements that make up their structure. Foams are comprised of bubbles that come together to form a thin film of liquid between bubble faces and the lines where the films meet are referred to as plateau borders. When these plateau borders meet to form a point in a connected network, the feature is referred to as a junction [49,50].

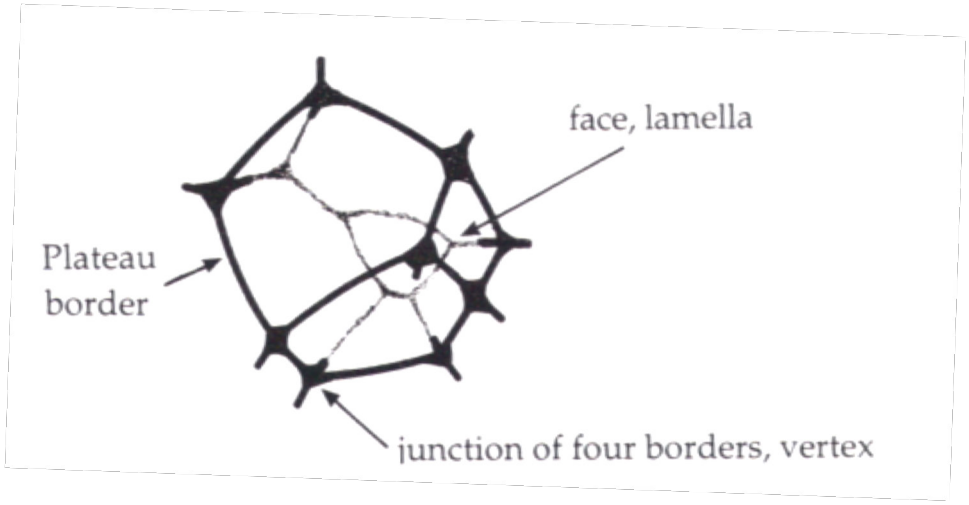

Figure 2.1. Illustration of a bubble in a foam [**49**].

These features are illustrated in Figure 2.1. The surface tension created in this structure is a driving force for the development of the foam. The pressure difference (Δp) across the liquid films can be described by the Laplace-Young law:

$$\Delta p = 4\gamma\kappa \qquad \textbf{2.4}$$

Where γ is the surface tension of a single film/air interface of curvature κ. The surface tension of the foam will be 2γ to account for both sides of the film and the curvature is calculated from the mean of the reciprocals of radii in two orthogonal directions. This can then be substituted into above to yield:

$$\Delta p = 4\gamma (1/r_1 + 1/r_2) \qquad \textbf{2.5}$$

This shows that smaller bubbles will lead to an increase in pressure across the film. The disjoining pressure of the films is used to describe the stability. The higher pressures across the film will eventually lead to the rupture of the film while low pressures lead to a stable bubble [50].

Coarsening is the process by which the structure of the foam changes as gas diffuses through the films, causing the bubbles to enlarge. This can be explained in part by the Laplace-Young law described above. Films with a large radius of curvature have a lower pressure and thus are more stable than those with a small radius. The high pressure in smaller bubbles drives diffusion of gas to the more stable large bubble, eliminating the small bubbles. The flux of gas through the films can be described using this equation:

$$J = \kappa A \Delta p \qquad \textbf{2.6}$$

Where A is the area of the film surface and κ is now defined as the permeability constant of the film. In a foam structure, plateau borders act to block diffusion of gas through the film, as they control the area of the film (Figure 2.2). Because this process follows the same laws as Ostwald ripening of isolated phases in alloys, it is possible to describe the area change in individual bubble using a geometric argument in Von Neumann's law. This states that in two dimensions the change in area of a cell with n sides is as follows:

$$dA_n/dt = 2/3 * \pi\gamma\kappa(n-6) \qquad \textbf{2.7}$$

As in grain growth, a bubble with 6 sides is stable; bubbles with more than 6 sides should grow while bubbles with less than 6 sides should shrink. This law agrees with what is seen experimentally in wet foams on average, however, a bubble with more than 6 sides has been shown to shrink rather than grow [49]. In ceramic foams, spatial effects can be seen during coarsening. As bubbles begin to coarsen, impingement from particles due to non-uniform distribution in the plateau borders can lead to the formation of cracks due to large coarse bubble alignment in the structure [51].

Figure 2.2. Diffusion of gas from bubble through the film. The plateau border acts as a barrier for diffusion [**49**].

2.4.1.1 Drainage

Drainage of the films is another process that affects the structure during foam evolution. As gas diffuses through the films, there is also the possibility of liquid draining from the films through the plateau border by gravitational forces (Figure 2.3) [50]. The mean velocity of gravitational drainage at angle θ from the vertical can be given by:

$$u(\theta) = f^{-1} (\rho g / \eta) A_p \cos(\theta) \qquad \textbf{2.8}$$

where ρ and η are the density and viscosity of the liquid, g is the gravitational force, A_p is the plateau border cross-sectional area and *f* is a dimensionless constant relating to the shape of

the plateau border (~49 in practice). This process leads to certain gradient of bubble size and behavior along the vertical direction of the foam. As drainage under gravity occurs, the foam will become dryer on the top while the bottom of the foam will be wetted from above. In addition, the average bubble size near the top of the foam is observed to be much larger than those at the bottom, as seen in Figure 2.4. This is partially due to buoyancy, as larger bubbles will rise through the wet foam. This phenomenon takes place because, as drainage occurs, the plateau borders decrease, which increases the rate of diffusion through the film, leading to a coarser structure [49].

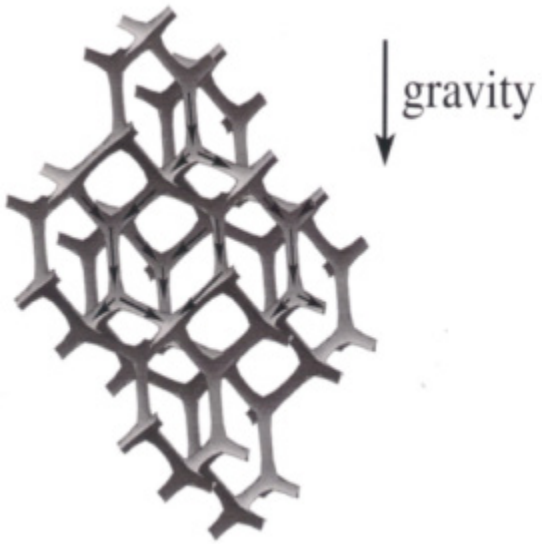

Figure 2.3. Drainage under gravity. Liquid will flow through the plateau borders under gravitational forces [**49**].

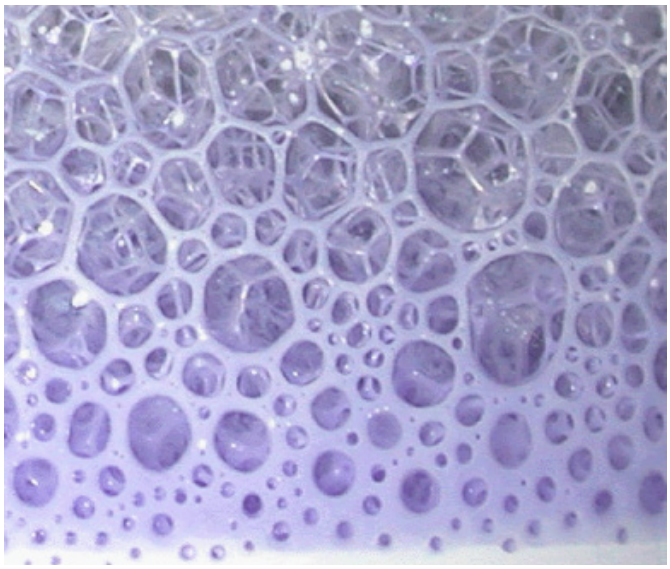

Figure 2.4. Vertical distribution of bubbles in a foam. Bubbles on top coarsen much more than those on the bottom [**52**].

When other components, such as surfactants, are added to the foam, the subsequent change in viscosity can greatly alter the foaming behavior such as the film drainage. With viscosity taken into account, the Young-Laplace law can be modified to:

$$\Delta p = 2\gamma\kappa + \lambda\nu \qquad \textbf{2.9}$$

Where ν is the normal velocity of the film during drainage and λ is a parameter which takes viscous effects into account. An increase in viscosity of the solution will further stabilize the film by reducing the pressure across the surface. The factor of 2 in this equation arises because this is a two-dimensional model [50,53].

Finally, in a wet foam, once these coarsening processes begin and the films between bubbles eventually rupture, the foam will collapse due to instability in the plateau borders. This can be prevented by adding surfactants to stabilize the bubbles in the wet foam. Further, when added to the aqueous component of the foam, particles can coalesce at the plateau borders and stabilize the structure [49]. When film rupture occurs in this situation, gates are created between the bubble faces leading to an open pore structure in the dry foam [50].

A surfactant molecule commonly contains a polar end with a lyophilic group and a nonpolar end with a lyophobic group. In aqueous solutions, the lyophilic end is hydrophilic and the lyophobic end is hydrophobic. These molecules can also be charged or uncharged. A nonionic surfactant will not ionize when dissolved. Anionic surfactants have a large lyophobic end and a smaller, negatively charge lyophilic end. In contrast, cationic surfactants have a positively charged lyophilic end. These charged surfactants can be used to stabilize wet foams in several ways. The lyophobic end can be absorbed at the air/water or oil/water interface in the foam, depending on the source of the bubble formation (surfactant adsorbed to a particle can be seen in Figure 2.5). These molecules can only be absorbed on bubble surfaces or particles to a certain critical amount, above which micelles will form, resulting in an increase in viscosity of the suspension caused by the excess surfactant [54].

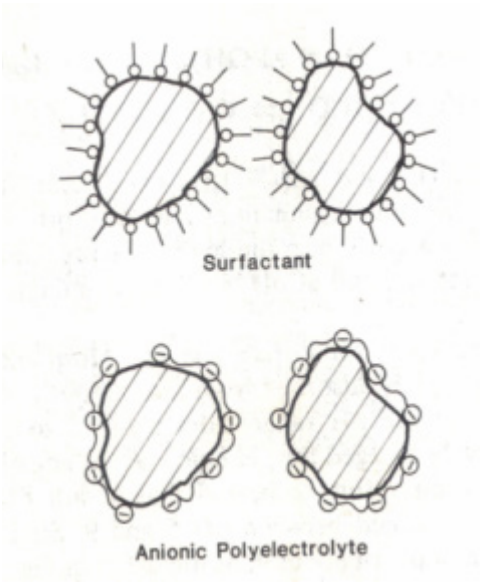

Figure 2.5. Illustration of surfactants and polyelectrolytes adsorbed to a particle surface [**54**].

Polymer electrolytes, molecules with charged side groups that can be absorbed at multiple sites on the surface of a ceramic particle, are common adsorbing molecules added to ceramic foam processing. The exposed side groups on the polyelectrolyte molecule create

repulsive surface forces between particles or bubbles in a suspension. To keep overall charge neutrality, an electrical double layer is formed at the surface in a polar liquid as shown in Figure 2.6 [54]. Oppositely charged ions and polar molecules from the bulk will be attracted to the surface forming a charge gradient from the surface to the bulk solution.

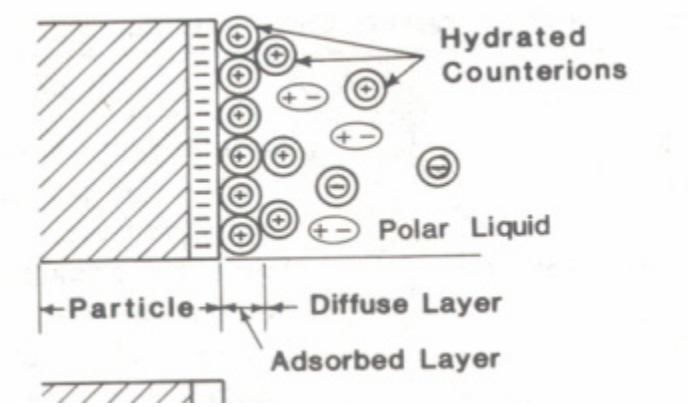

Figure 2.6. Electrical double layer formed at the surface of a particle with an anionic polyelectrolyte adsorbed [**54**].

For ceramic foams, both surfactants and polyelectrolyte dispersants are commonly used. There are significant interactions between these two types of molecule at the bubble film interface depending on the specific charge used. For surfactants and polyelectrolytes with similar charges no significant change is observed in surface tension in the aqueous solution, though there may be a local decrease in polyelectrolyte concentration due to repulsive forces since the surfactant will form a layer at the air/solution interface. There is a significant effect on the film thickness in this case and films will rupture at much lower pressures when compared to foams with no polyelectrolyte added. Kristen and von Klitzing [55] attribute this to the mobility of the polyelectrolyte at the interface causing an unstable film. When the surfactant and polyelectrolyte are of opposite charge, complexes can form due to electrostatic and hydrophobic forces that will lower the surface tension. The magnitude of this effect is dependent on many variables, including the degree of the charge and rigidity of the polyelectrolyte molecule, as well

as the chain length of the surfactant. The film between bubbles will become more stable as an excess of either component is added. An excess of surfactant will create complexes that absorb to the surface while an excess of polyelectrolyte will drive the polyelectrolyte back into solution and a surfactant stabilized film is formed [55].

2.4.2 Ceramic Foams

2.4.2.1 Mechanical Incorporation of Air Into a Ceramic Slurry

The most common way to create a ceramic foam is the mechanical incorporation of air bubbles into a ceramic slurry. This has been demonstrated in the literature using many different methods. Air has been incorporated into a ceramic slurry containing a foaming surfactant by methods ranging from mechanical shearing [47,51,56] to forcing air through the holes in a Buchner funnel [47]. However, without something to stabilize the bubbles in the wet foam during the drying process, large amounts of coarsening will occur leading to foam collapse. Several techniques have been developed to solve this problem, one of which is the addition of a gelling agent to stop the coarsening of the wet foam. Common gelling agents include polymers derived from seaweed, such as sodium alginate and agar powder [47,57]. In this case, the slurry must be heated to temperatures above 70°C to dissolve the polymer and subsequently cooled to 4°C to set the gel. While this prevented foam collapse, the quick setting nature of these gels prevented adequate coarsening and impingement of air bubbles needed to create a fully open foam.

Another technique developed uses surfactants to stabilize the bubble surfaces in the wet foam [48,51]. This solves some of the problems seen with gelation because open porous foams more fully develop. With the addition of short chain surfactants, the particles were surface

lyophobized by a strong adsorption of the anchoring group leaving the hydrophobic tail in contact with the aqueous solution (seen in Figure 2.7). This drew the particles to the air/solution interface, stabilizing the air bubble formed by mechanical shearing. In standard foams, a large amount of film drainage occurs during coarsening, however, bubble were impinged by the particles, limiting drainage and coarsening, leading to a uniform structure upon drying with windows between pores.

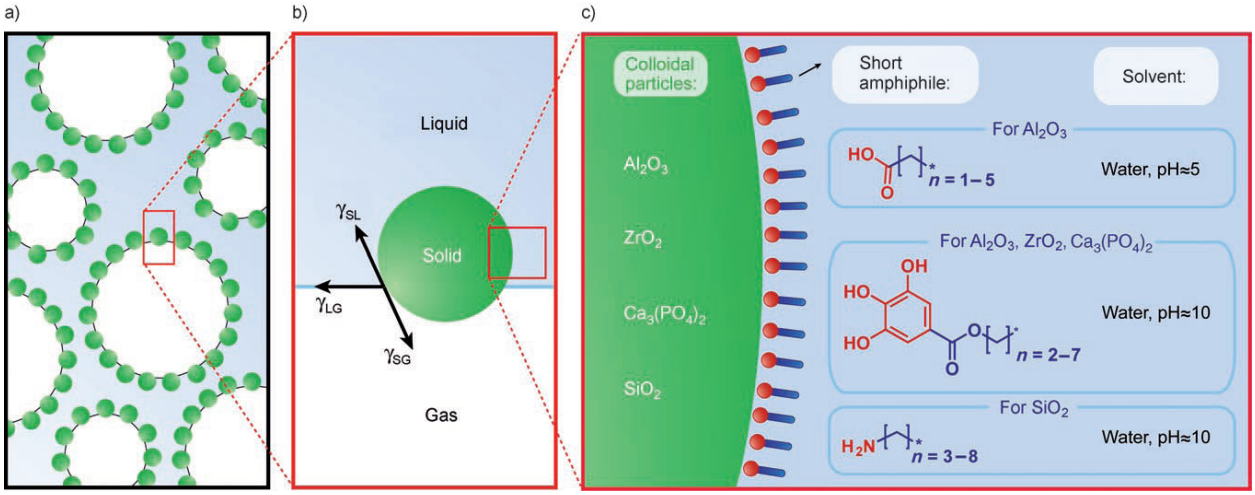

Figure 2.7. Particles stabilized the air/liquid interface by the use of adsorbed short chain surfactants [**48**].

2.4.2.2 Ceramic Embedded Polymer Foams

The use of well-controlled polymer foaming methods has also been investigated. A porous ceramic can be easily created using the replication method, in which a foam, usually polymeric, is coated in a ceramic suspension and pyrolysed during the sintering process to leave a ceramic with the same structure as the polymer [51]. Several groups have also researched suspending ceramic particles in a polymer. Polyurethane is well studied, showing that foams can be created with a controlled pore size and morphology. Ceramic foams have been created by suspending particles in the prepolymer before it is allowed to foam. Open porous foams were created due to particles segregating at the plateau borders and junctions so as the polyurethane is

pyrolysed and the films are burnt out and the ceramic in the plateau borders sinters [58]. The use of silicone surfactants during the foaming process has been shown to aid in the rupturing of films in a wet foam leading to an open structure before pyrolysis [59].

2.4.2.3 Emulsion Foaming Techniques

A foaming technique has been developed by using an emulsion. Volatile alkanes are emulsified into a ceramic slurry and as the alkane evaporates, a porous foam is created upon drying [52,56]. Barg et al. [52] have shown that an open porous foam with pore fractions as high as 97% has been created by emulsifying heptane into an alumina slip containing cationic, anionic or nonionic surfactants. The pH was adjusted to allow for the inclusion of the surfactant in the suspension. By using an ionic surfactant, bubble stabilization occurs in the emulsion and as the alkane evaporates through paths created by liquid film rupture, highly porous ceramic forms. Without a charged surfactant the foam did not show full development, while the ionized surfactants created more porosity in the final structure [52]. Because the point of zero charge for alumina is pH 9.1, a large positive charge can be created at the surface by dropping the pH of the suspension to 5.5. The addition of a cationic surfactant to this suspension leads to a large repulsive force between the lyophilic end of the surfactant molecule and the bulk liquid, leading to even greater stabilization of the alkane droplets [53].

By further controlling the microstructure with the use of surfactants and an alkane with a lower vapor pressure, Barg et al. have created a fine pore ceramic using a high alkane phase-emulsified suspension (HAPES). The use of anionic surfactant in a basic solution created a large negative zeta potential in the alumina slurry. This surfactant stabilized decane bubbles after the suspension was emulsified at 70% alkane by volume. All structures produced by this method had a porosity around 78% that was mostly open. By altering the mixing speed at which the

decane was added to the slurry, the average pore size in the ceramic ranged from 20 μm to 6 μm as the stirring speed used to prepare the suspension increased from 800 to 2500 rpm. These structures have a much finer pore structure than that of previous foams created with an emulsion of a more volatile alkane. Furthermore, graded structures have been created using HAPES foams of different porosities by utilizing a two-step casting process [60].

2.5 LIVER CELL BIOLOGY AND IN-VITRO CULTURING

2.5.1 Liver Cell Biology

The focus of this proposal will be the growth of human adult liver (HAL) cells to form functional liver tissue. Before techniques for grow these cells in vitro can be discussed, basic liver biology and definitions must be presented. The liver is an important organ in the body that performs a multitude of functions. It is responsible for: the detoxification of the blood, the synthesis of proteins such as albumin, and the production of bile used in the digestion process [61]. The liver contains many different cell types, the most abundant of which are the hepatocytes that participate in many liver functions. These cells are responsible for the synthesis of several proteins, mainly those involved in transport and blood clotting. Albumin is one of the most prominent proteins produced by the liver and is commonly used to identify liver cells in culture. This protein is used in the transport of different hormones and fatty acids in the body, as well as being used to regulate the osmotic pressure of the circulatory system. Additionally, these cells are responsible for synthesizing the bile salts that aid in the digestion of fats in the body. Finally,

the metabolism and detoxification of harmful compounds such as drugs and other toxins in the bloodstream occur in hepatocytes [61].

As the liver is developing in the fetus, pre-hepatocytes or hepatoblasts are present. These cells are precursors to the mature liver cells. While hepatoblasts participate in similar processes to hepatocytes, they synthesize α-fetoprotein (AFP) and only produce a small amount albumin. AFP is secreted in smaller amounts as time goes on and albumin begins to be produced as the cells mature into adult hepatocytes, at which point only albumin is produced [4]. While most liver cells fully differentiate, there is a small population of liver stem cells, between 0.5-2.5% by number, that reside in the Canals of Hering (bile ducts in between hepatocytes) [6]. Blood stem cells (CD34+) are another population present in the fetal liver that disappears during maturation. These cells migrate to the bone marrow as the fetus matures and no longer reside in the liver [62].

Along with hepatocytes, several other cell types are present in the liver, serving different tissue functions. Two of the most prominent cells will now be discussed. Endothelial cells form the walls of the vasculature in the liver that facilitate blood and bile flow through the organ. The second type of cell is the stellate (or Ito) cells that store fat in the liver. Excess lipids that cannot be digested by the bile are stored as droplets in these cells. They can also be activated during injury or disease and are prominent in fibrosis (scarring) during liver failure. Lastly, several different extracellular proteins are present in the liver that support the structure of the cells and provide different signals to cell function, the most abundant of which is collagen [61,63].

2.5.2 In-Vitro Niche Construction

The stem cell niche can be defined as a microenvironment in which stem cells reside along with a support structure that controls the differentiation or expansion of the cells [64,65]. A stem cell is a cell with the ability to differentiate to form a number of different types of mature cell. These can be omnipotent in the case of embryonic cells which can differentiate into any cell type in the body, pluripotent which can form multiple mature cell types, or unipotent which can only form one type of mature cell [66]. As seen in Figure 2.8, there are three types of niches where the main purpose is to keep a population of the cells undifferentiated while facilitating the differentiation into daughter cells as necessary. The first is a simple niche where the stem cell is supported by a partner cell, usually a mature cell and attached at a junction. Signals from the partner cell will interact with the stem cell to create a daughter progenitor cell that can form a mature, fully differentiated cell where needed. This can be seen in the bone marrow where blood stem cells will attach to bone cells (osteoblasts) and will differentiate and leave whenever signaling chemicals dictate that a certain blood cell is needed. The second type of niche is referred to as a complex niche. In this scenario, two or more different types of stem cells are supported by partner cells. These occur where neural stem cells reside to facilitate the repair and growth of the nervous system. The final niche, a storage niche, differs greatly from the first two types discussed. Here, the stem cells are maintained by partner cells and signals from outside the pocket are used to recruit the cells. The stem cells will then migrate to where they are needed and will differentiate. These are most commonly found in hair follicles [64].

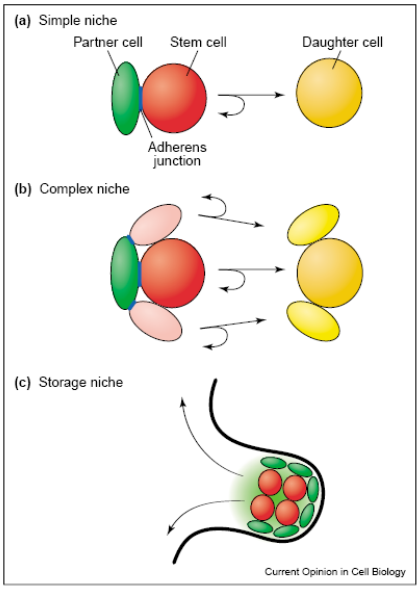

Figure 2.8. Illustration showing the three different categories of stem cell niches [**64**].

The most common way to culture cells is in two dimensions on a polymer plate. There are obvious disadvantages to this when creating most tissues in the lab. Most organs, aside from a select few tissues like skin, have a complex three dimensional architecture [67] in which the extracellular matrix (ECM) supports this structure in the body. Generally, ECM is a protein based fibrous network that controls cell function and facilitate the diffusion of nutrients and other factors that support cell growth [68]. As seen in figure 2.9, cells cultured in a 3D environment more closely replicate the structures observed in nature as compared to standard 2D culturing [67].

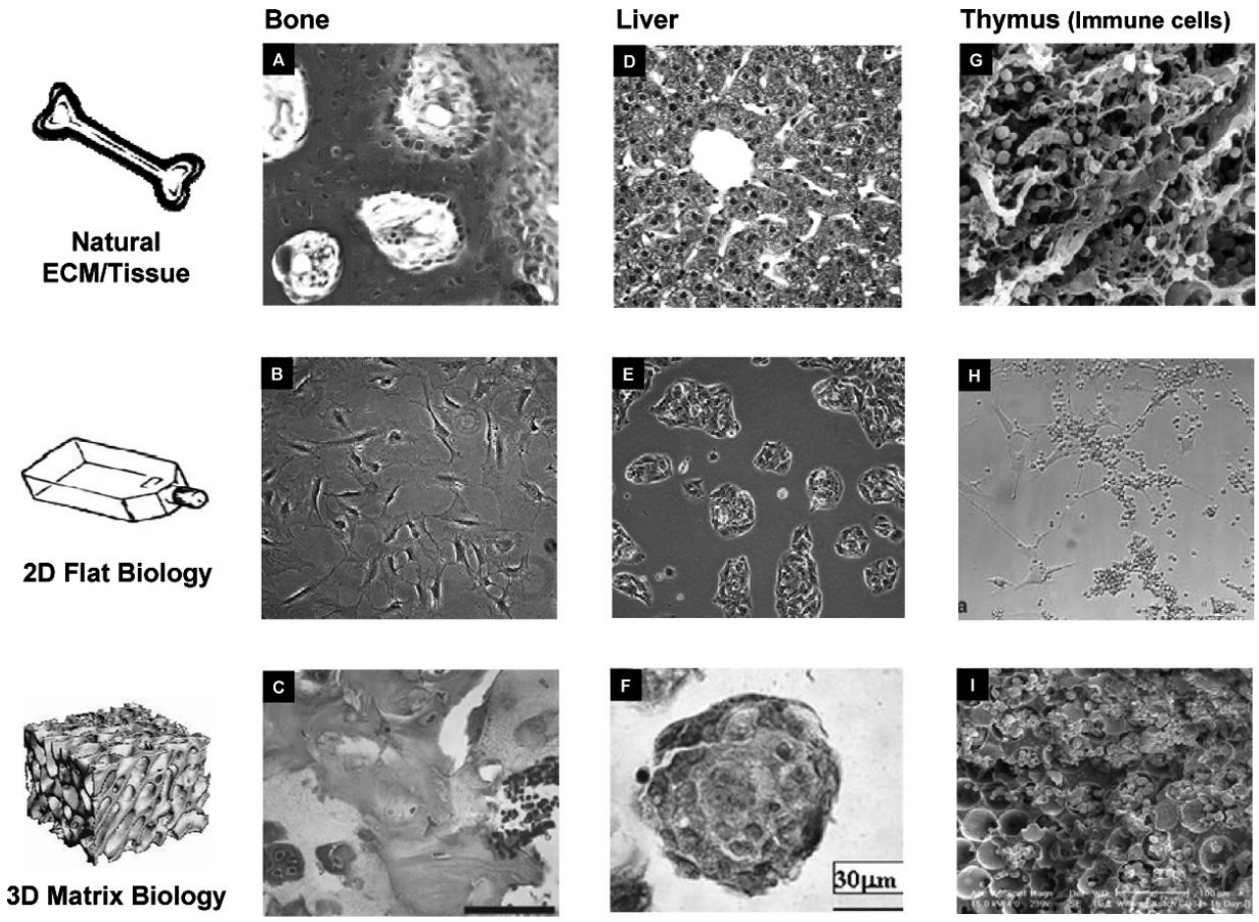

Figure 2.9. Diagram showing the growth of cell in their natural environment (A,D,G), in 2D culture (B,E,H) and 3d culture (C,F,I) [**67**].

One approach to 3D culturing is decellularized natural tissue which can be used as an extracellular matrix. The cells are first digested, leaving behind the 3D scaffold of extracellular matrix. Cells can then be re-seeded into the scaffold to develop a new organ. Some success has been shown in these structures including the growth of both heart [69] and liver cells [70]. However, there continues to be issues with culturing of larger cell masses, and the fact that an organ must be sacrificed to create this scaffold.

Another 3D culturing method introduces an extracellular matrix for cell culture using an injectable porous hydrogel. A hydrogel is network of hydrophilic polymer chains in water [71]. These gels have been made from several synthetic polymers such as poly(acrylic acid) and

poly(ethylene oxide) [68], and have been shown to successfully grow cells in culture [68]. Alginates have also been used and while they come from a natural source (seaweed) they are not found in the body and do not show significant interactions with cells [68]. However, they have been used to encapsulate cells such as liver [3] and islets of Langerhans (pancreatic cells responsible for producing insulin) [68] for injection into the body to treat disease. Porous 3D scaffolds made from alginate gel have also been used to grow human liver cancer cells in culture, showing much greater cell activity than those grown on a PS plate [72]. Natural polymers found in the body, however, can be more desirable due to their known presence in stem cell niches. Collagen, the most abundant protein in the body, can be found in most organs [66]. This protein has a triple helix structure and can be processed into a gel by dissolving it in an alkaline solution and heating [68]. These gels, which will degrade over time and can also be digested by the enzyme collagenase. Collagen gels are widely used in cell culturing because of its prevalence in the body, including skin cells [73], bone cells [68], and liver cells [63]. In fact, the widely regarded "gold standard" of hepatocyte culturing is the collagen sandwich method, which involves culturing a monolayer of hepatocytes between two layers of collagen hydrogel. This has shown to maintain functional hepatocytes from several species in culture for long periods of time [74].

Hyaluronic acid (HyA, $(C_{14}H_{21}NO_{11})_n$ seen in figure 2.10) has also been used in cell culturing because of its prevalence in the body, especially in wound healing [68]. This glycosaminoglycan can be formed into a gel by covalently crosslinking the structure with a hydrazide derivative. The hyaluronan can be extracted and purified from various sources such as rooster combs [68] and from bacteria cultures [6]. As with collagen, these structures can be broken down with enzymes secreted from cells, specifically hyaluronidase [68]. These gels are

used widely in cartilage repair [75] and, increasingly, in the culture of liver cells. Specifically, hepatoblasts are cultured in hyaluronan gels because of the presence of hyaluronan receptors on the surface of the cell (surface marker CD44). Schmelzer et al has shown that these gels can support the growth of liver stem cells without affecting the differentiation of the cells in culture for 10 days [4].

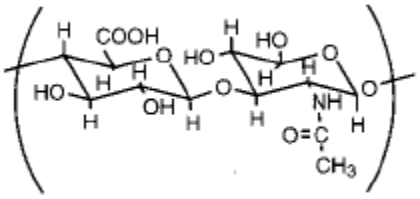

Figure 2.10. Chemical structure of hyaluronic acid [**68**].

Once the correct ECM is chosen for culture, the last aspect of culturing viable tissue *in-vitro* is vascularization of the construct. This has been a well-documented in bone tissue engineering as well as other systems [76,77]. This is necessary in three dimensional culturing to delivery nutrients to the center of the construct to avoid necrosis in the interior and is seen as a pitfall in current tissue engineering strategies [76]. Several methods have been shown to induce vascularization in cell cultures including material choice, morphological changes, mechanical stimulation and the addition of certain growth factors to the culture medium [76]. The most common method of inducing vascularization in-vitro is by adding growth factors to the culture medium, specifically vascular endothelial growth factor (VEGF) in combination with other factors specific to the desired tissue [76]. A problem with this method is the short half-life of these molecules as well as the prohibitively high cost [76,77]. The three-dimensional scaffold itself can also be used to induce endothelial cells (EC) for vascular tissue by creating a surface suitable for the actin filaments of the ECs to attach, as well as providing a microenvironment

either from the scaffold or from the culture medium suitable for cell proliferation [76,77]. Casting techniques have also been developed to guide ECs to form vascular tissue in channels in a construct. Recently, Miller et al. formed cylindrical channels in a hydrogel by rapid casting of amorphous carbohydrate vascular-like networks. A hydrogel, embedded with cells, was then casted around these networks and saline was perfused through the channels to dissolve the amorphous carbohydrate. These channels were then seeded with ECs and vascular-like channels formed in culture [78]. One disadvantage of this technique is the ~48 hr. time it took for the network to dissolve [78]. Ideally perfusion through these networks would be available as soon as possible after the cells were injected to prevent any cell death in the interior of the construct.

As discussed earlier, HAp scaffolds have been used to culture many different cell types including liver cells. Most notably, porous HAp discs have been seeded with rat hepatocytes and cultured in the lab for 3-6 days to ensure that the cells were attached to the disc. These were then implanted into the abdomen of the rats and left for 21 days. After the discs were excised from the rat it was found that blood vessels had grown into the structure creating blood flow to the cells in the scaffold. Additionally, the authors suggest that long term growth of hepatocytes on the scaffold can be accomplished due to the maintenance of these cells during the experiment [9]. Human hepatoblasts have also been cultured in porous HAp carriers [79].

While hydroxyapatite has been used to culture liver cells, there is no reasoning provided for this material selection decision. One promising reason for using calcium phosphates as scaffold material for liver tissue culturing is the role of Ca^{+2} ions in both hepatocyte and vascular cell growth. Calcium ion channels on the surface of the cell are important not only in the function of vascular endothelial cells, but also in their formation. These channels imperative for the expression of mature endothelial genes including von Willebrand factor, it is also thought

that they play a crucial role in the expression of vascular endothelial growth factor (VEGF), a necessary factor in vascular tissue formation [80]. Calcium is also important to hepatocyte proliferation *in vitro*. It was shown in a study by Eckl et al. that a Ca^{+2} ion concentration of 0.4mM in the culture medium greatly increased proliferation of adult rat hepatocytes. Proliferation of these cells increase as the Ca^{+2} ion concentration to this point and then it began to decrease at higher concentrations. Despite this the proliferation of the cells was still higher at the higher concentration when compared with cultures containing no calcium [81]. These two findings are integral to the foundation of this work. Local environments rich in Ca^{+2} ions are beneficial for the culture of several liver specific cell types.

2.6 BIOREACTORS

2.6.1 Types of Bioreactors

A bioreactor is a vessel in which cells are cultured in an environment controlled for pH, temperature, and nutrient concentration [82]. These are used extensively in the food industry (fermentation) [82], wastewater treatment (enzymatic water purification) [83], and pharmaceuticals [82]. There are two main types of reactors: stir tank and fixed bed. A stir tank reactor, pictured in Figure 2.11, is a vessel where cells float freely in cell culture medium (a solution containing components such as nutrients, growth factors and antimicrobials, which supports the culture of cells) as the suspension is constantly mixed. These reactors are ideal for non-adherent cells. Carriers made from biocompatible polymers and ceramics can be used for

cells that are apt to grow on a surface (adherent cell). The cells can attach to the carriers which are then suspended in the reactor [82].

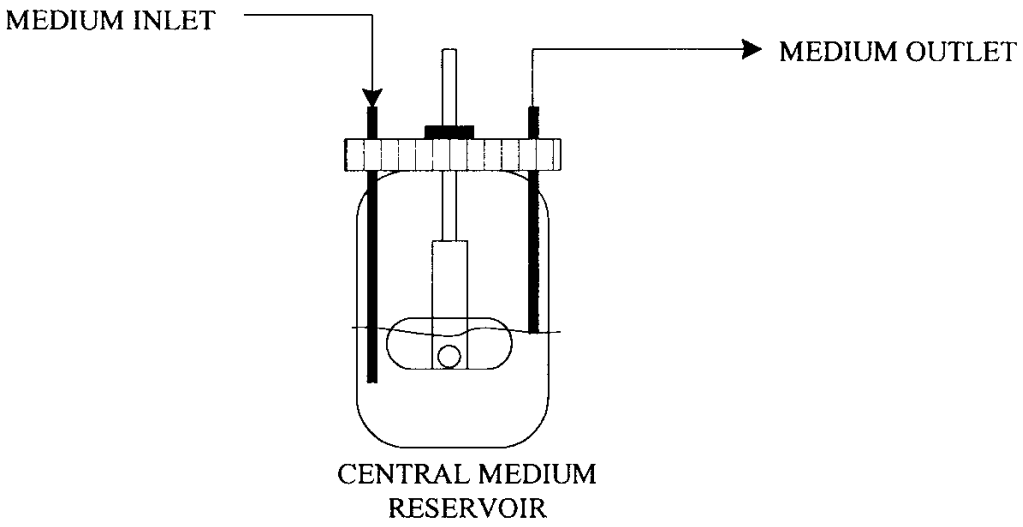

Figure 2.11. Diagram of a standard stir tank reactor [**84**].

The second type of bioreactor can be described as a fixed bed reactor. In this type of reactor, cells are cultured in a fixed chamber or core that the culture medium is then perfused through. In many cases, hollow fiber membranes can be used to perfuse medium and oxygen into and out of the chamber (Figure 2.12). Human fetal and adult liver cells have been observed to grow successfully in reactors of this nature. By setting up a 3D environment, these cells have been seen to spontaneously reorganize in the core to resemble tissue structures [14, 67].

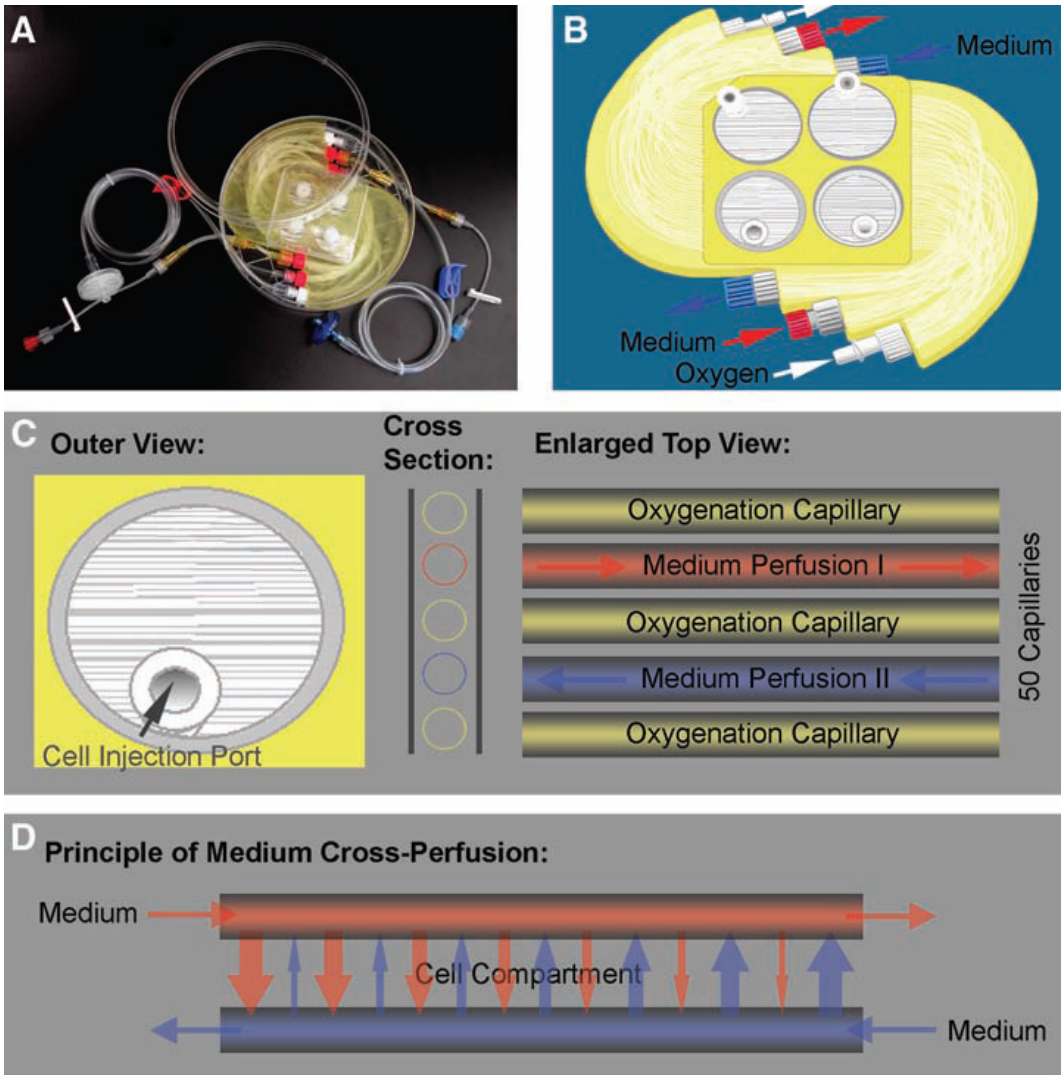

Figure 2.12. Example of fixed bed reactor using hollow fiber membranes [**4**].

2.6.2 3D Networks in Bioreactors

Different polymeric scaffolds have been used to grow liver cells in a bioreactor core. Cellulose beads have been used to culture a human liver cancer cell line with rat epithelial cells in an attempt to recreate liver tissue in a perfusion reactor. Liver structure formed in the beads; however, cell function was seen to decrease over the 13 day culture [85]. Hydrogels have also been used to support cell growth in a bioreactor core. HyA gels have been used to culture human

fetal liver cells in a bioreactor and without perfusion. It was seen that after 10 days, significantly more differentiation to mature liver cells was seen in the bioreactor compared to the negative control. This was shown by the increase in albumin production in the cells as well as by the presence of mature detoxification enzymes in the culture [4].

Calcium phosphate scaffolds have been used for several different cell types in a perfusion reactor. β-TCP scaffolds have been used to culture sheep mesenchymal stem cells in 3D. A porous TCP cylinder was created and seeded with the stem cells and then they were then either perfused or kept in static culture. The cell viability was significantly higher in the scaffolds that had cell culture medium perfused over the course of 28 days in comparison with the static control [85]. Perfusion bioreactors have also been implemented to develop liver tissue using an apatite scaffold. Similar to the cellulose bead experiment described above, human liver cancer cells and rat endothelial cells were cultured in a bioreactor containing a porous degradable scaffold made from single crystal HAp fibers for 17 days. Again, tissue structures were seen in the scaffold after removal from the bioreactor. In this study, the scaffold was then implanted into a rat abdomen and kidney after culture in the bioreactor. After 8 weeks the cells were still showing healthy liver cell function including the production of albumin [10]. This finding shows the validity of culturing liver cells on bioactive ceramics. This proposal will examine the culturing of human liver cells on calcium phosphates for future use in a perfusion bioreactor.

3.0 HYPOTHESIS

It is proposed that it is possible to create a bioreactor core suitable for human liver cell proliferation and reorganization by controlling the pore size of a ceramic/hydrogel composite, using the phase distribution resulting from high temperature decomposition of HAp, and incorporating a vascular pore network.

4.0 TECHNOLOGICAL RELAVANCE

This study is of importance because a three dimensional support structure is needed for the growth of large masses of implantable tissues in-vitro. These structures must be rigid enough to maintain the microenvironment in the reactor core and also dissolve as the tissue grows. It is thought that this could be accomplished using a hydroxyapatite/collagen 1 hydrogel composite, and by decomposing HAp to resorbable phases during sintering. The growth of human adult liver cells (HAL) on these materials must be accomplished to create viable liver tissue. While liver specific cells have been successfully grown on HAp [11,12], they were not able to form tissue for transplantation. The ceramic emulsion foaming technique used in this study also allows for the creation of a multiscale porous structure, which can be used to immobilize the cells and also to create a guide for growth of a vasculature system. Finally, by placing these structures in a perfusion bioreactor, the simulated physiologic conditions could allow spontaneous reorganization of human liver cells into tissue like formations [10]. These tissue-like structures would form within the 3D ceramic scaffolds and eventually remodel the bioreactor core.

5.0 OBJECTIVES

1) Preparation of a ceramic/hydrogel composite structure and the culturing of liver cells.

   Further refinement of the emulsion foaming technique and examination of the composite structure was needed to create the three-dimensional support structure for culturing the cells. The pores of the ceramic must be between 250 and 1000 μm to support the formation of liver plates. The pore size cannot be significantly larger than 1000 μm so that nutrients can be sufficiently delivered to the center of the pore through the hydrogel. Cell culturing experiments were completed as a proof of concept that HAL cells can successfully grow on the materials studied here.

2) Effect of porosity on the high temperature transformation of HAp and consequent effects on dissolution.

   The ceramic in the composite structure must be able to resorb over time as the tissue begins to form. It is possible to create suitable porous biphasic structures by using the high temperature decomposition of HAp. The effect of emulsion foam variables on the transformation behavior were examined, as well as their dissolution behavior in both static and perfusion conditions.

3) Effect of a vascular structure on the pore structure of the foam.

   Multiscale porous ceramics have been created using the positive-negative casting technique; more complex geometries, however, must be created to facilitate the creation

of a natural vascular system. Surface properties and spacings of the positive vascular copy were examined. The validity of using these structures as a surface for endothelial cell attachment were also evaluated by the cell culture experiments performed in objective 1.

6.0 EXPERIMENTAL PROCEDURES

6.1 EMULSION FOAM PROCESSING

6.1.1 Emulsion Processing

HAP powder (Sigma-Aldrich) was calcined at 900°C for 1 hour to ensure phase purity, and then milled in water with alumina ball for 24 hours. The powder was then dried and crushed using a mortar and pestle and used to make emulsion foams [52]. To create the foam, a suspension was made using 30% by volume of prepared HAp powder with deionized water, an ammonium polymethacrylate polyelectrolyte dispersant (Darvan C, RT Vanderbilt Co.), and hydrochloric acid that was used to adjust the pH to 5.5. The pH was adjusted to facilitate an addition of a cationic surfactant to stabilize the alkane droplets later in the foaming process. This suspension was subsequently mixed at a speed of 2500 RPM for 20 minutes to assure proper dispersion. Then a cationic surfactant (benzethonium chloride, Sigma) or an anionic surfactant (sodium dodecyl sulfate, Sigma) was added to stabilize the emulsion and various amounts of heptane were added and mixed at high speed for 2 minutes to create the emulsion. Heptane was added at 0, 2.5, 5, 7.5, 10 and 20% by volume. Following its creation, the emulsion was then poured into a paper mold and kept at 24°C and 60% relative humidity for one hour inside of a humidity

controlled desiccator. Afterwards, the foam was allowed to dry at 40% relative humidity overnight.

Once dried, the foam was heated in a furnace at a rate of 2°C/minute to 900°C where it was held for 1 hour to burn off the paper mold. After burn out, the foams were transferred to a high temperature furnace and heated at a rate of 5°C/minute to 1300°C for 4 hours to fully sinter the foam.

6.1.2 Pore Size and Characterization

Scanning electron microscopy (SEM) analysis was done on machined and polished sections of foams as well as fracture surfaces. For the planar sections, the foams were first impregnated with a low viscosity resin to preserve the foam structure during machining. These samples were then cut to obtain a through thickness cross section and a horizontal cross section of the interior of the sample (Region 2 of figure 3.1). Afterwards, these were mounted in the same low viscosity resin and ground with 45 μm and 30 μm diamonds, pre-polished with 15 μm diamonds, and then polished with 6 μm and 1 μm diamonds.

These samples were then coated with palladium using a sputter coater and examined in a Phillips XL30 scanning electron microscope. Backscattered images were taken of the through thickness and horizontal cross sections of all samples to enhance the contrast between the ceramic and pore phases.

For quantitative analysis of the pore structure, nine images were taken at randomly selected locations on the planar sections. The images were then thresholded using ImageJ where black pixels were pore space and white pixels were ceramic. The percentage of white pixels equated to the solid fraction of ceramic V_s in the foam where the pore volume fraction $V_p = 1-V_s$.

These same images were used to calculate the two average pore intercept lengths that were defined differently. For both measurements, six randomly located lines were drawn on each of the nine images. Pore/solid intercepts per unit length of test line, P_L^P were then counted. At high pore volume fractions, the microstructure contained continuous pore phase, even in the 2 dimensional sections. This allowed for a distinction to be made between pore sections that are surrounded by the solid phase (internal pores) and pore sections that are part of the continuous pore phase in the samples. The pore boundary intercepts for internal pores, P_L^{IP} were then recounted separately from the intercepts of the continuous pore phase P_L^{LP}. The surface to volume ratio can then be calculated for each of these intercept measurements. For example, the surface to volume ratio for all pores S_v^p is given by:

$$S_v^p = 2P_L^p \qquad \textbf{6.1}$$

Each surface to volume ratio can then be used to define an average pore intercept. For example the average pore intercept length for all pores is given by:

$$\lambda_p = 4V^p / S_v^p \qquad \textbf{6.2}$$

At low pore volume fractions the pores are isolated and this parameter represents a measurement of the average pore size, conversely, at high pore volume fractions this measurement may involve both the size of pore sections isolated in the solid phase and the average distance between the continuous pore boundaries through the continuous pore phase. This added complication for the analysis of highly porous foams can be somewhat mitigated using the distinction between intercepts for the internal pore boundaries and the boundaries of the larger continuous pores. In particular, for foams with more than 80 vol% pores, the number of continuous, large pore boundaries per unit length of test line P_L^{LP} was used to define a pore intercept length, λ^{LP}, which is best interpreted as the "mean free path" through the continuous pore phase in the foam. In this case the pore volume fraction of the continuous pore phase V_p^{LP}

must also be determined by reprocessing the images to fill in all the internal pores and redetermining the pore fraction. Thus the pore intercept length through the continuous pore phase is given by:

$$\lambda^{LP} = 4V_p^{LP} / S_v^{LP} \qquad \textbf{6.3}$$

Intercept lengths can also be defined for the solid phase using the same intercept data. In this study the total solid intercept length λ_s was calculated as:

$$\lambda_s = 4(1-V^p) / S_v^p \qquad \textbf{6.4}$$

Again this parameter is easily interpreted at low pore volume fractions when the pores are isolated and the intercept length represents the average pore separation. At high pore volume fractions the interpretation is complicated because the solid can be made up of struts containing closed pore sections. Without internal pores, the average intercept length could have been interpreted as the average strut thickness. However, the presence of internal pore sections requires a new definition of λ_s^{LP} based on P_L^{LP} and the V_p^{LP} as follows:

$$\lambda_s^{LP} = (1-V_p^{LP}) / S_v^{LP} \qquad \textbf{6.5}$$

This intercept length is a measurement of average strut thickness for a situation where the solid phase contains small isolated pores.

Finally, machined surfaces that had not been impregnated with resin or polished were examined to give qualitative information about the topology of the pore structure.

Figure 6.1. Image of pre-sintered foam to illustrate the 3 regions produced. 1)'surface region', 2)'foamed region' and 3) 'dense region' which is ceramic that did not foam during the emulsion process.

6.1.3 Effect of Alkane Vapor Pressure on Pore Morphology

An alternate emulsion technique was used to examine the effect of alkane vapor pressure on pore morphology. High alkane phase emulsion suspensions (HAPES) are used in the manner described in section 2.4.2.3. Heptane, octane, nonane, and decane were used as the alkane phase. 20 g of HAp powder was suspended in Darvan C and NaOH to achieve a pH of 9.5. Subsequently, this was mixed at 2500 RPM for 10 minutes to ensure full suspension. Afterward, sodium dodecyl sulfate was added to stabilize the ensuing emulsion. Next, alkane was added at 50 vol% and mixed for 2 minutes. The emulsion was then poured into a paper mold and allowed to coarsen and dry at ambient temperature and humidity for 72 hours. Lastly, the foams are sintered as described above.

6.2 HUMAN ADULT LIVER CELL CULTURING

Human hepatocytes from male donors were obtained from discarded grafts (BD biosciences). This population contains mainly hepatocytes; however, small populations of non-parenchymal cells were also present, preserving all cell types necessary for liver formation. These include, but are not limited to vascular endothelial cells, bile epithelial cells, and stellate cells (fat storing liver cells of mesenchymal origin).

Four-well polystyrene tissue culture plates were prepared with two wells containing hydroxyapatite (HAp) foam prepared from the "surface region" of an emulsion foam (figure 6.1), providing two negative controls per plate without the presence of a scaffold. The plate was sterilized using γ-irradiation and the scaffolds were sterilized using an autoclave. Before plating, 1E6 cells were lysed for RNA and genomic DNA testing to be performed later. Two extracellular matrix hydrogels were prepared for the study. Hyaluronic acid gel (HyA, Glycosan) was prepared by dissolving freeze-dried hyaluronan in 1 mL of sterile water at 37°C. To decrease gelation time, 125 µL of a crosslinker (extralink, Glycosan) was added, and the prepared cell fraction was suspended in the mixture at a concentration of 1E6 cells/mL of gel. Collagen 1 gel (C1) was prepared by mixing 0.665 mL collagen type 1 (rat tail, BD Biosciences) with 1.5697 mL sterile water, 0.25 mL sterile 10x PBS and 15.3 µL sterile 1M NaOH. Cells were again suspended at a concentration of 1E6 cells/mL of gel. To each well of a 4-well cell culturing plate, 250 µL of both gel/HAL mixtures were added. Additionally, cells suspended in cell culture medium were added at a concentration of 1E6 cells/mL to a flat plate to be used as a second negative control. 250 µL of Williams E (WE) complete media, a medium specifically used to culture adult hepatocytes [87], was added to each well. Table 1 below shows the composition.

Table 1. WE Complete Formulation

William E Complete Medium	**For 500 ml**
WE #12551032 (Invitrogen)	438 mL
Nicotinamide (contains 1 mg/L)	
Glutamax	5 mL
Anti/Anti	5 mL
Insulin	0.5 mL
Transferrin	0.5 mL
Selenium	0.5 mL
Hydrocortisone	0.5 mL
FBS	50 mL

After plating, the cells were cultured in an incubator at 37°C and 5% CO_2 for between 5 and 28 days. The WE complete medium was replaced every 2 to 3 days during culture to replenish nutrients and remove waste products. Additionally, the aspirated medium was saved for future protein analysis. For all experiments, cultures were kept for 5, 15 and 28 days. At each time point a piece of scaffold was extracted using a scalpel and fixed in 4% paraformaldehyde for 30 minutes at room temperature for microscopy. Afterwards, both samples (scaffold and no scaffold) were lysed using RLT Plus cell lysis buffer and kept for RNA isolation and genomic DNA quantification.

Five methods were used to analyze the cell cultures. The first of these, enzyme linked immunosorbent assay (ELISA), is used to examine protein secretions in the aspirated medium. In this procedure, an antigen of interest is attached to the surface of a 96-well plate which will

attract the antibody of interest from the medium samples. After a series of reactions, the plate can be read using a spectrometer where the intensity of the color in each well corresponds to the amount of antibody in the medium. Albumin levels in the medium were examined as a test for mature liver cell function.

RNA was extracted from the cell lysate using a kit from Qiagen. Reverse transcription polymerase chain reaction (PCR) was subsequently performed on the RNA, resulting in c-DNA samples. Real-time PCR (RT-PCR) was used to examine the cell types in the culture through gene expression. 25 ng of c-DNA from each sample was used and tagged with fluorescent TaqMan probes (invitrogen), which bind to specific gene sequences of interest. The following list shows the 7 markers used and their significance:

1. β-actin – one of six actin isoforms found in all human cells. This is used as a control gene to normalize the gene expression data.
2. P450-CYP3A4 - a detoxification enzyme found in mature hepatocytes
3. Albumin (ALB) - a protein found in mature hepatocyte populations
4. α-smooth muscle actin (ASMA) - a marker of stellate cell formation (fat storing cells of the liver)
5. von Willebrand Factor (vWF) – a marker of mature vascular endothelial cell
6. Cytokeratin 19 (CK19) – a marker for both bile epithelial cells and hepatocyte progenitors
7. Antigen KI67 – a marker of cells in a proliferative state

For the repeats using donors 5-7, prior to RNA isolation, the lysates were passed through a column to isolate genomic DNA from the samples. This was then quantified using a Qubit fluorometer (invitrogen) and a double stranded-DNA assay kit and compared to the DNA of a

known number of cells. For these samples, an extra well was prepared so that the entirety of the culture can be lysed to ensure that all cells were counted provided an entire well for microscopy.

Immunohistochemistry was used to analyze where the cell types appeared in each sample. An Olympus Fluoview confocal microscope was used at the University of Pittsburgh's Center for Biological Imaging, allowing for the concurrent use of 3 lasers. All samples were stained for DAPI (Diamidinophenylindole dihydrochloride, Sigma), a nuclear stain which binds to DNA; Phalloidin (invitrogen), a toxin which unspecifically binds to the cytoskeleton of the cell; and one specific cell marker of interest. For the purpose of this experiment, samples were stained for CK19 to determine if high gene expression was due to expansion of bile epithelial cells or hepatic progenitors. Morphology of the cells in culture was also used to identify cell types.

6.3 HEAT TREATMENT

6.3.1 High Temperature Phase Transformation Behavior of Hydroxyapatite Foams

First the effect of sintering temperature was examined for dense pressed HAp discs and replicated foams. To make dense ceramics, the powder was pressed at 85 MPa. The green density of the pellets was 45%. To create the foams, polyurethane precursor tiles (Polyaddition type, PPI 30 soft foam, Modulor, Berlin, Germany) were coated with a 33.5 vol% HAp suspension (Sigma) dispersed with Darvan C. The foams were allowed to dry overnight and both the foams and pellets were heated at 1°C/minute to 800°C to allow the polyurethane to burn out, and then sintered at temperatures in the range of 1350–1550°C for 1 hour. To further

examine the phase transformation, pellets and foams were also held for 0 hours at 1350–1450°C following the same heating program as before.

Once the sintering was complete, the density of the pellets was measured using the Archimedes method based on ASTM C373, in which the suspended weight was measured after the sample had been evacuated, and then immersed in water for 12 hours. Both the bulk density (solid volume fraction) and apparent density (calculated with the volume of solid and closed pores) were determined.

For scanning electron microscopy (SEM) analysis, pellets sectioned parallel to the pressing direction and foams were vacuum impregnated and mounted in a low viscosity epoxy resin. Then, the samples were ground with 45 μm and 30 μm diamonds, pre-polished with 15 μm diamonds, and then polished with 6 μm and 1 μm diamonds. Phase analysis was determined by x-ray diffraction (XRD) on the external surface of the pellets, ground pellets and ground foams.

6.3.2 Effect of Pore Size on High Temperature Phase Transformation of Hydroxyapatite

For quantification of α-TCP contents a calibration curve was created using XRD. Known mixtures ranging from 100wt% α-TCP to 100wt% HAp were examined by scanning between 30 and 33°2θ. The ratio of the (2 1 7) α-TCP peak to the (2 2 1) HAp peak was then plotted with respect to wt% α-TCP and fitted with a linear line. This was used in subsequent experiments to quantify relative phase amounts in sintered scaffolds.

To examine the effects of pore size on the high temperature phase decomposition of HAp, foams were created as seen in section 6.1.1. These foams were sintered at 1500°C for 1

hour and analyzed as in section 6.2.1. The peaks of the XRD scan were used to quantify α-TCP contents using the calibration curve.

6.3.3 Dissolution Behavior of Biphasic Calcium Phosphate Foams

Foams were created as described in section 6.1.1 using 10 vol% heptane. These were sintered at four temperatures ranging from 1350°C to 1500°C for 1 hour to obtain α-TCP contents ranging between 2.16% to 62.59%. Tris-buffered saline (50 mM tris(hydroxymethyl)aminomethane-HCl, 150 mM NaCl) at pH 7.3 was used to approximate culture conditions. The dissolution of these foams was examined under two conditions, static and perfusion, for 28 days. For static experiments, three 30 mg coherent pieces from each sample were placed in 2 mL tubes and covered with 1.5 mL of saline for each time point and placed in an incubator at 37°C. Six time points were used: 20 minutes, 1 hour, 24 hours, 72 hours, 1 week and 4 weeks. At each time point the saline from each sample was aspirated and tested for Ca^{+2} ion concentration using a Ca^{+2} ion Accumet probe (Fisher). The three samples from the 4 week time point were washed with DI water and dried to measure mass loss over the duration of the experiment and for SEM. For the perfusion experiments, again three 30 mg coherent pieces of each sample were placed in the chamber of a 3D Kube bioreactor (3D Biotek). These reactors where then connected to a pump with ¼" tygon tubing and 1 L of tris-buffered saline (TBS) was continuously perfused at a rate of 5 mL/min to approximate perfusion bioreactor conditions. The experimental setup is shown in Figure 6.2. 1 mL samples of saline were taken at the same time points as the static experiments. After 4 weeks, the reactor chamber was flushed with DI water and the scaffolds were extracted and dried to measure mass loss and for SEM.

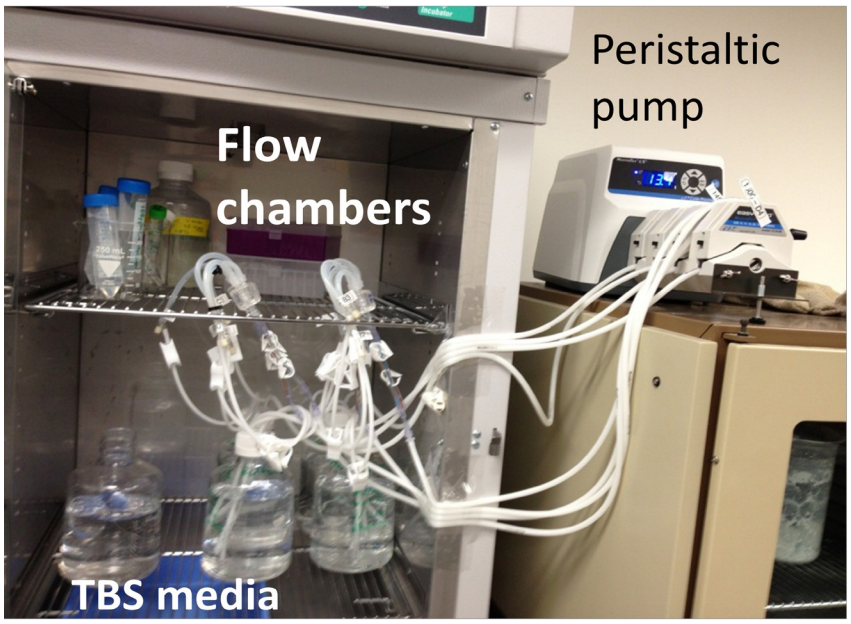

Figure 6.2. Experimental set up for perfusion dissolution experiments.

6.4 POSITIVE-NEGATIVE CASTING TECHNIQUE

6.4.1 Initial Positive-Negative Casting Experiments

For the purpose of preliminary experiments, polystyrene tubes (diameter~3mm) will be used as the vascular network copy. These tubes were fixed to the bottom of a paper mold in square arrays with the edge spacing equal to 1D, 2.5D and 5D. An emulsion was prepared following the method outlined in section 6.1.1 with a heptane content of 10 vol%. These foams were then sintered, sectioned and polished and then qualitatively examined following the procedure outlined in 6.1.2.

6.4.2 Effect of Coatings on Polystyrene Tubes

To address the problem of foam collapse between closely spaced tubes, surfactant coatings were examined. Polystyrene tubes were coated in both Darvan C and benzethonium chloride (dissolved 1:20 in DI water). These, along with uncoated tubes, were then fixed to the bottom of a paper mold in a square array with one-diameter edge spacing. The same 10 vol% heptane emulsion foam was used as in the previous section and the dried foams were sintered at 1300°C for 4 hours. Next, the foams were impregnated with epoxy and sectioned parallel to the channels formed by the tubes. After following the previously described polishing procedure, the sections were examined using SEM and the distance from the top of the foam to the collapsed foam between the channels was measured using imaging software.

6.4.3 Positive-Negative Casting Around a Closely Spaced Nylon Array

More complex vascular preforms were used to simulate a natural vascular system. A square, woven nylon mesh was used with 4 mm edge spacing. These arrays were either used as is or coated in a 5 wt% solution of either benzethonium chloride (a cationic surfactant) or sodium dedecyl sulfate (an anionic surfactant) for 24 hours. The HAPES foaming technique was used as described in section 6.1.3 with 25 vol% octane and 29 vol% HAp. The square arrays were fixed horizontally in a paper mold and the emulsion was poured in completely covering the array. These molds were then placed in a desiccator at saturation humidity for 10 minutes and allowed to dry at ambient conditions for 72 hours. These samples were then sintered following the above conditions and fracture surfaces were examined using SEM.

While they were not used in this study, polymeric copies of a rat's liver vascular system has been produced in Dr. Gerlach's lab. To create the positive cast of a vascular system, a small gauge catheter is inserted into the liver portal vein between its exit site at the intestine and its entrance site at the liver. Once inserted, the liver is flushed with saline and then polyurethane or silicone is injected at a slow, fixed rate. After the polymer is cured, the liver tissue is digested using solvents. The resulting structure is shown below.

Figure 6.3. A silicone rat liver vascular system copy.

7.0 RESULTS AND DISCUSSION

7.1 EMULSION FOAM PROCESSING

As described in the first objective, a porous HAp structure must be created to be used as a scaffold in liver cell culturing. This scaffold must be over 80% porous with completely interconnected porosity so that the pores of the ceramic can be injected with cells and cell culture medium can be flowed into and out of the structure. Additionally, these pores must be between 250-1000 μm so that essential nutrients can be delivered to the center of the pore and interconnection must be at least 75 μm in size to ensure cells can be easily injected.

7.1.1 Emulsion Foam Technique Development

After the emulsion is foamed, three distinct regions can be observed (Figure 6.1). Region 1 is found at the top surface and is comprised of a thin, open porous foam. This region is in direct contact with the environment during the foaming process and consequently dries well before the rest of the emulsion. Region 2, the most important with regards to this study, is an open porous foam in the center of the sample. These pores are larger than those seen in region 1 because the heptane bubbles have more time to coarsen in the emulsion and the slower drying kinetics of the ceramic phase can lead to further coarsening of air bubbles after the heptane evaporates. Region 3 appears at the bottom of the cast along with the surfaces of the mold. This region is relatively

dense containing a limited amount of mostly closed porosity. A relatively dense skin is observed at the surfaces of the mold as seen in polyurethane integral skin foams [88]. This is most likely due to the ability of heptane bubble to wet the mold surface or the electrostatic repulsion of the surfactant coated bubbles and similarly charged species on the surface. Also, film drainage under gravity in the wet foam will lead to a more dense region at the bottom of the mold [50]. The amount of regions 1 and 2 are dependent on the stability of the wet foam which is influenced by humidity during drying, surfactant concentration and heptane content among other variables [53]. The effect of varying the heptane content on the foam structure created is discussed below.

7.1.2 Effect of Alkane Content on Foam Morphology

The effect of emulsion heptane content on the pore fraction in the sintered foam can be seen in Figure 7.1. As expected the porosity of region 2 increased as the heptane content increased. At 0 vol% heptane there is 8.5% closed porosity due to air incorporation during mixing. Figure 7.2 shows the calculated pore and solid intercept lengths from stereology (calculated from the equations in section 6.1.2). From these two figures, three distinct microstructural types can be seen over the 6 heptane contents examined. The first group consists of foams that contain a small amount of isolated, closed pores. At 0 vol% heptane the average pore size is 42 μm and the pore separation is much larger at 451 μm. As the heptane is increased to 2.5 vol% the pore fraction increases to 23% but the structure is still comprised of closed pores (Figure 7.3a). The pore size increases to 66 μm and the pore separation is greatly reduced to 220 μm. When the heptane content is increased to 5 vol%, a dramatic change in the microstructure to an open porous foam is seen (Figure 7.3b). The pore fraction has increased greatly to 80% and is almost entirely continuous. The average pore intercept, which is more accurately interpreted as a mean

free path through the pore phase, is 632 μm, while the average solid intercept length, which is more accurately interpreted and the strut thickness, is 161 μm. This discontinuous change in the morphology is due to the heptane at this amount being able to expand and coarsen to create the classic polyhedral wet foam structure [51]. As the gas bubbles expand, they begin to impinge on each other forming liquid film faces surrounded by ceramic slurry in the bubble edges, creating the foam struts. As the foam dries, the liquid films burst leaving a connection or gate between the pores. These are necessary for a bioreactor core because the gates will facilitate the flow of culture medium through the structure. This open foam structure contains smaller, isolated bubbles in the struts. There is therefore a need for additional microstructural parameters that separate the continuous porosity from the remaining isolated porosity within the solid struts of the foam as described in section 6.1.2. The newly defined λpLP, seen in Figure 7.2, is a more accurate mean free path through the continuous pore phase since it does not include intercepts from the isolated pores within the struts. For 5 vol% heptane this value is 852 μm. The difference between λpLP and λp is indicative of the amount of close porosity in the struts. It is important to remember that although the pore sections are isolated in 2 dimensions it is not possible to confirm that all of these pores are actually isolated from the continuous pore phase in 3 dimensions. Therefore, this interpretation represents an approximation. When the heptane is further increased to 10 vol% the pore fraction increases to 93%, almost entirely comprised of continuous porosity. The difference between λpLP and λp is also increased with values of 1.6 mm and 1.2 mm respectively. This is due to the fact that the average solid intercept length remains relatively constant between 2.5 and 10 vol% heptane. This suggests that the foam evolves due to the coarsening of large bubbles which would increase the mean free path as the number density of bubbles is increased (heptane content). Finally, when the heptane content is

increased to 20 vol%, another structure is observed. The foam collapses significantly during drying due to the large amount of bubble coarsening as seen by the through thickness section shown in Figure 7.4. Here the large elongated pores and large ceramic feature result from the coarsening and collapse of the structure. Also note that region 3 in the 20 vol% sample is large due to substantial drainage in the wet foam that accompanies collapse. There is a slight decrease in pore fraction to 60% however, λp decreases greatly to 658 μm due to a larger fraction of isolated porosity in the collapsed ceramic phase. If these isolated pores are removed from the analysis, as described above, the mean free path is 1.9 mm illustrating further coarsening in the collapsed structure. Figure 7.3c shows the cross-section of region 2. It is clear that the structure is mainly comprised of pore phase with large ceramic feature containing many small isolated pores.

From these results it is clear that foams produced with 5 to 10 vol% heptane are most suitable for cell culturing applications. The open pore structure produced in this range of heptane contents will facilitate cell seeding and the subsequent fluid flow through the connected pore network. The open pore structure seen with 10 vol% has the most desirable structure for cell culturing and will be used going forward.

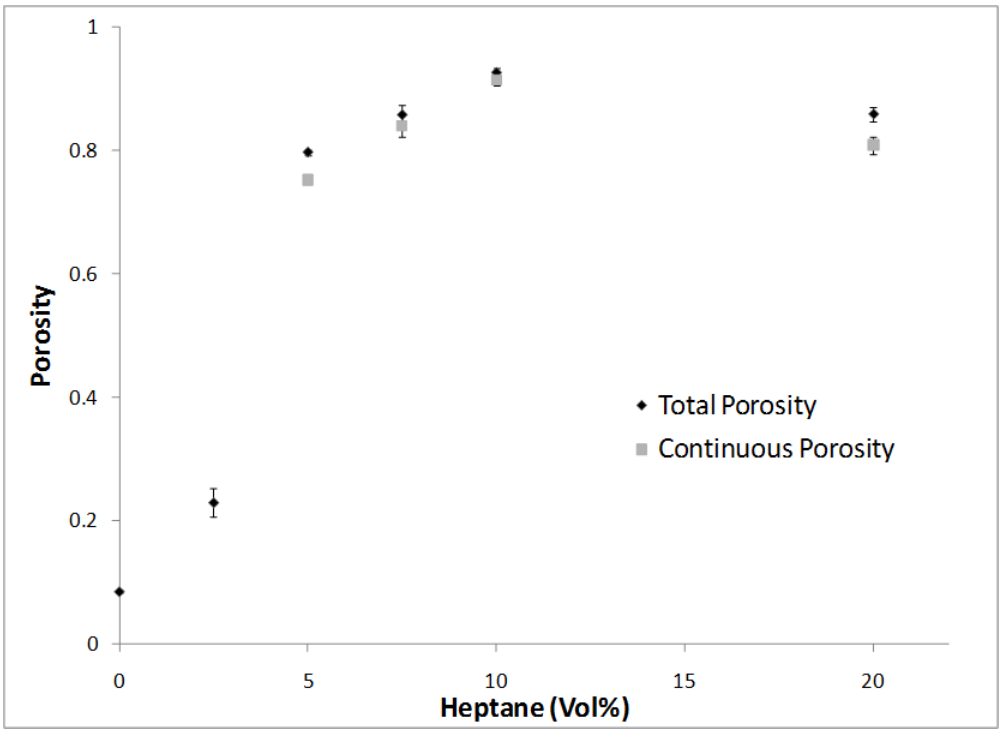

Figure 7.1. Effect of heptane content on the pore volume fraction of the sintered foam both for total porosity and the open continuous porosity.

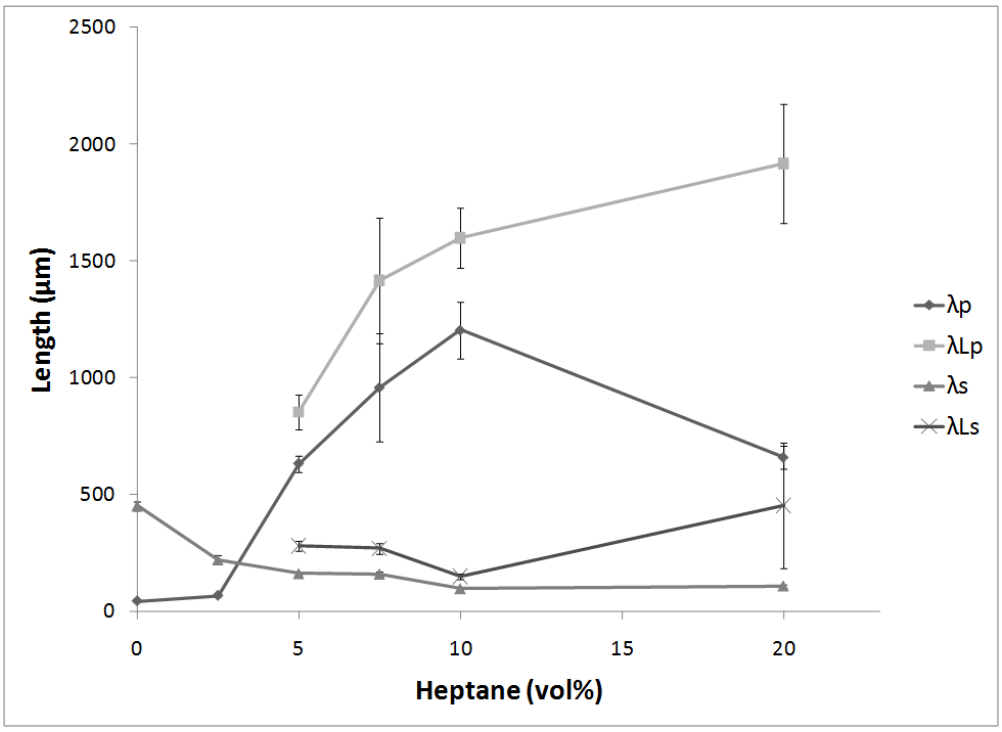

Figure 7.2. Effect of heptane content on the average intercept lengths for: the total pore phase λp, the continuous pore phase λLp, the total solid phase λs and λLs which is the solid phase with the internal small pores removed.

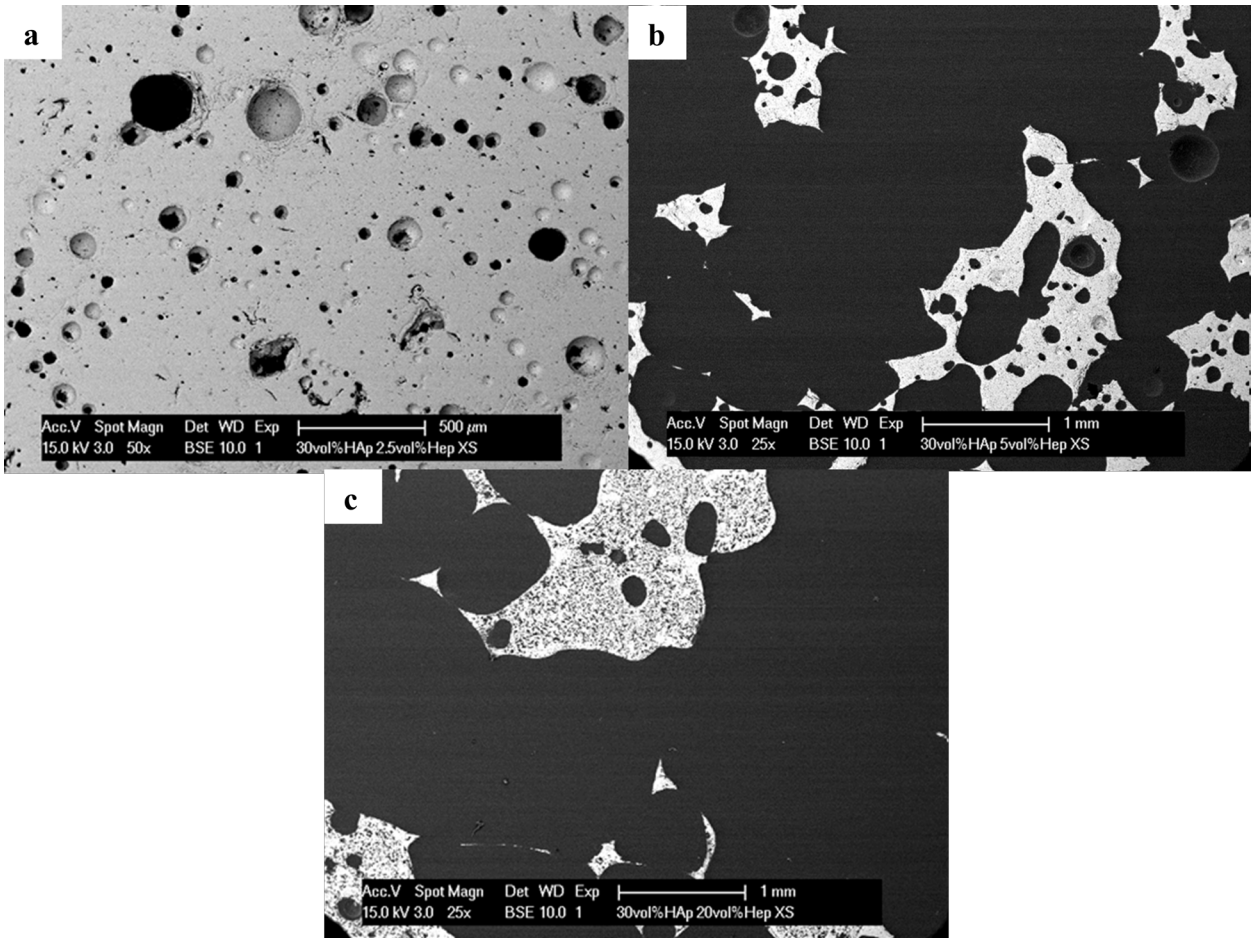

Figure 7.3. SEM micrograph of a polished section of a sintered ceramic processed with: (a) 2.5 vol% heptane (50x), (b) 5 vol% heptane (25x) and (c) 20 vol% heptane(25x).

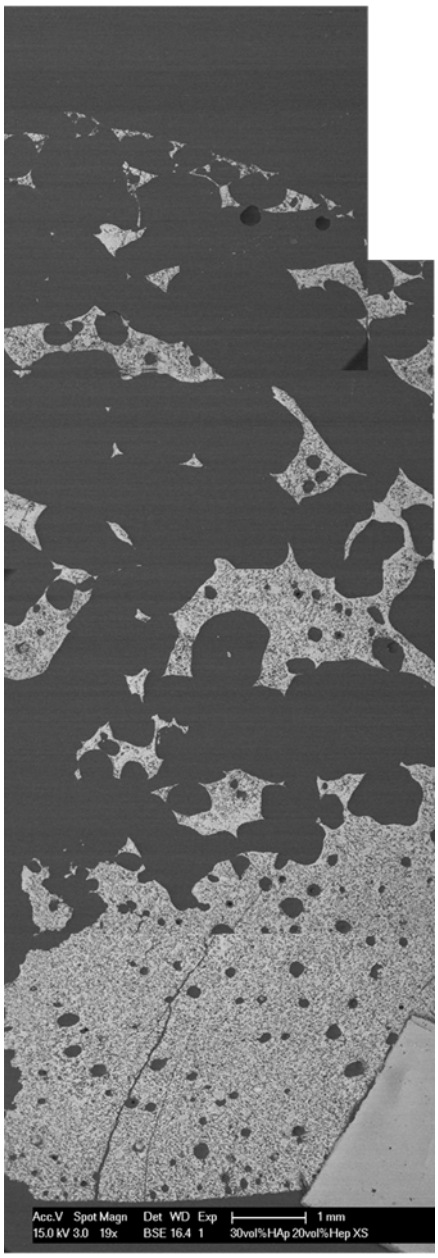

Figure 7.4. SEM image of a polished vertical cross section of foam made with 20 vol% heptane.

7.1.3 HAPES Foam Processing: Effect of Alkane Vapor Pressure on Pore Morphology

In order to closely examine the effects of alkane vapor pressure of the development of pore structure, a HAPES foaming technique was utilized [60]. Expansion in these foams are much

lower than the previous technique because the use of a different surfactant, lower vapor pressures of octane, nonane, and decane, and the higher volume fraction of alkane decreases the mobility of the alkane droplets in the emulsions, leading to less coarsening during drying. First, the density of each of the four samples was measured using Archimedes principle. Bulk density measurements show that there was no significant expansion in the foaming process (Figure 7.5). The density was around 45% in each condition, similar to the 50 vol% alkane that was added to the emulsion. This finding was not expected, as more volatile alkanes should produce expansion due to their higher rate of evaporation. In contrast, the lower vapor pressure alkane emulsions show no evidence of evaporation. Further analysis of this data found that the percentage of interconnected porosity reached almost 100% of the bulk porosity, proving coalescence of the bubbles during drying in all cases despite the absence of observed expansion. With all density measurements being the same regardless of vapor pressure, the microstructure must be examined to see differences in the structure.

Looking at the fracture surface of the samples prepared with decane (the lowest vapor pressure of alkanes examined, 0.195 kPa compared to heptane which has a vapor pressure of 5.33kPa) at low magnification, some large pores exist, most likely caused by air incorporation during mixing of the emulsion (Figure 7.6a). If the structure is examined at higher magnification, an intricate pore structure is seen (Figure 7.6b). These pores are quite small, on the range of 5 μm, and exhibit the morphology seen in open porous foams. This is expected due to the low volatility of the alkane reducing the driving force coarsening of the droplets during drying.

As the vapor pressure of the alkane is increased the pore size is also greatly increased. In foams created with heptane, the porosity can be seen at low magnifications (Figure 7.6c). These

pores are much larger than those created with decane and are on the order of 200 µm. When this structure is examined at higher magnifications, the intricate pore structure seen in the foams prepared with decane are not seen. Instead, the droplets fully coarsened and created large connections between pores (Figure 7.6d). While this structure is not suitable for a bioreactor core, it does demonstrate the effect of vapor pressure on foam development. Higher vapor pressures lead to more coarsening of alkane droplets during evaporation, which in turn leads to the coarse pore structure in the foam. In contrast, alkanes like decane with low vapor pressures will produce a structure with micro-porosity, which can be useful in other applications but are not large enough for seeding and perfusion of the bioreactor core. This study exemplifies an alternate method to control porosity.

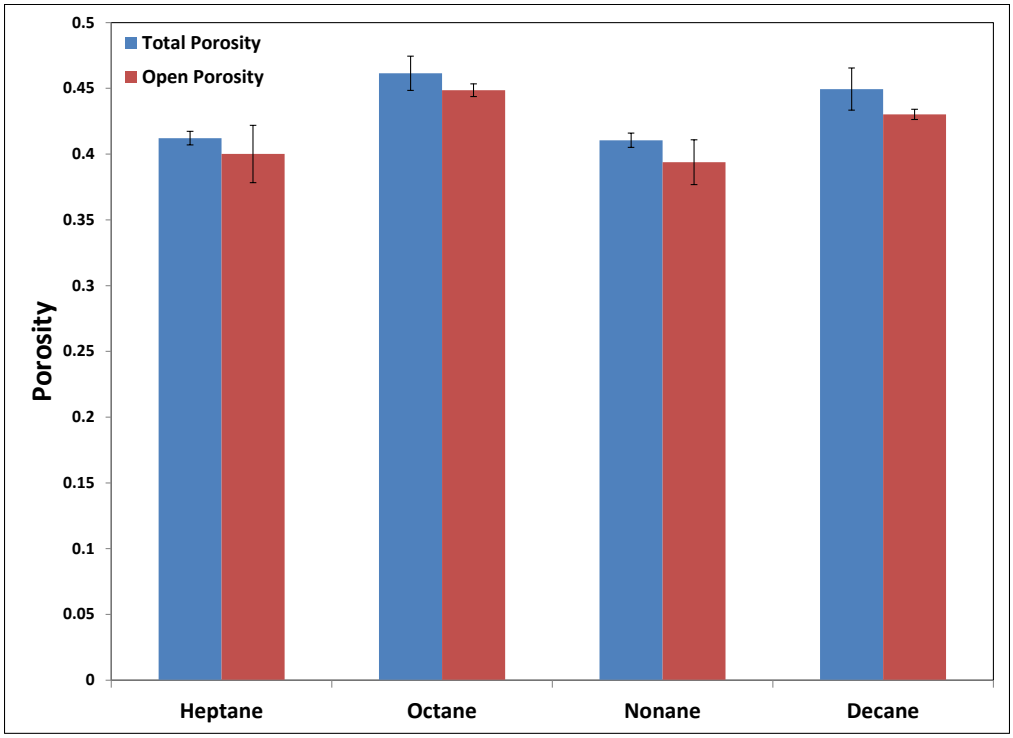

Figure 7.5. A graph representing the ratio of total and open porosity in the samples as a function of alkane used.

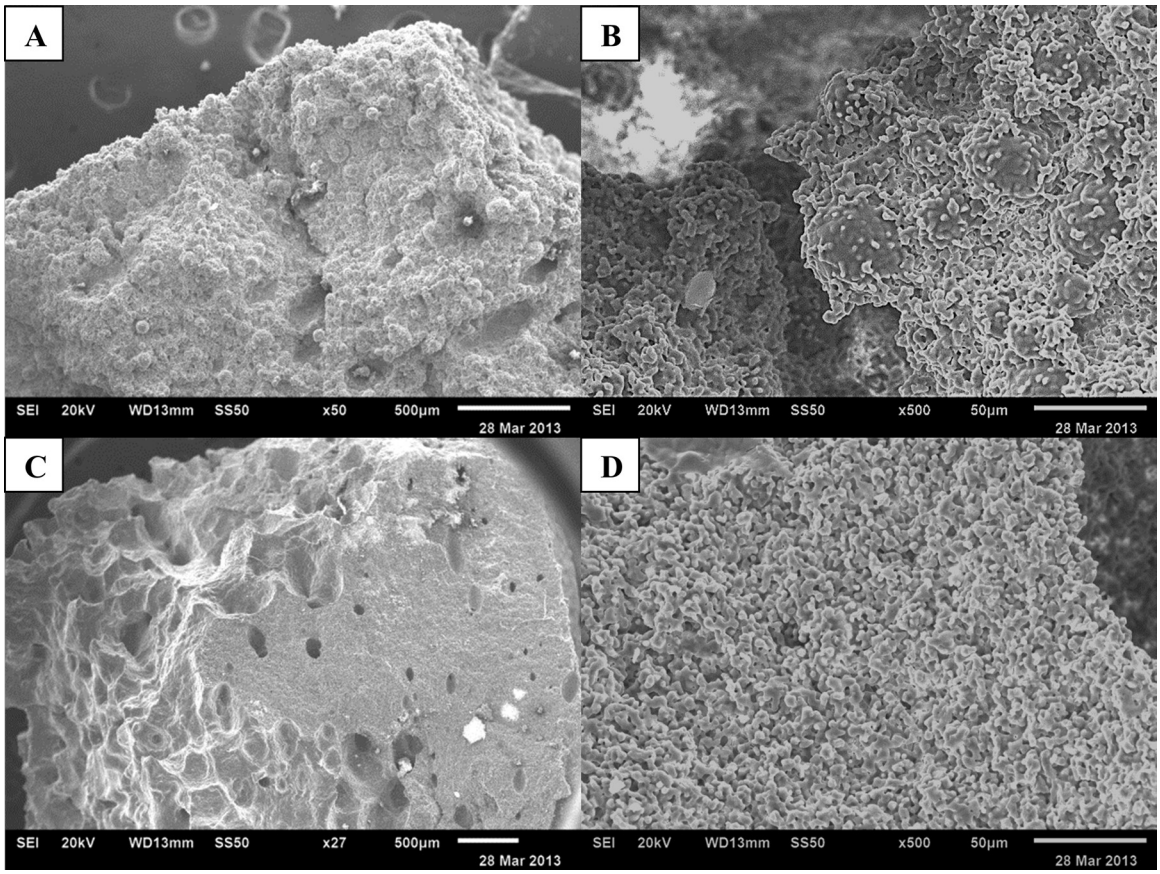

Figure 7.6. Fracture surface micrographs of HAPES foams created with Decane A) 50X where the only pores seen are caused by air incorporation and B) 500X where the fine pore structure can be seen, and Heptane C) 50X where the large pores are formed by heptane droplet coalescence and D) 500X where the pore structure seen in (B) is absent.

7.2 HUMAN ADULT LIVER CELL CULTURING

The original intended cell source for this study was human fetal liver cells. After five biological repeats, successful preliminary results were unable to be repeated as few cells survived in culture, regardless of culturing conditions used. Human adult liver cells were used with much higher success, and the results are presented below. Human fetal liver cells remain an attractive

option for future experiments. These cells have the ability to divide and expand at far greater rates than adult liver cells and have been shown to differentiate to mature liver cell types in perfusion bioreactors [4].

7.2.1 Genomic DNA Data and Culturing Observations

Seven organ donors were used in this study whose cells yielded viability (the amount of live cells compared to the total amount of cells) between 65-83%. This wide range was low due to the nature of these cells, having been obtained from discarded transplant grafts that had been rejected due to various reasons including: cirrhosis (hepatocyte death), steatosis (fatty liver), fibrosis (fibrous tissue), and excessive time passage between extraction and delivery to hospital (which causes cell death). Six material conditions for cell culturing were examined: hyaluronic acid hydrogel (HyA), collagen 1 hydrogel (C1), and no hydrogel (NG) all with both HAp scaffold and no HAp as a negative control. The cell number was calculated by measuring the total amount of DNA in each sample and comparing this number to the DNA from a known amount of cells. To address this variability between donors, cell number results were normalized to the day 15 C1 condition, the optimum culture condition found in the literature [74]. The numbers presented below are a ratio of the cell number to the 15 day time point of the C1 gel sample. A vast drop in overall cell number was seen between day 5 and day 15 in culture, which was expected as cells begin to attach and proliferate in each specific construct (Figure 7.7). Not all cells attach to the scaffold and are removed during medium changes, leading to the observed decrease in cell number after five days. This is most likely caused by cell injury during the time between extraction from the tissue sample and delivery to the lab (as much as 24 hours at a temperature below 4°C) and during the pipetting of cells during plating [14]. After the initial

drop off, most cultures continued to lose cells due to cell death over the 28 day period with the exception of the C1/HAp composites and, to a lesser extent, the C1 hydrogel. Of the six culturing conditions examined, the maintenance of cells in culture was clearly best in these two conditions, with the C1/HAp composite having almost two times as many cells after 28 days than any other condition ($p<0.05$). C1 hydrogels are a common culturing model for liver cells because of its abundance in natural tissue. This ECM provides an environment similar to native liver tissue and might be expected to be the best hydrogel for supporting the culture of adult liver cells. It is more surprising that the HAp scaffold contributed to the best result.

When cells suspended in a hydrogel are plated, the cell embedded gel forms a 1 mm thick layer that conforms to the shape of the polystyrene well. The HyA gels used in this study were robust and kept their structural integrity, or original shape and rigidity, throughout the experiment. In contrast, the C1 gels begin to degrade over time. If a HAp scaffold is not present, the gel would detach from the surface of the well after 15 days, completely losing structural integrity. This would be detrimental to tissue formation, as the goal of the project is to create a scaffold in the shape of the desired tissue. If the hydrogel collapses, the tissue will not form in the intended shape. When porous HAp is present, the composite structure kept it shape during the entirety of the culture, allowing the cells to expand in 3D. While the gel degraded, it remained attached to the ceramic so the cells remained in the pore space of the foam. It is thought that the surface of the HAp scaffold provides ample area for collagen fibers in the gel to attach. In the absence of a hydrogel, cells attached to the polystyrene surface regardless of HAp usage. As in the condition without a scaffold, the cell number continues to drop off in C1 sandwich cultures after 15 days. The composite structure provides cell maintenance during the last two weeks of culture which is an improvement both over the negative control and also the

C1 sandwich cultures [74]. Cells cultured on a HAp scaffold without gel exhibited cell attachment to the ceramic surface in addition to the cells attached to the plate.

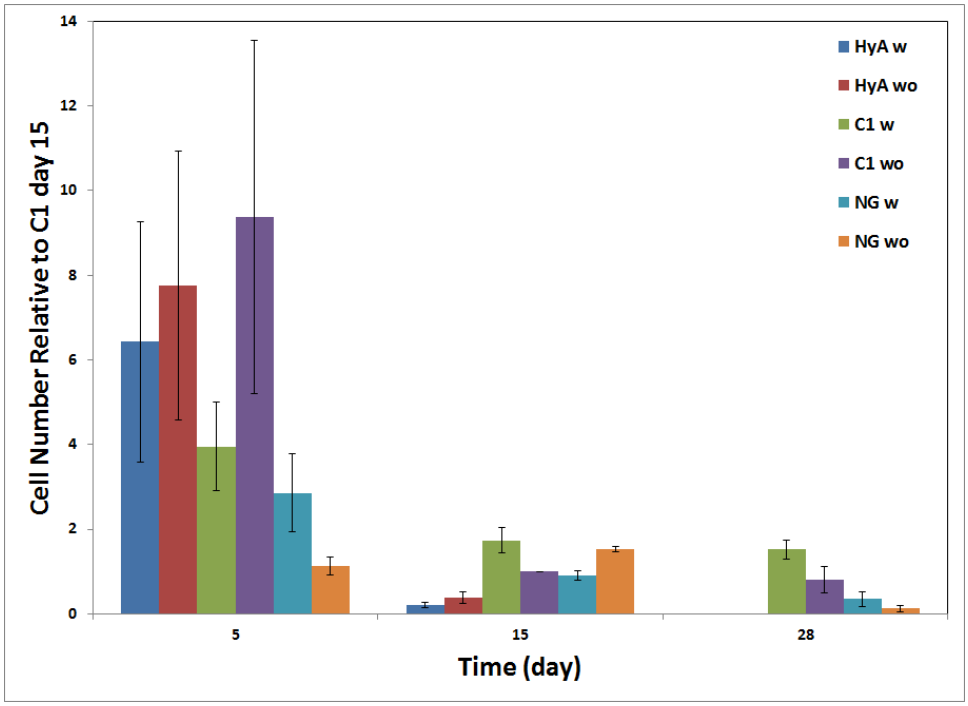

Figure 7.7. Normalized cell numbers as determined by genomic DNA.

7.2.2 ELISA

Albumin ELISA has been performed for all seven donors. This test measures the amount of albumin in the medium samples produced from hepatocytes in culture. Albumin secretion is indicative of mature hepatocyte function. The main conditions of interest are those of the hydrogel/ceramic composites and the negative controls, as this cell culturing method will be necessary to keep the cells in 3D culture, rather than in a flat layer on the surface of a petri dish. As discussed above, this will be necessary to create viable tissue for transplantation or in-vitro models [2-4,14,67]. When examining the albumin secretion, cells cultured in C1 hydrogels exhibit much higher activity over 28 days. Figure 7.8a presents the normalized, cumulative

albumin secretion for C1 hydrogel cultures with and without a HAp scaffold. This data was normalized to the total secretion after 28 days in the C1/HAp composite for each repeat to address variability between donors, with day 28 in this condition set to 100 so the secretion can be represented as the percentage of the total of this condition. Without a scaffold, hepatocytes from HAL cells cultured in C1 gel had an increase in albumin secretion over 18 days. After this point, there is no significant increase in albumin secretion through the remainder of the experiment ($p>0.05$), with values no more than 80% of the C1/HAp condition. When the cells are cultured in the C1/HAp composite, this drop of in production is not observed. When the secretion from the C1 gel cultures level off, the amount of albumin produced is significantly higher in the composite than the previous point through 28 days ($p<0.01$), over a 30% increase between day 18 and day 28. The comparatively small error bars, representing a 95% confidence interval, proves that the trend in this condition is significantly similar between repeats. In contrast, without a HAp scaffold, the error bars are much larger, representing great variability between donors. This variability was also seen in the four other culturing conditions used. The total albumin secretion of HyA gel cultures was never more than 30% of the C1/HAp composite cultures and was statistically similar with and without HAp. When looking at all three conditions that involve HAp, the C1 composite is clearly the best for repeatable, continued production of albumin over long time periods. This result is ideal because the continued secretion shows mature hepatic function [4]. This also proves that the cells in culture maintained their mature hepatocyte lineage over the course of the experiment rather than reverting to a less mature lineage. When the mean albumin values for each time point of the C1/HAp composite culture are compared to C1 sandwich cultures in the literature that use similar cells [74], it is found that the scaffold produced in this study maintains albumin secretion better over 28 days, as

the sandwich cultures cease production between day 14 and day 21 due to cell death over that time period (Figure 7.8c). This increased albumin secretion as well as the repeatability between donors can be attributed to several factors. First, by culturing in three dimensions, instead of the monolayer model used in the sandwich cultures, hepatocytes can spontaneously form into structures similar to those seen in native tissue because natural liver tissue is not a two dimensional layer of cells [2,4,14,67]. Next, the composite structure not only provides a protective environment for the cells in culture; it also provides Ca^{+2} ions that are liberated from the ceramic over time, which can be beneficial in hepatocyte proliferation and function [80,81]. Finally, the presence of non-hepatocyte cell types can be beneficial to the growth and maintenance of hepatocytes in culture as Yarmush et al. saw when hepatocytes were co-cultured with mesenchymal stem cells in an alginate gel, or when fibroblasts were used in co-culture [3,89].

Two additional controls were examined to see if there were any material effects on these albumin productions. First, all six material conditions were prepared without cells and blank WE complete medium was exchanged during the first 15 days of the experiment. Afterwards, albumin was not detected in any of the cases. This experiment was then repeated with 10 μg/mL human albumin added to the medium in order to test if the gels were absorbing albumin during culture. Subsequently, it was found that without the presence of hydrogel, the levels of albumin during the 15 day experiment were either the same or slightly higher than those of the original medium, most likely due to evaporation of water in the medium during culture rather than absorption to the polystyrene surface. When a hydrogel, either HyA or C1, is present, albumin readings were anywhere from 10-30% lower than those found in the original medium regardless of the ceramic being included. Complete medium extraction can be impaired by medium being

trapped in the small pores in the hydrogel and ceramic. These results should be accounted for when comparing the albumin readings of different conditions with one another. As seen in Figure 7.8, the no gel, no HAp condition has similar albumin production to the C1/HAp composite, albeit with much higher variability. With these results, it can be inferred that the secretion in the no gel, no HAp condition is actually lower than the secretion in the C1/HAp composite due to difficulty in extracting the entirety of the medium from the composite.

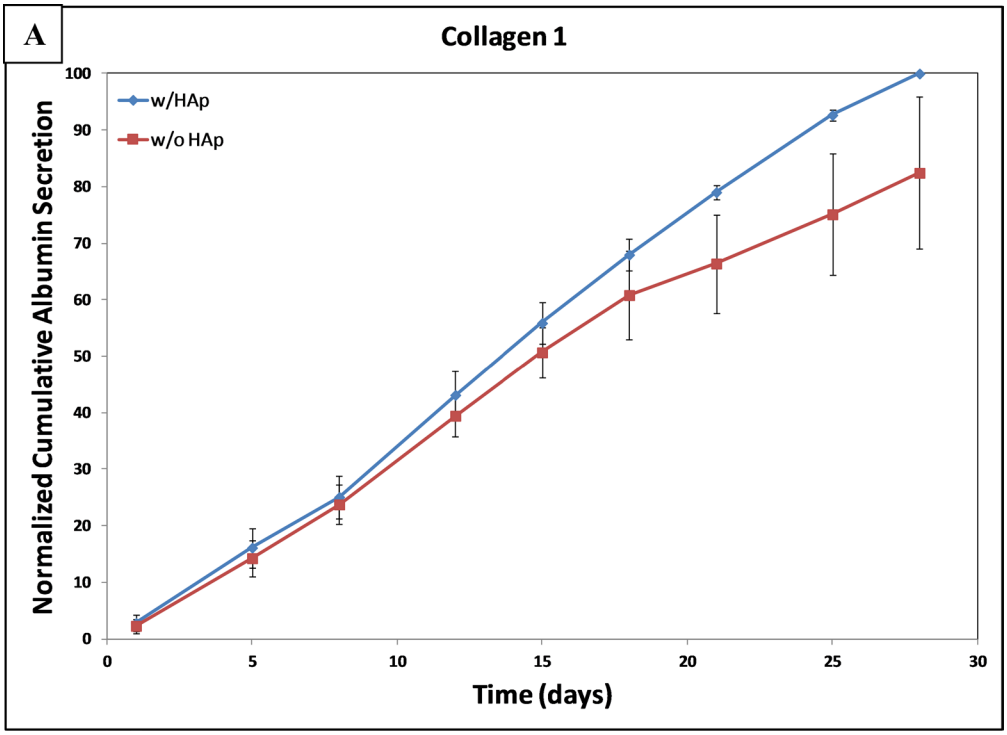

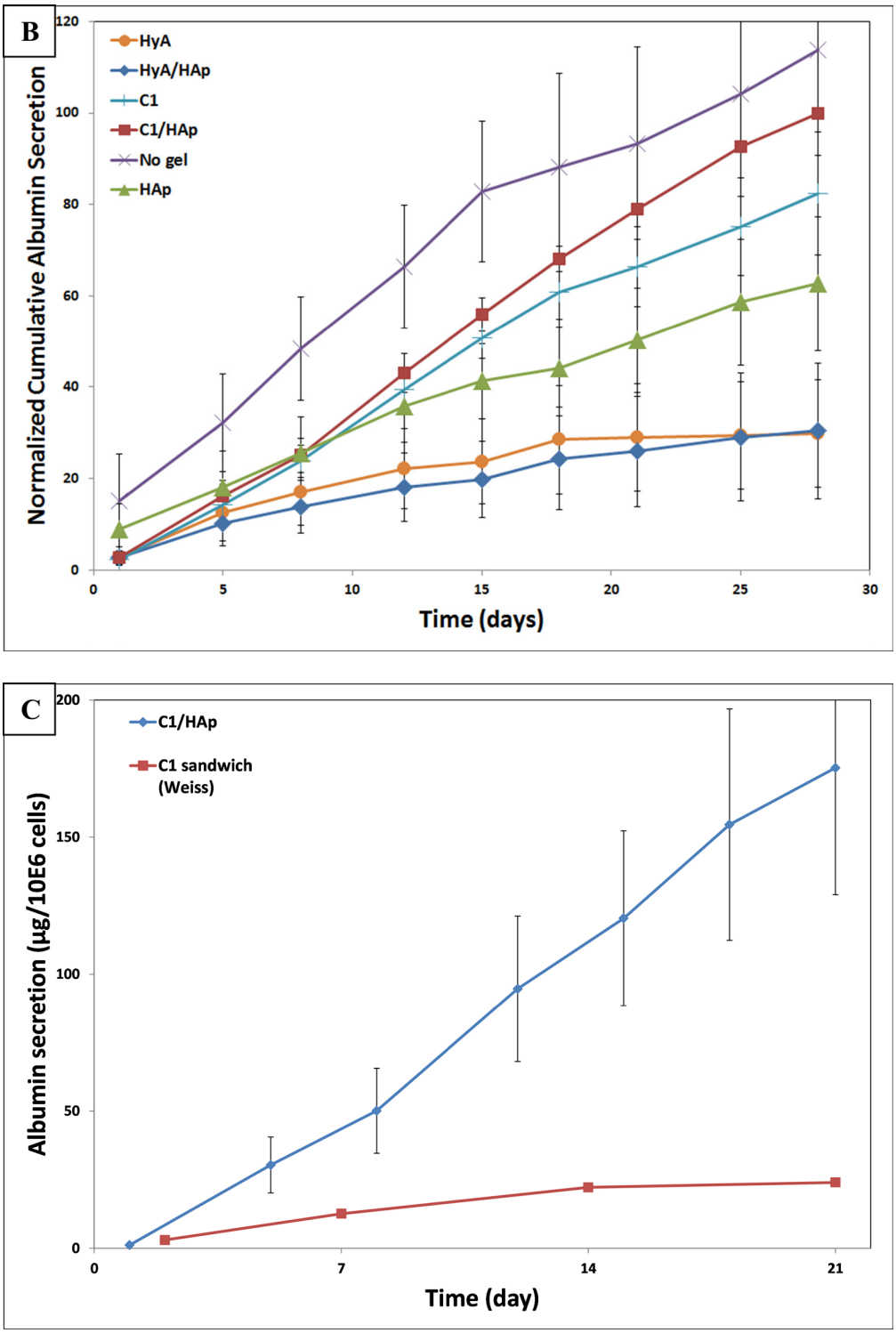

Figure 7.8. Graphs of Cumulative Albumin secretion for a) comparing C1 hydrogel cultures to C1/HAp composites, b) a comparison of all six material conditions, and c) a comparison of the secretion data from C1/HAp cultures and C1 sandwich cultures from Weiss et al. [**74**].

7.2.3 RT-PCR

Real-time PCR was used for gene expression in all samples. This measurement gives insight to the relative amounts of cell types present in each culture. Six genes were examined: vWF, CK19, CYP450-3A4, albumin, ASMA, and KI67 and are discussed below. There were few significant results found in this study due to several factors. First, most of the cell types that were tested for were only present in small amounts in the original cell fraction including vascular endothelial cells, bile epithelial cells, hepatoblasts, and stellate cells. These cells are present in small amounts compared to hepatocytes, not only because they appear in comparatively smaller amounts in the tissue, but also because the method of cell isolation used by the provider of the cells focuses on isolating a cell fraction that is mostly comprised of hepatocytes. In addition, the large variability in cell viability between donors had a greater effect on the non-hepatocyte cell types and CYP450 genes, the detoxification enzymes which indicate hepatocyte functionality.

Several genes exhibited significant differences between the culturing conditions as shown below in Figure 7.9, the first of which is the vWF expression in conditions without a hydrogel. Because it is only present in mature endothelial cells, vWF was chosen as the gene of interest for these cells. When the data is normalized to the negative control in order to account for variability between repeats, it is seen that vWF expression is as much as 12 times higher in cells cultured on HAp compared to cells cultured without scaffold after 28 days ($p<0.05$). This is also observed when vWF expression is compared with cells that are cultured in either of the hydrogels. This shows that the surface of the HAp scaffold is the best condition examined to expand endothelial cells and serves as a proof of concept for using HAp to promote the formation of vascular-like channels in a scaffold construct. As discussed in section 2.6, Ca^{+2} ion channels play an important role in endothelial cell growth and subsequent vascularization. The

resorption/dissolution of the material should create a microenvironment near the surface of the HAp should be rich in these ions. Also described in section 2.5, calcium ions contribute to the maintenance of endothelial cells and also the formation of vascular tissue by passing through channels on the surface of these cells to initiate these events. The rough 3D surface provided by the scaffold also creates an ideal environment for ECs to attach and proliferate. In positive-negative cast scaffolds, the vascular-like channels formed are expected to be devoid of gel, and endothelial cells could be injected here and will ideally attach to the HAp surface.

CK19, the second gene of interest, is present in both bile epithelial cells and hepatoblasts and only those two cells types in the liver. This gene is expressed in high amounts in all culturing conditions, as seen in Figure 7.9b, where the y-axis is normalized to the original total cell fraction. At 28 days, CK19 expression is over 100 times greater than for original cells in all six conditions, which is indicative of either bile duct formation or a large expansion of hepatoblasts. This is surprising because this is a result that is generally seen in perfused bioreactor experiments, not as much in static cultures [14]. Specifically, HyA gels support this expression, which is of interest because of a marker on the surface of hepatoblasts, the progenitor cell for hepatocytes, is specific for hyaluronan, leading to preferential attachment to these gels and suppressing differentiation into mature hepatocytes [4]. This finding has not yet been confirmed by microscopy. Secondly, CK19 is highly expressed in C1/HAp cultures, showing significantly higher expression than the negative control after 15 and 28 days. This result is also important as a proof of concept for the positive-negative cast scaffolds. In this technique, the cells will be injected into the interior of the core with a hydrogel. Bile duct structures must form in culture to create functional tissue, as seen in the previous work of Gerlach [14]. This result

must be confirmed with immunohistochemistry, confocal microscopy using gene specific fluorescent dyes, to see if these structures are present.

The CYP450-3A4 gene, a detoxification enzyme found in functional mature hepatocytes which is responsible for metabolizing toxins, was also examined. Expression of this gene quickly fades in cell culture as seen in the literature, and is caused to reduced transcription of this gene in hepatocytes outside of the body (Figure 7.9c) [90]. It was found that the condition producing the highest expression of this gene was the HyA hydrogel cultures, both with and without HAp. This was result was wildly variable between donors, exhibiting no expression in some and large amounts in others and stayed much higher than the donor cells after 28 days, up to 40 times higher. This can be attributed to one sample having an abnormally large expression at 28 days. If this repeat is omitted, the average of the other 6 donors has only 0.5 times the expression of the original cell fraction. Cell culture in C1 gel had a more consistent expression between donors, with no significant difference of expression regardless of HAp presence. This expression was, on average, within error of the original cell fraction until day 15, after which expression was significantly lower. As expected, without an ECM hydrogel present, cultures expressed little to no CYP450-3A4 at each time point, since functional hepatocytes are not generally observed in these culturing conditions in the literature [4, 90].

Albumin was the next gene examined. This can be used as a marker for hepatocytes; however, the expression of this gene is complex and is down regulated by increased production of albumin from the cells [91]. As expected, albumin expression was highest in HyA gel cultures as they produced the least amount of albumin measured by ELISA. Overall, the expression was relatively constant in all conditions over the duration of the experiment and was

near the expression of the donor cells until day 28 when most conditions exhibited a drop in albumin expression, most likely caused by cell death.

α-smooth muscle actin (ASMA) is a gene found in stellate cells in the liver and can be used as an indicator for fibroblast growth if expression is high. This gene had low expression in all donor cells which lead to highly variable results. Cultures without a hydrogel were the only conditions to have ASMA expression in every donor. ASMA was not detected in six biological repeats in HyA gel cultures and four biological repeats of C1 gel cultures. The high expression seen in C1 cultures after 5 days (24.6 times the donor cells with HAp and 36.6 times the donor cells without) is from three of the seven donors. The relatively low expression of ASMA in most samples suggests that there was no overgrowth of fibroblasts in culture in most cases, a problematic event in which fibroblast cells expand and become the main cell type in culture. This result is supported by microscopy.

The final gene examined was KI67, a marker for cells in their proliferative state. This gene is present in cells of any cell type that is undergoing cell division and expansion. One result shown in Figure 7.9f is that expression of KI67 is low in HyA gel cultures, less than the expression in the donor cells. Expression was higher than the donor cells in both the C1 gel conditions and the no gel conditions, which is expected because of the higher cell numbers present in these cultures as compared to the HyA cultures. This expression was again highly variable between donors and offers little insight into the differences between culture conditions.

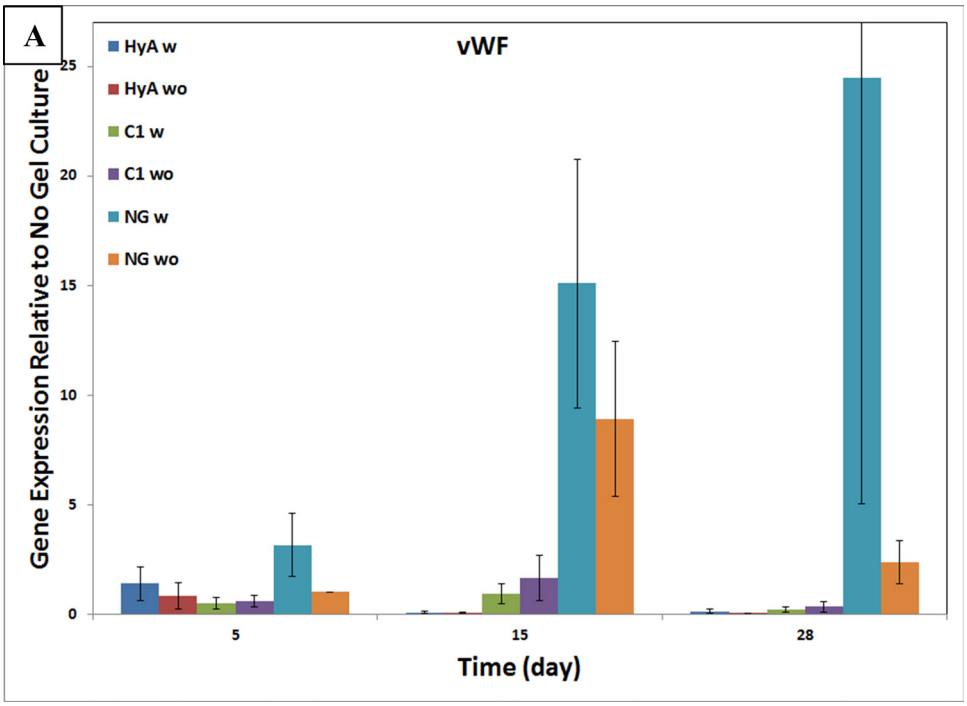
A
vWF
HyA w
HyA wo
C1 w
C1 wo
NG w
NG wo
Gene Expression Relative to No Gel Culture
25
20
15
10
5
0
5
15
28
Time (day)

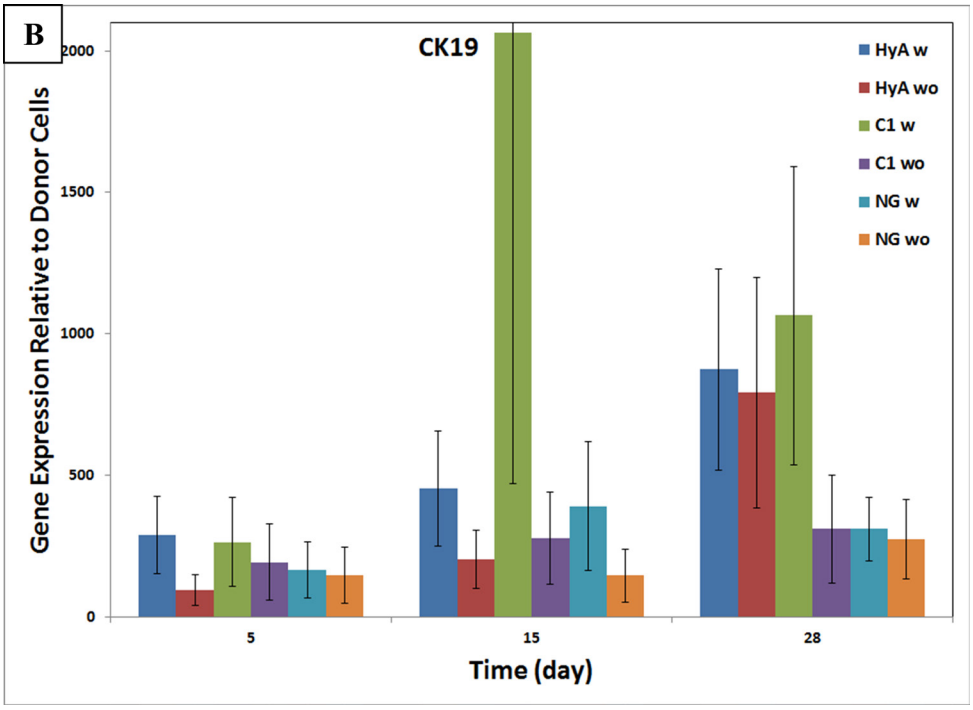
B
CK19
HyA w
HyA wo
C1 w
C1 wo
NG w
NG wo
Gene Expression Relative to Donor Cells
2000
1500
1000
500
0
5
15
28
Time (day)

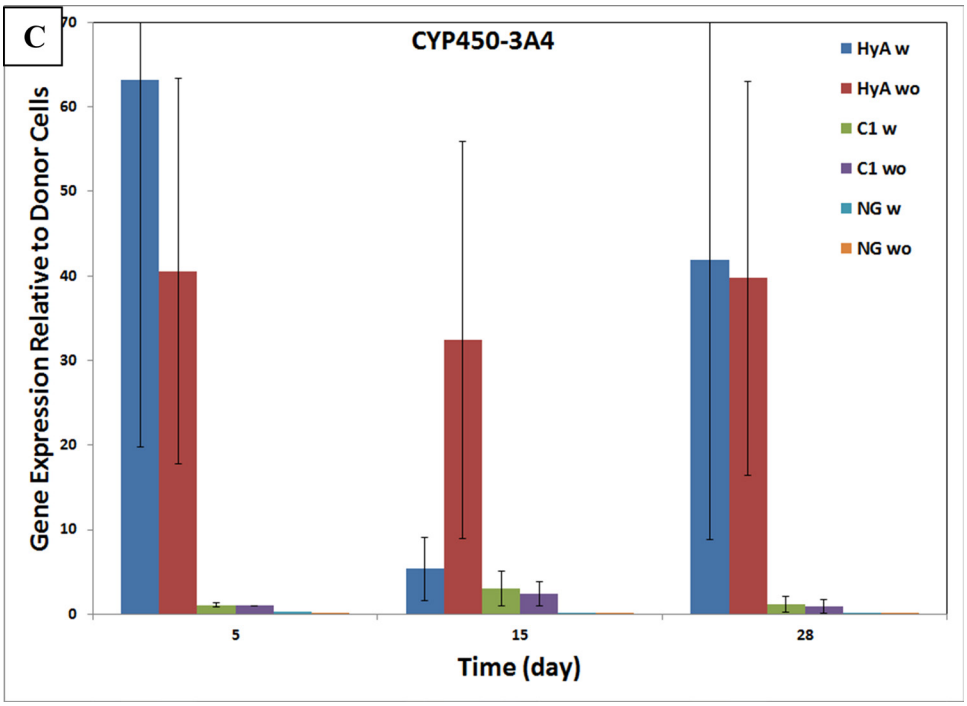
C
CYP450-3A4
Gene Expression Relative to Donor Cells
70
60
50
40
30
20
10
0
5
15
28
Time (day)
HyA w
HyA wo
C1 w
C1 wo
NG w
NG wo

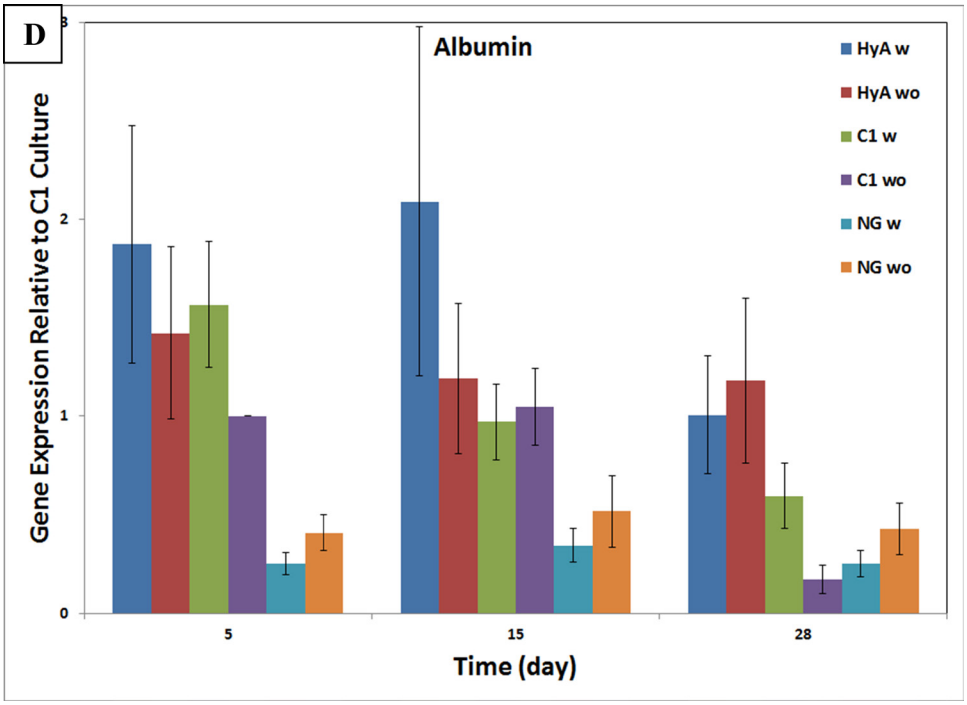
D
Albumin
Gene Expression Relative to C1 Culture
2
1
0
5
15
28
Time (day)
HyA w
HyA wo
C1 w
C1 wo
NG w
NG wo

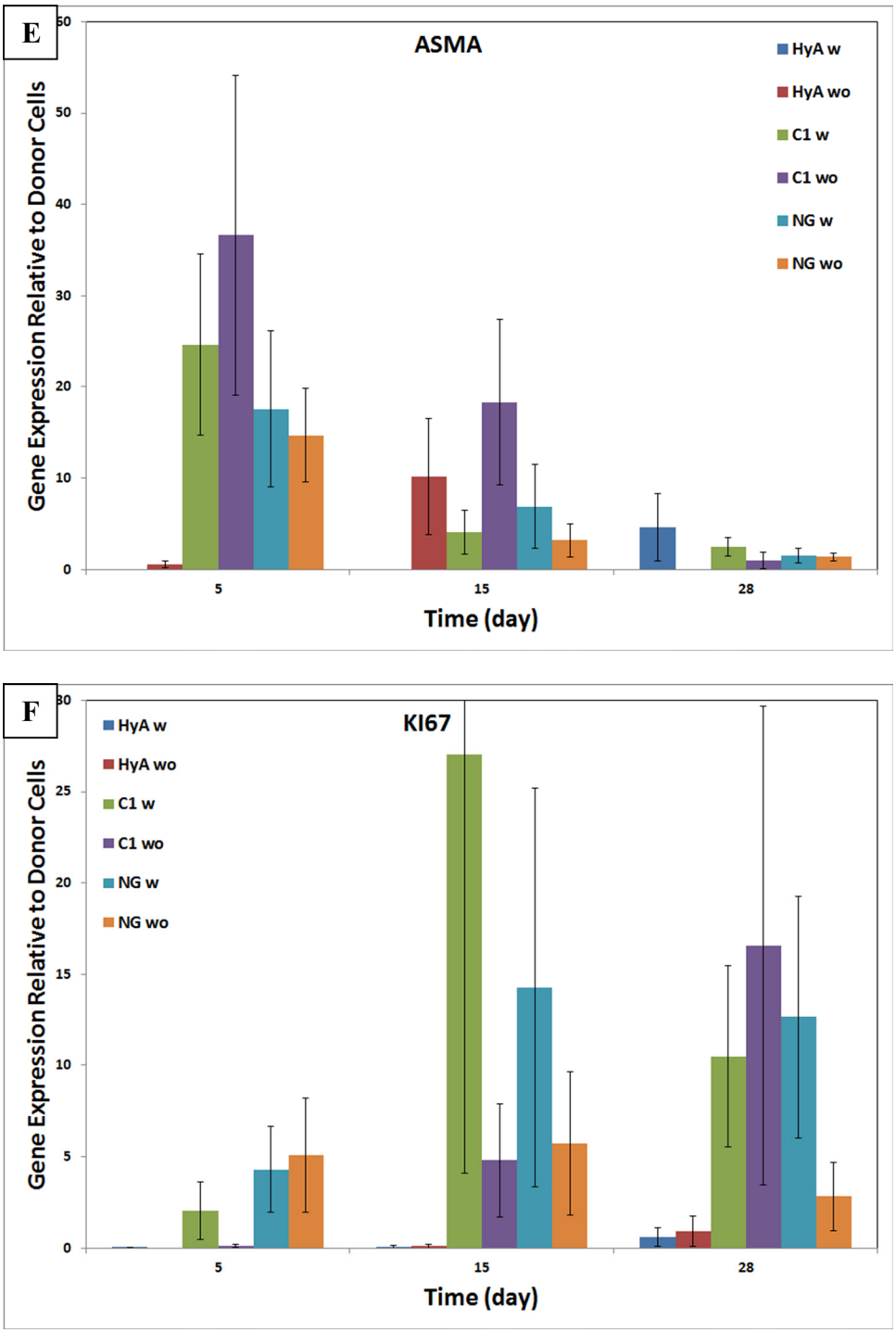

Figure 7.9. Gene expression data for a) vWF normalized to day 5 of the no gel, no HAp condition, b) CK19 normalized to the donor cells, c) CYP450-3A4 normalized to donor cells, d) albumin normalized to day 5 of the C1 gel condition, e) ASMA normalized to donor cells.

7.2.4 Immunohistochemistry

Confocal microscopy was used to examine the cultures. Fluorescent stained were used to attach to specific antibodies for genes of interest as described below. This will help explain the large expression of CK19 found in RT-PCR and provide a view of the cultures and how close the morphology of the cells mimic liver tissue. Microscopy samples were stained for CK19 to observe the morphology of cells that were positive for the gene (green, 488 nm). This was done to examine any evidence of bile duct formation in the cultures based on the PCR results. The samples were also explored for hepatocytes and liver plate formation with the phalloidin cytoskeleton stain (red, 568 nm), due to their distinct morphology. This stain attaches to the cytoskeleton of every cell to show the morphology of the cell. This allows for the micrographs to be compared to natural tissue and the morphology of cell types of interest. DAPI (4',6-diamidino-2-phenylindole) was used to stain the nucleus of each cell by binding to DNA (blue, 358 nm). HyA samples were not examined because the thickness of the gels created difficulty in resolving cells due to the small focal length of the aperture. This was not really of interest because DNA data indicated that there are not many cells present in these cultures.

As discussed in section 7.2.1, the C1 hydrogels began to degrade over time and lose their original shape in the absence of a HAp scaffold, as clearly seen in Figure 7.10a and b. This can be seen from the cells forming into strands due to the gel degrading and detaching from the well (marked with an arrow in Figure 7.10b) After 15 and 28 days in culture, hepatocytes are present in large numbers and exhibit the cube-like morphology seen of cells arranged in liver plates (Figure 2.9d). This is important as it indicates that the cells are forming into structures similar to natural tissue. There are also several cells in each of the conditions that are positive for CK19, represented in green. These cells appear regularly in between the hepatocytes; there is not,

however, enough evidence from the microscopy to identify biliary structures in these cultures. This does not mean that these cells are not bile epithelial cells, but only that these cells are not yet forming biliary structures.

Micrographs of samples cultured in a C1/HAp composite after 15 and 28 days look superficially similar to the negative control. However, there are several differences, the first being the presence of biliary-like structures. CK19 positive cells were seen to form a circular structure similar to a bile duct as seen in Figure 7.10c (marked with an arrow). While this occurrence was not common, no similar structures were found in the negative control. The effects of culturing in a gel are also evident. The cells seen in C1 hydrogels form in between the fibrils of the gel, as it exhibits collapse at this time point in culture. When a scaffold is present, the gel remains attached in the pores of the ceramic, providing 3D structure on which the cells can form tissue. This further exemplifies the benefits of this culturing method. This result is why HAL cells are maintained better in this condition over the negative control, and these structures seen in the microscopy are consistent with the high albumin secretion seen in ELISA data and the high expression of CK19.

Finally, expected results are observed in cells cultured on HAp without a hydrogel. From the micrograph shown in Figure 7.10e, there are no signs of hepatocytes or CK19 positive cells anywhere on the structure. These cells appear to be fibroblasts, from stellate cells, and/or endothelial cells due to their ‘stretched-out’ morphology, as the actin fibers of the cytoskeleton have elongated over the surface of the HAp. The presence of fibroblasts are confirmed by using an ASMA dye (488 nm, Figure 7.10f), where positively stained cells were seen to attach to HAp and have similar morphology to cells seen in Figure 7.10e. Cells that are not stained green could be endothelial cells because of high vWF gene expression in this sample. The lack of

hepatocytes highlights the importance of having a C1 hydrogel present in the pore space of the ceramic in order to support hepatic cell growth in 3D. As described in the objectives, it is intended that liver plates form in the pores of the ceramic as the ceramic resorbs, which includes bile ducts and fine vasculature.

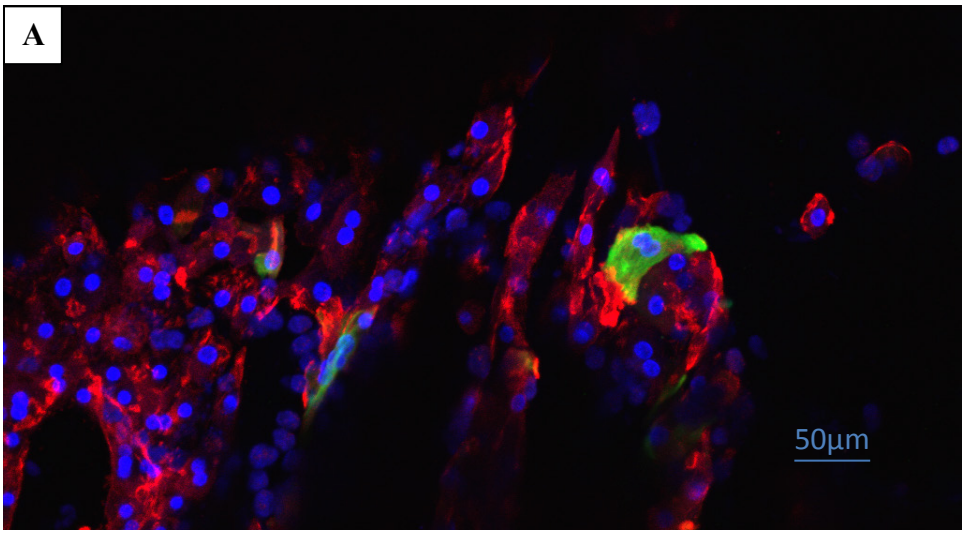

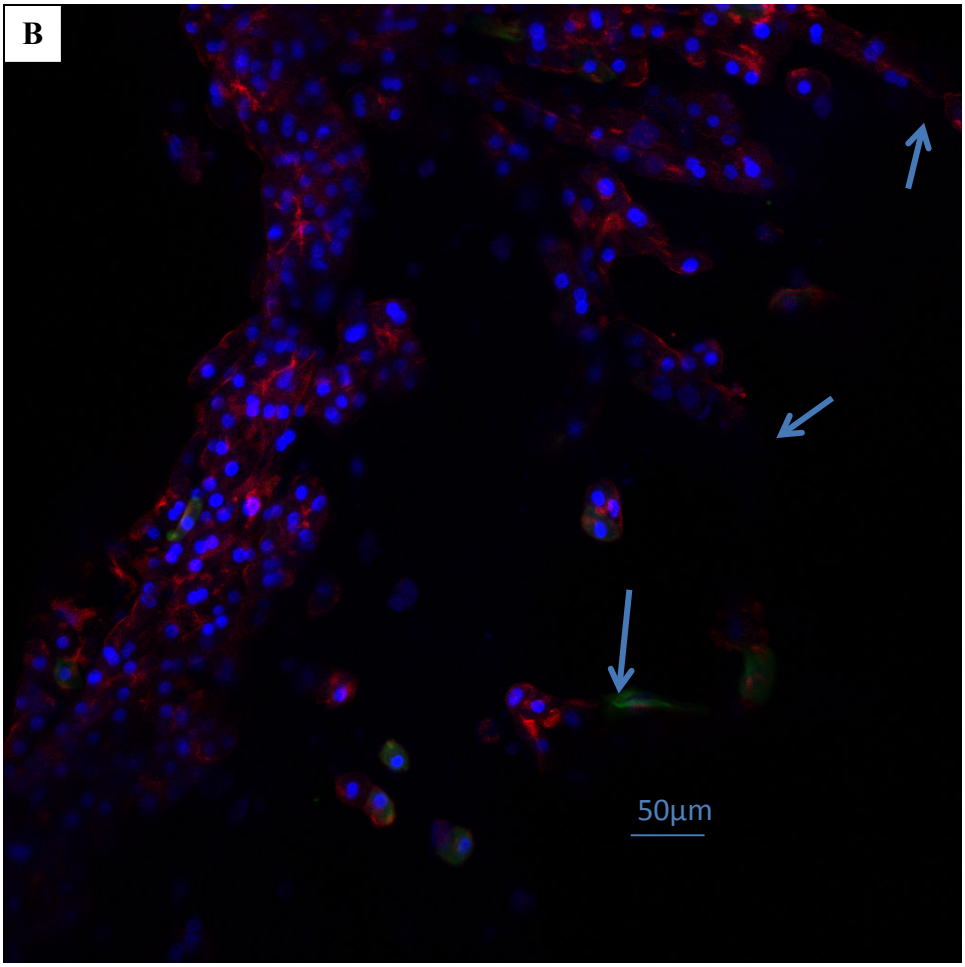
B
50µm

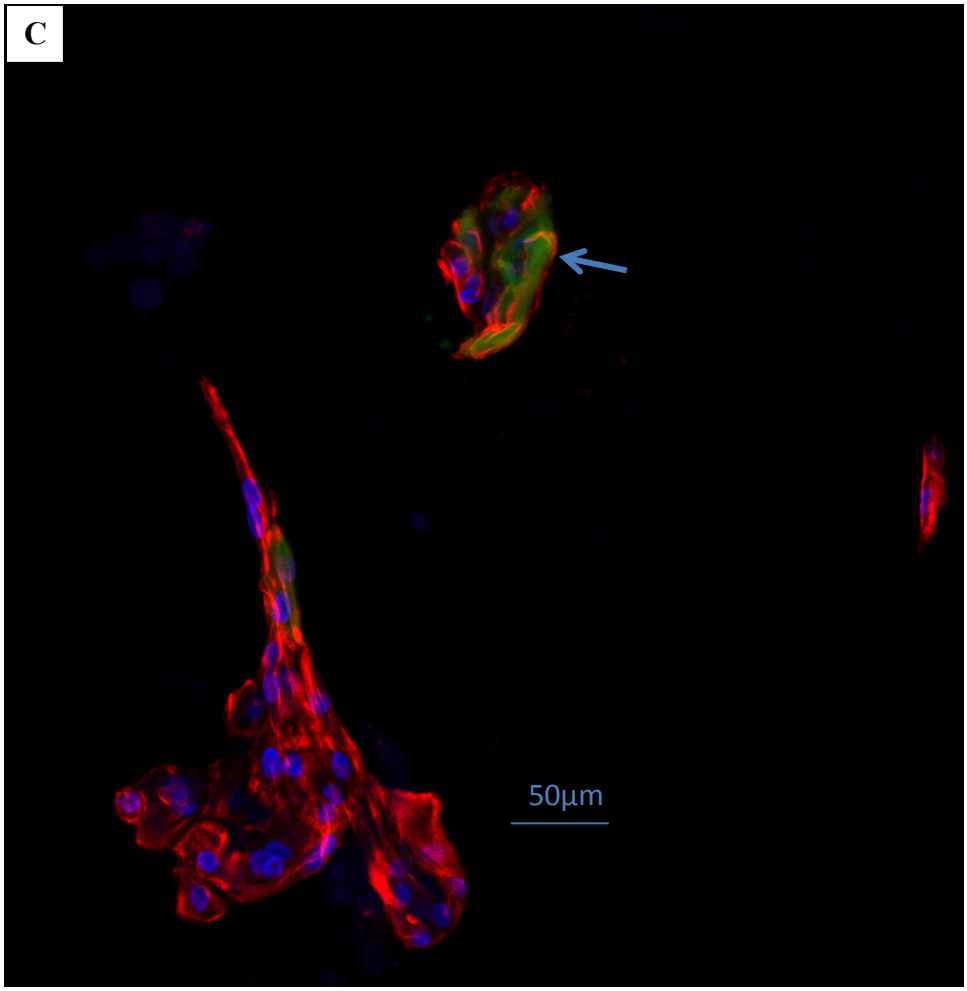
C
50µm

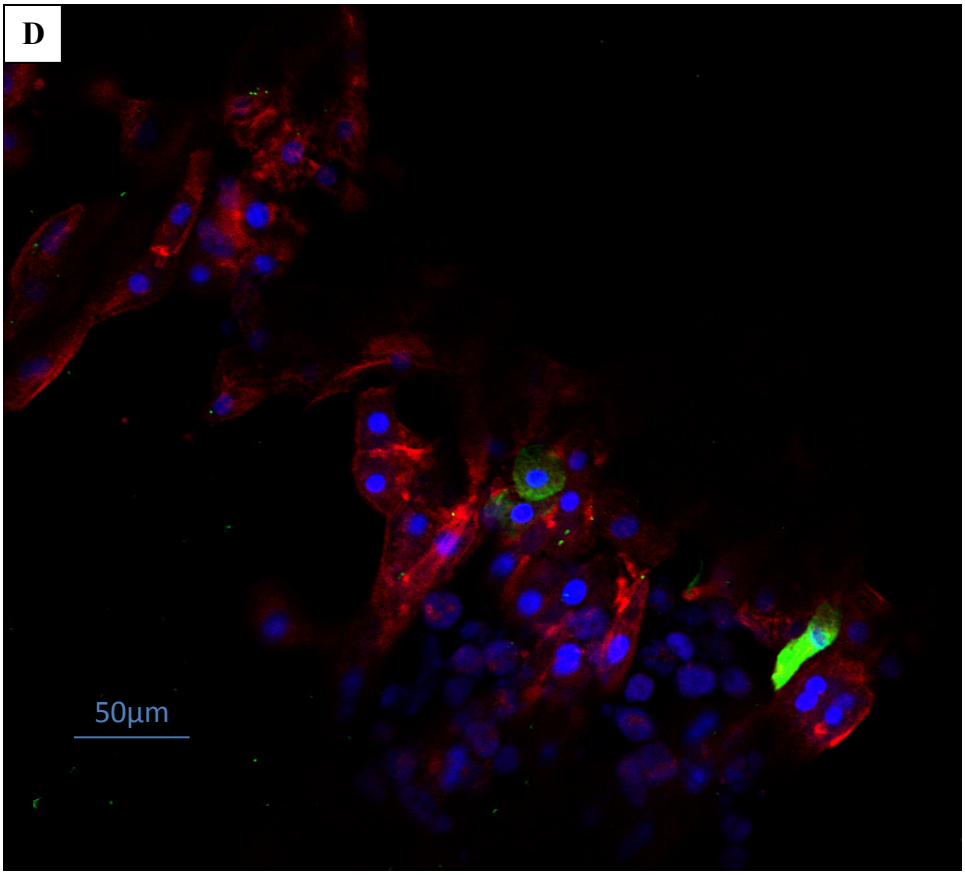
D
50µm

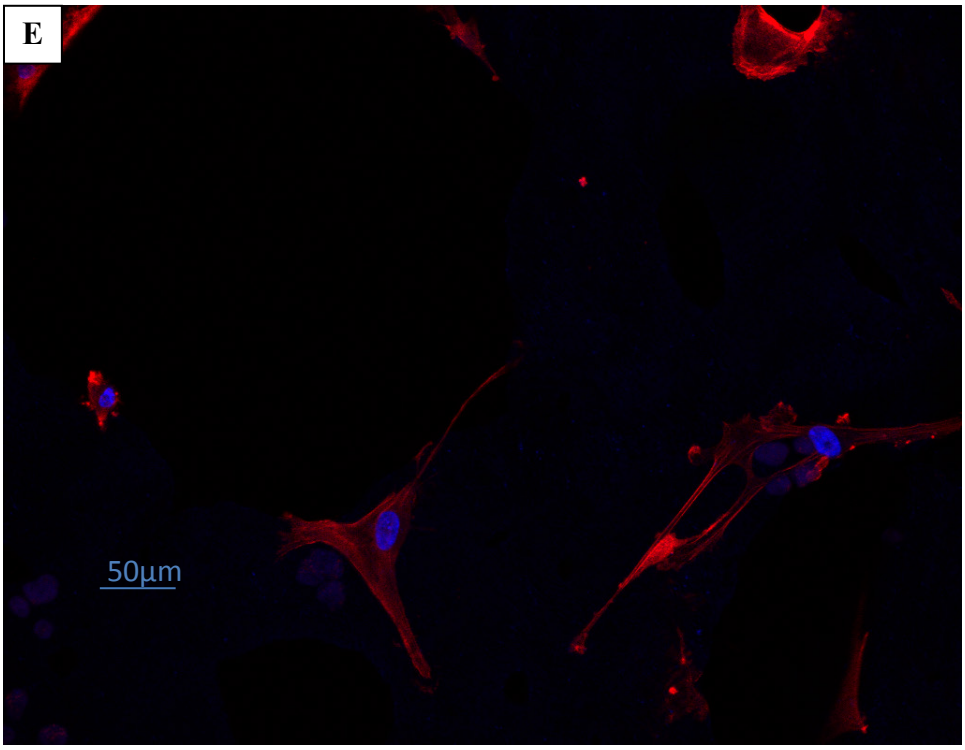
E
50µm

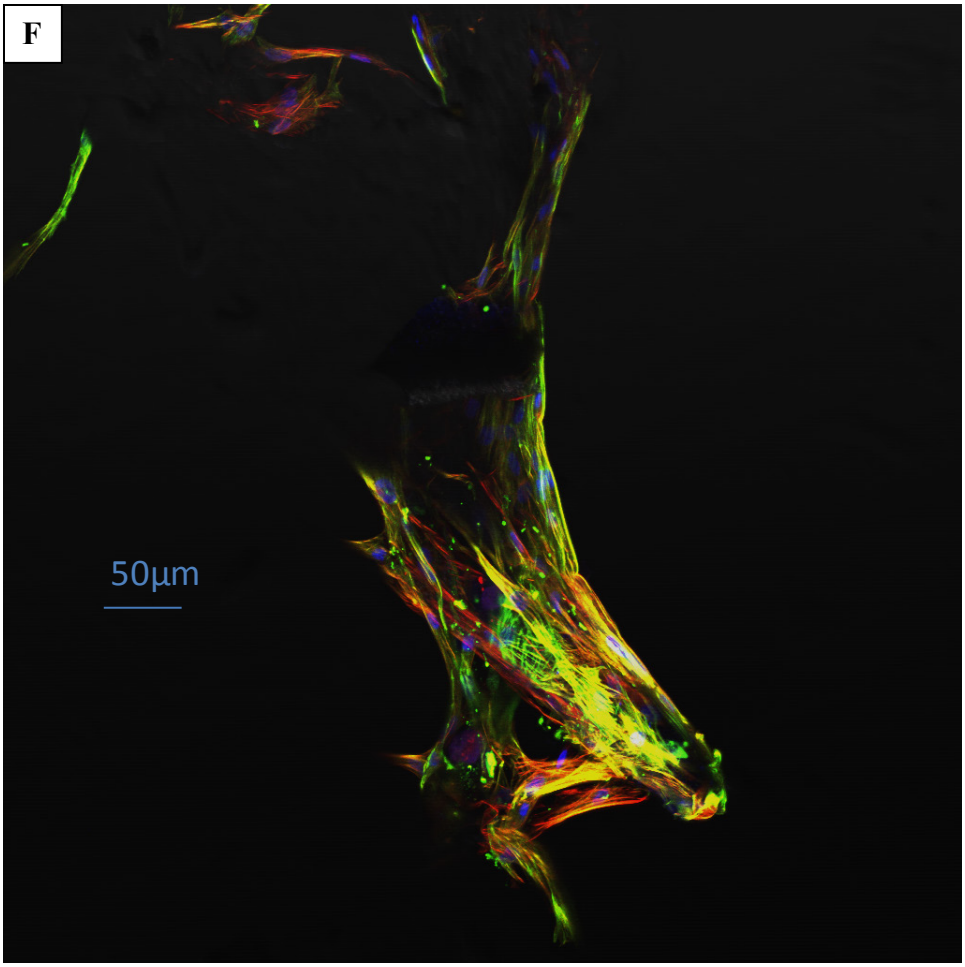

Figure 7.10. Confocal microscopy images. The nuclei of all cells are stained blue (DAPI), the cytoskeleton is stained red (phalloidin), and CK19 is stained green for: a) C1 15 days, b) C1 28 days, c) C1/HAp 15 days, d) C1/HAp 28 days, e) HAp 28 days, and f) with ASMA stain (green) for HAp 28 days.

7.2.5 Preliminary Al_2O_3 Comparison

One donor was used to explore the effects of a bioactive ceramic (HAp) compared to alumina, a bioinert material which does not dissolve in culture or release ions in the local environment. Al_2O_3 scaffolds were prepared in the same methods as the HAp scaffolds, with the solid loading of ceramic powder increased to 35 vol% to account for the difference in powder morphology. The HAp powder used for this study is a chemically prepared powder with large surface area

while the Al_2O_3 are spherical particles with much lower surface area. Both scaffolds were injected with HAL cells dispersed in a C1 hydrogel to create a composite. The albumin secretion after 28 days was almost identical in both cases, continually increasing over the course of the experiment to 500 μg/10E6 cells (Figure 7.11a). This result might be expected because the hepatocytes are supported in the C1 hydrogel within the pore space of the scaffold. This implies that the hepatocytes in the pores of the ceramic are unaffected by the ceramic material. The HAp composite cultures, however, contained drastically higher amounts of cells. Cell number is essentially maintained throughout the 28 days with HAp (around 80,000 cells/well), while in the alumina composite, the cell number drastically drops off from 97,000 cells/well to 30,000 cells/well at 15 days (Figure 7.11b). This is surprising given the similar albumin production, therefore leading to the conclusion that the HAp composite must be supporting the non-hepatocyte cell types better necessary for long term culturing in this donor, because albumin is only produced by hepatocytes. The gene expression data supports this conclusion, since vWF expression increases over the duration of the experiment while it is not expressed in the $C1/Al_2O_3$ composites (Figure 7.11c). This illustrates how Ca^{+2} ions liberated from the HAp could influence endothelial cell growth as seen in the literature [80]. One gene that appeared to be expressed in much higher amounts in the alumina composite was CK19. This expression increased over the 28 day experiment to 1090 times the expression in the original donor cells. CK19 expression was well maintained in the C1/HAp cultures, around 200 times the expression in the donor cells at all time points, which shows growth of these cells even though it is not as high (Figure 7.11d). ASMA was not found to be expressed in any condition and CYP450-3A4 was barely expressed in any conditions for this donor. Albumin expression was only slightly different between the two conditions, only 20% or less of the expression in the donor cells.

Finally, KI67 was much higher in the C1/HAp composites at 15 days, 131.7 times the expression in the donor cells compared to 28.5 times, but was not measurable in either condition at 28 days. This experiment begins to show the importance of a bioactive ceramic being used, specifically Ca^{+2} ion liberation at the surface, especially beneficial of endothelial cells as discussed above, though further biological repeats must be completed in the future to confirm these findings.

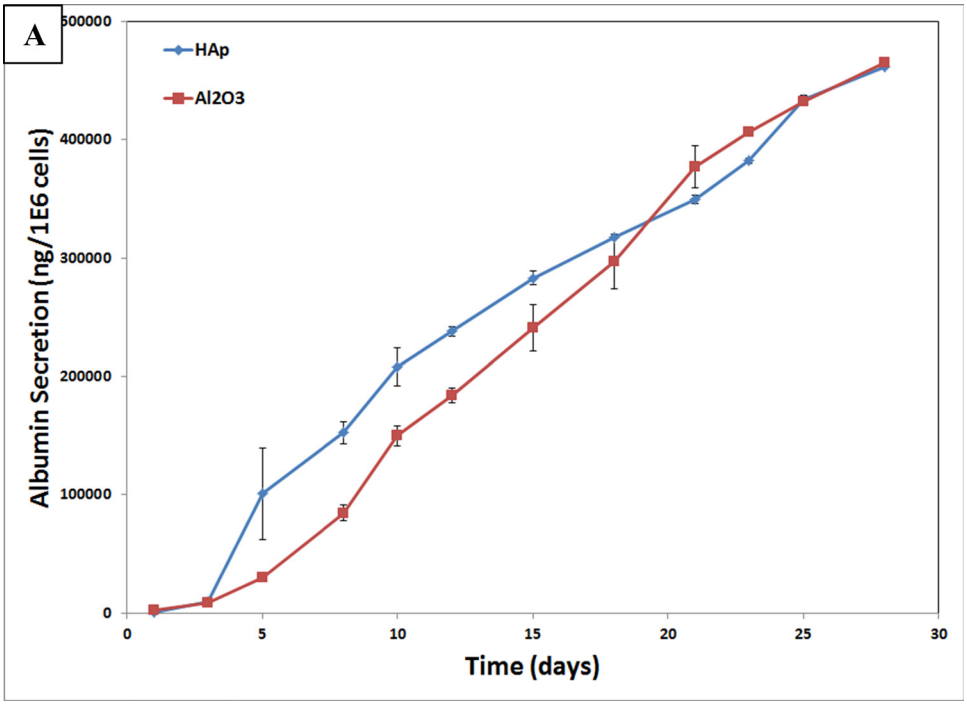

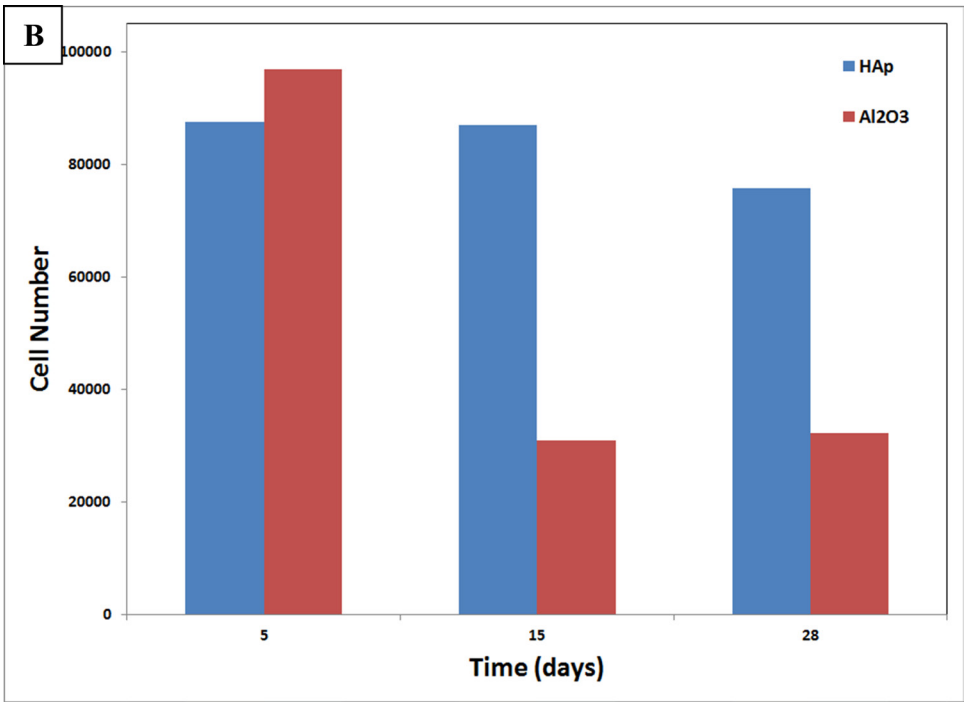
B
100000
80000
60000
40000
20000
0
Cell Number
HAp
Al2O3
5
15
28
Time (days)

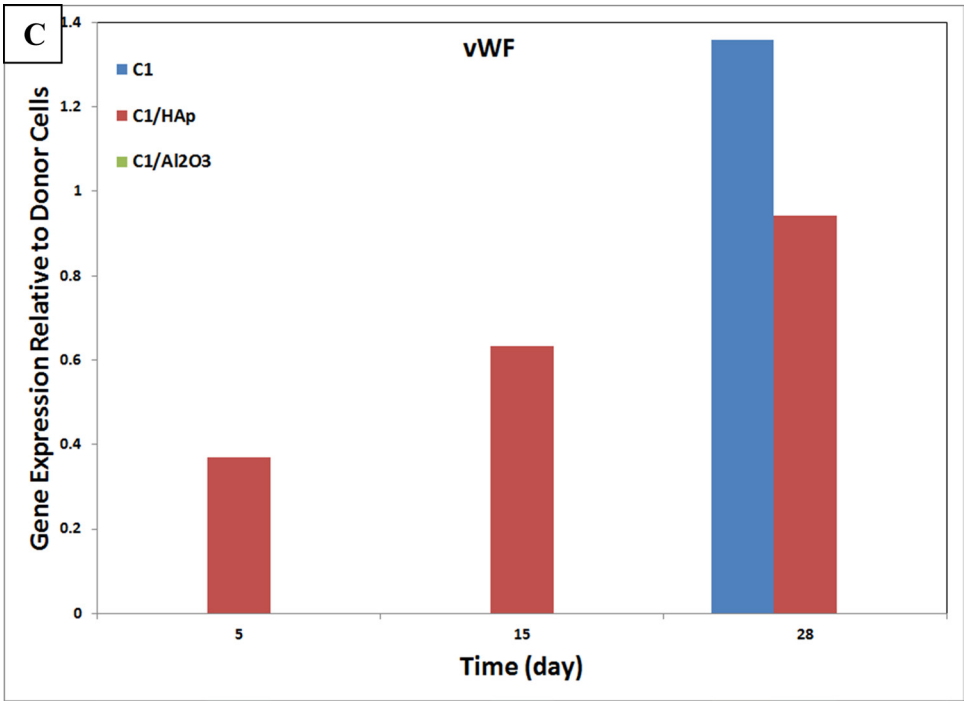
C
vWF
C1
C1/HAp
C1/Al2O3
1.4
1.2
1
0.8
0.6
0.4
0.2
0
Gene Expression Relative to Donor Cells
5
15
28
Time (day)

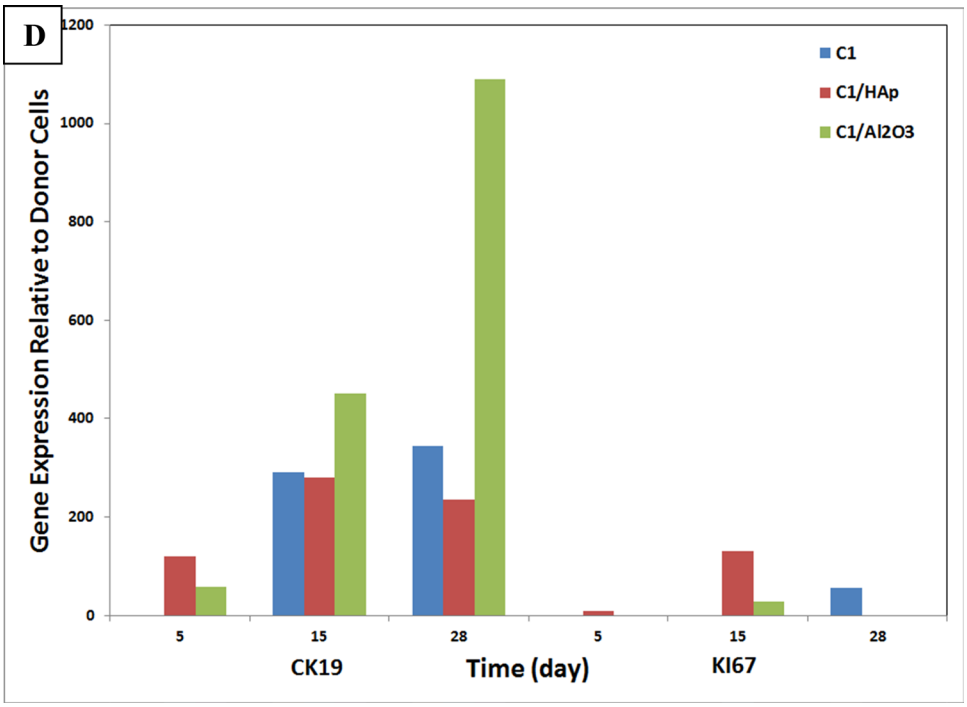

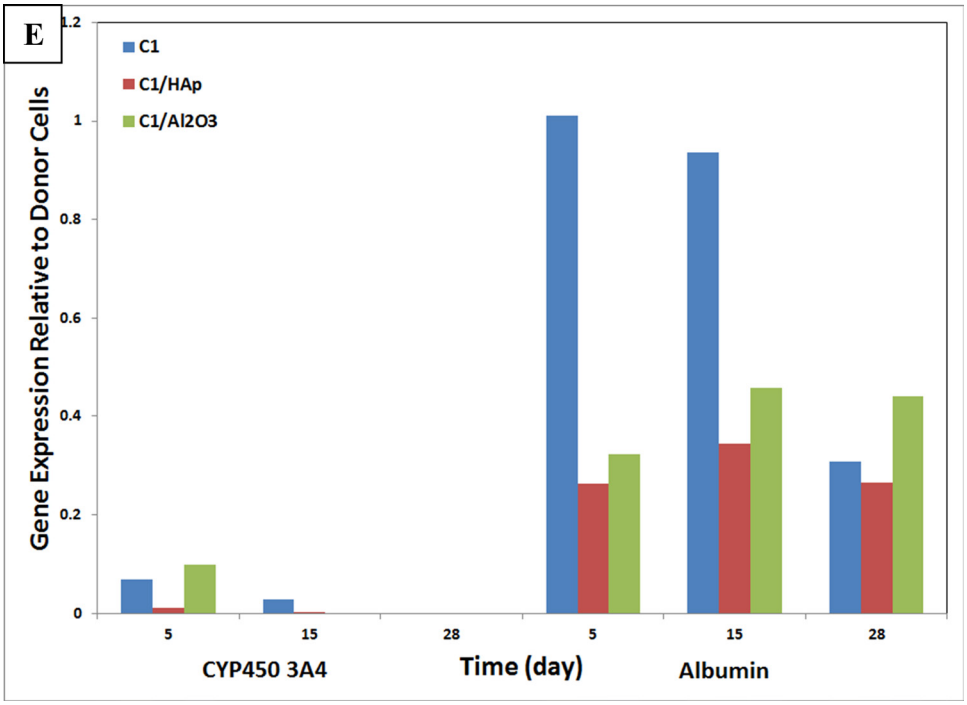

Figure 7.11. A) shows albumin secretion for C1/HAp and C1/Al2O3 composite cultures. B) is the cell number as determined by genomic DNA quantification. C-E Shows gene expression normalized to donor cells for vWF (C), CK19, KI67 (D), CYP450-3A4, and albumin (E).

7.3 HEAT TREATMENT

Creating a resorbable ceramic is imperative for the success of this project. Using the high temperature transformation of HAp to resorbable phases, it is possible to make a resorbable CaP scaffold. Creating a scaffold that can completely resorb in the 4-8 week culturing time in the bioreactor is necessary so that functional tissue can be extracted from the core.

7.3.1 X-ray Diffraction

Figure 7.12 shows x-ray diffraction patterns for pellets and replicated foams fired at different temperatures: 1350°C, 1450°C, and 1550°C. Figure 7.12a shows that HAp and TCP were present in the ground pellets, which represent the entire volume of the pellets. It is apparent that HAp is the main phase found at all sintering temperatures for the pellets. It was not until 1550°C that evidence of TCP was seen in the diffraction pattern. This result was expected because the reaction is seen at the surface of dense HAp samples at a small percentage of the total thickness of the pellet. Predictably, XRD patterns from the surface of the pellet show a much different picture than the ground pellets (Figure 7.12b). At 1350°C, there is already a significant TCP peak at 30° 2θ. This shows that TCP has already formed on the surface of the pellets at the lowest firing temperature although the diffraction pattern of the crushed pellet shows that this did not extend into the interior. This is quite consistent with the transformation occurring at the surface of the already dense ceramic observed in previous studies [11,43]. At 1450°C, there is more growth of TCP on the surface of the pellets along with an apparent increase in the intensity of the HAp peak at 32.2° 2θ. This unusual increase in HAp peak intensity could be attributed to the formation of CaO which also has a peak at that position which is 43% relative to the max

peak for CaO. X-ray diffraction of the ground foam shows different behavior from that of the pellets or the powders (Figure 7.12c). TCP formation was seen at temperatures as low as 1450°C but does not increase dramatically between 1450°C and 1550°C. Again, the formation of a higher proportion of TCP at the lower sintering temperatures is consistent with the high surface-to-volume ratio of the foam relative to the bulk ceramic.

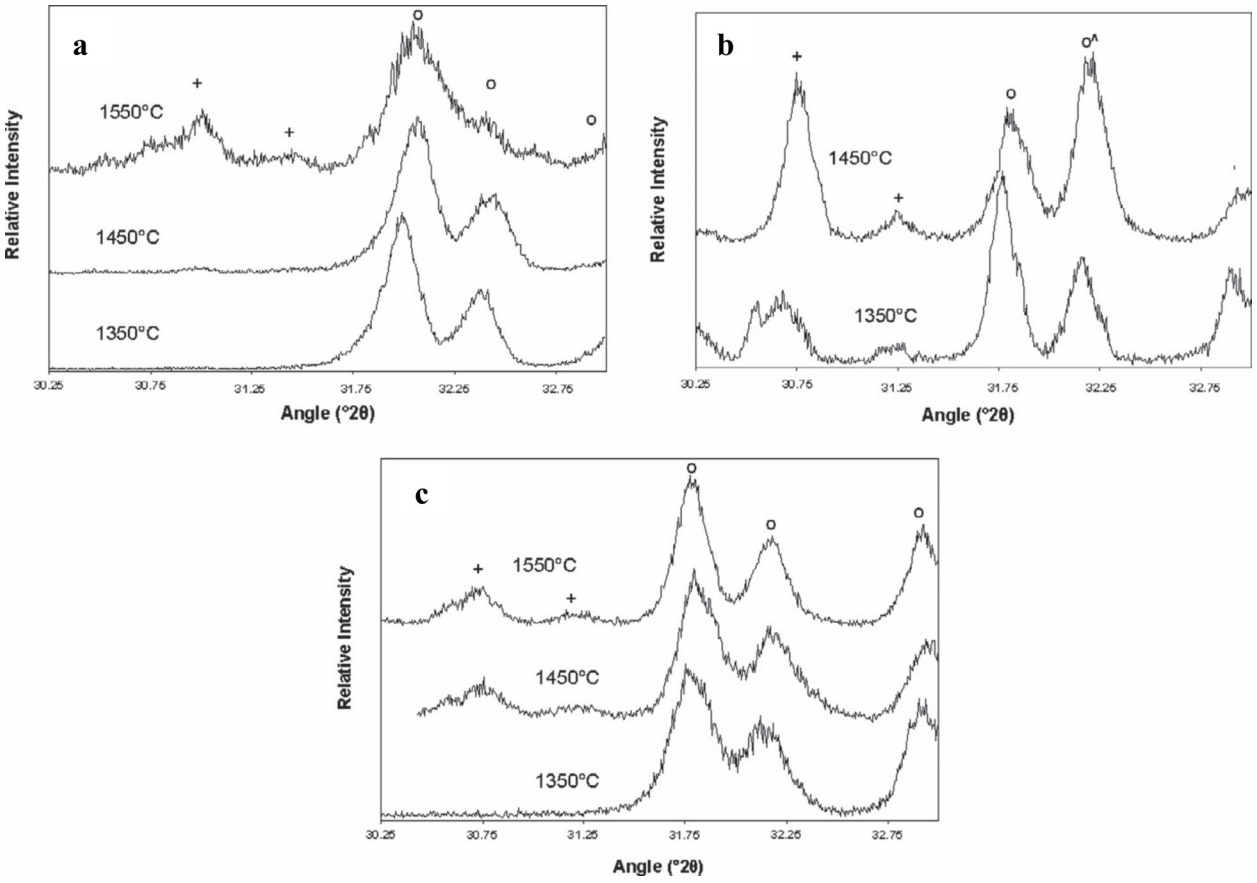

Figure 7.12. X-ray diffraction patterns of (a) ground pellets, (b) pellet surface and (c) ground foams. Peaks marked (o) correspond to hydroxyapatite, peaks marked (+) correspond to tricalcium phosphate and peaks marked (^) correspond to the presence of CaO.

7.3.2 Scanning Electron Microscopy

Microstructural analysis of sections through the HAp pellets clearly shows the phase transformation behavior of the pellets at high temperature. At 1350°C, the pellet is dense with little sign of damage caused by the phase transformation. As the temperature is increased from 1400°C to 1500°C, a visible transformation layer is seen on the surface of the pellet and cracking is found that extends from the surface of the ceramic into the interior (Figure 7.13a and b). At temperatures at or below 1450°C this layer appears to be pure α-TCP with small amounts of amorphous CaO as suggested by Cihlar et al. [11]. This is consistent with the effect of sintering temperature on the mechanical strength of HAp observed in previous studies. After sintering at 1400°C, the layer is not continuous and only appears in spots along the surface; above this temperature, a continuous layer is formed as observed in previous studies [11,43]. Because these cracks appear to initiate at the phase interface, they probably open due to the volume increase associated with the phase transformation (Figure 7.13c). The reaction layer in the 1500°C sample appears to have a third phase on the surface (Figure 7.13c). By EDS, the relative Ca/P ratios measured suggest that the bulk phase is HAp (1.44), the reaction layer is α-TCP rich due to a lower Ca/P ratio (1.36) and the lighter contrast phase closest to the surface of the pellet appears to be either rich in CaO and/or TeCP due to a higher Ca/P (1.51). These numbers were not absolute because of limitations in the calibration of the EDS used. For reference, the Ca/P ratio of HAp is 1.67. At these temperatures, CaO will react with α-TCP to form TeCP. CaO and subsequent TeCP formation on the surface could be caused by preferential phosphorus evaporation at the surface at high temperatures creating a calcium rich area, because phosphorus has a much higher vapor pressure at these temperatures compared to calcium [92]. The presence of these phases was unable to be confirmed with XRD and EDS, due to the relatively small

amounts and the presumably low crystallinity of these compounds, but this is expected in accordance with the literature [11].

The thickness of the reaction layer increased with the temperature. At 1350°C, the pellet did not have a distinguishable and continuous layer. At 1400°C, the reaction layer was 8(±2) μm; at 1450°C, it grew to 43(±6) μm and finally was 97(±8) μm thick at 1500°C which are similar to transformation behavior seen in the literature [11]. The layer formed at 1450°C in this study is within error with the results seen by Cihlar et al. [11]. When the pellet was fired at a temperature of 1550°C, severe damage is sustained in the pellet due to transformation occurring throughout the sample (Figure 7.13d). The water vapor formed during decomposition of HAp appears to cause large voids destroying the sample heat treated at 1550°C. The reaction products are also disbursed throughout bulk samples fired at this temperature. This is consistent with the density measurements of the pellets. Samples fired between 1350°C and 1500°C had a relative bulk density that averaged 97%. Similar densities were found in the samples fired at 0 hours at 1350–1450°C, showing that much of the densification happened before the samples reached the sintering temperature. When the sintering temperature was increased to 1550°C, the density dropped to 45% due to the porosity associated with internal decomposition.

The foam exhibits a much different microstructure when fired at high temperatures when compared to the pellet. At 1350°C, the struts of the foam appear to comprise dense HAp. At 1400°C, significant fine cracking was seen in the struts and a second phase was distinguishable throughout the thickness of the foam struts (Figure 7.14a). These cracks appear to originate at the external surfaces and internal voids where decomposition occurs. Once the sintering temperature is increased further to 1450°C, the cracks begin to heal by creep and the newly formed TCP densifies (Figure 7.14b). The improved densification of the TCP foams continues

up to 1550°C, the highest temperature used in this study. Importantly, the large cracks observed in the bulk samples (pellets) were not observed in the foams. The average strut thickness was found not to vary over the range of temperatures examined and was found to be on average 48(±4) μm. This distance can be used to explain the difference in microstructure seen between dense and porous structures in the next section.

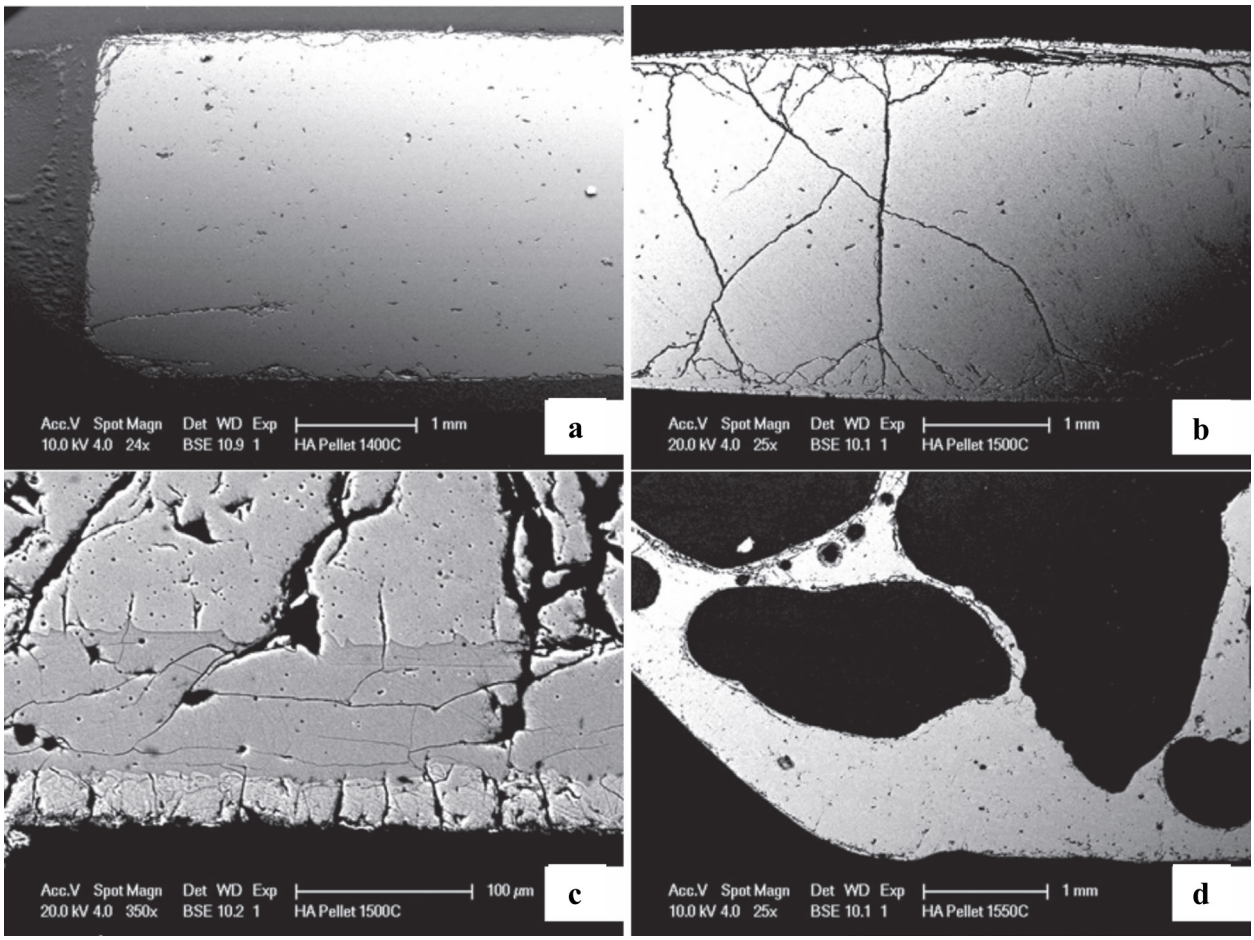

Figure 7.13. SEM micrographs of HAp pellets. (a) and (b) show damage due to transformation at 1400°C and 1500°C respectively. (c) shows the three phase layer that develops on the surface of samples sintered at 1500°C and (d) illustrates the large voids created during transformation at 1550°C.

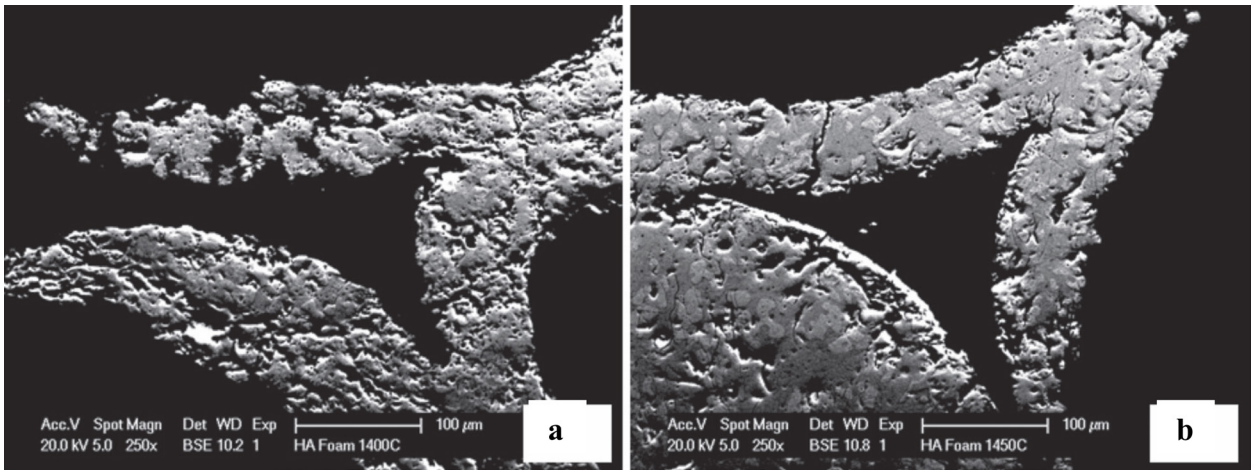

Figure 7.14. Cross sections of HAp foams are shown. (a) illustrates damage created by transformation at 1400°C, and (b) shows healing of those cracks due to densification of TCP at 1450°C.

7.3.3 Difference Between Dense and Porous Samples

Based on the microstructural and phase analysis of HA pellets and foams fired at high temperatures, it is clear that the foams behave very differently from dense pellets. The formation of these reaction products on the surface of the pellet can be explained by the sintering behavior. The density of the pellet fired at 1350°C sintered for 0 hours was found to be 94%. This shows that the pellet has densified during heating to the sintering temperature. Therefore, the only material in contact with the atmosphere at the sintering temperature was the surface. For the reaction to occur, diffusion to the surface of OH^- is necessary to remove the newly formed water vapor at the surface. This creates the layer of TCP and CaO on the surface of pellets fired at high temperature. This also creates strain due to the volume changes associated with the formation of the new phases as compared to the HAp. This strain creates cracks which extend into the interior of the sample and lower the mechanical integrity of the pellet (Figure 7.13c). Once the temperature reaches 1550°C, the transformation occurs throughout the sample and

forms water vapor, creating large voids that destroy the pellet which is not seen in the foams. The reason for this is mainly due to the effective diffusion distance for decomposition of the foam compared to the pellet. The struts of the foam are 48 μm thick while the pellet is on average 2.9 mm thick. At 1350°C, the pellet and foam behave similarly, both comprising dense HAp. At 1400°C, the behavior begins to deviate. An 8 μm reaction layer appears on the surface of the pellet and cracks begin to form. The strut thickness of the foam is greater than 8 μm and when transformation occurs, the cracks created damage the foam structure but do not cause the foam to disintegrate. Samples fired at 1450°C deviate even more. The pellet follows the same trend as before and the reaction layer grows to 43 μm and cracking is more severe. This reaction layer is now almost of the same size as the strut thickness in the foam and the reaction product can be observed throughout the foam structure. Importantly, the TCP formed by the transformation begins to sinter and creep, thereby healing the finer damage created by the transformation. As temperature is increased to 1550°C, crack healing continues to occur because of further sintering and creep of TCP. The distortion of the structure due to creep is shown in Figure 7.15. In contrast, the transformation in the bulk materials at temperatures above 1400°C is restricted to the surface due to the much larger diffusion distance. This causes much larger cracks that extend into the interior of the pellet and cannot be healed by sintering at higher temperature.

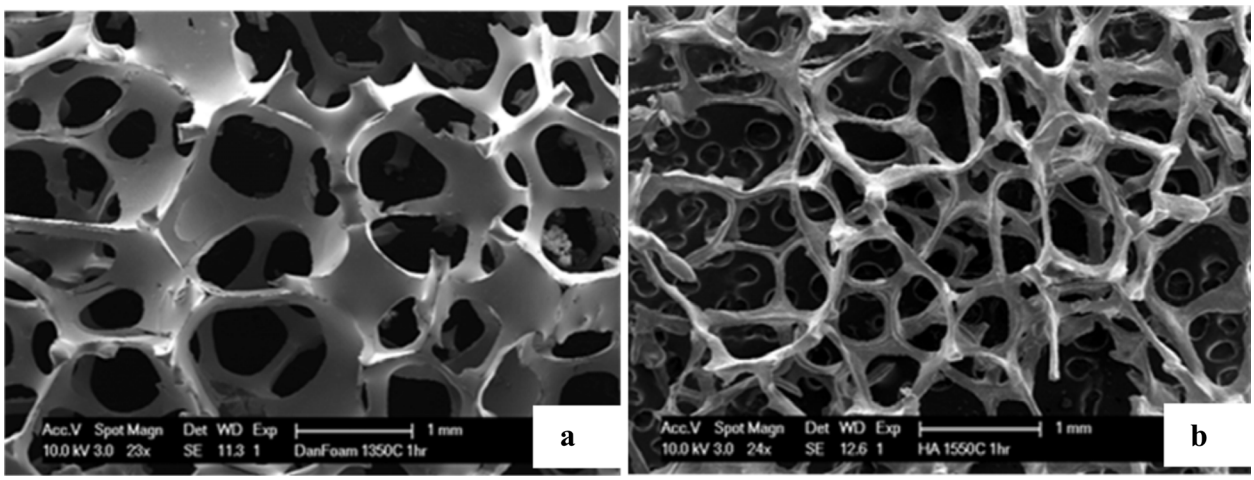

Figure 7.15. Representation of the compliance of the foam structure. Hollow HAp struts shown in (a) are allowed to creep to accommodate the phase transformation occurring at 1550°C (b).

7.3.4 Effect of Pore Size on Decomposition of HAp

While the differences in high temperature behavior between dense and porous HAp were described in the previous section, the effects of porosity on this transformation must still be addressed. Six distinct porosities were chosen, two of which have mostly closed porosity and four having a highly interconnected pore network with varying morphologies. It is expected that as the size of open pores increase or the effective diffusion distance decreases, the percentage of α-TCP in the ceramic will gradually increase.

XRD results show a range of TCP contents produced after the six foams were sintered at 1500°C for 1 hour (Figure 7.16a). Foams produced with low heptane contents lead to low amounts of α-TCP created during sintering. Using the calibration curve described in section 6.3.3, the amount of α-TCP in these structures ranged from 9.5% to 16% relative to HAp. After the creation of a continuous pore network in foams made with heptane contents ranging from 5-10 vol%, the amount of α-TCP formed rose greatly to 28.1% to 33.2% relative to HAp. At 20

vol% heptane, the TCP composition decreased to 22.6% relative to HAp, which is most likely due to the structure collapsing as seen in section 7.1.2.

To further explore these results, horizontal cross-section SEM micrographs were collected, exhibiting familiar results. A closed pore structure with high distances between pores results in transformation behavior quite similar to that of a dense sample. The bulk of the transformation occurs near the surface of the foam (Figure 7.17a), while the interior shows little transformation product, most of which is present near the surface of the closed pores (Figure 7.17b). Foams with a continuous pore network behave more closely to the reticulated foams observed in the previous section. When 5 vol% heptane (160.7 μm solid intercept length) was used in foam creation, α-TCP contents were 15% greater than the more closed porous structure created by 2.5 vol% heptane (219.9 μm solid intercept length). The cross-sections show a similar phase distributions as seen in other open porous foams (Figure 7.17c). When the amount of heptane was increased, the strut thickness in the resulting foam decreased, leading to an increased amount of reaction product, seen both in the XRD data and SEM micrographs (Figure 7.16a and Figure 7.17d). When the amount of heptane was increased to 20 vol%, the structure collapsed, as seen in previous research. This data point is interesting, as it does not fall into the general trend seen with the other foams (Figure 7.16a and b). When TCP content is graphed as a function of solid distance between pores (108 μm), the amount of transformation is much lower than in structures with similar distances (7.5 and 10 vol% heptane). When the strut thickness (452 μm), the size of the solid features discounting internal porosity, is used instead of the raw solid distance value, the solid length is in the range of the closed pore structure examined (450 μm at 0% heptane). This α-TCP content is significantly higher than contents found in those

foams. This suggests that the seemingly closed internal porosity within the collapsed struts influences the transformation behavior of the structure.

While these values were only calculated for the foamed region of the samples, vertical cross-sections of the entire foam were examined. Figure 7.18 shows a representative structure of open porous foams that is seen regardless of pore morphology. The transformation product is highest at the top, or skin, region of the foam, while sections closer to the bottom of the sample do not seem to exhibit this decomposition. Micrographs show that the structure becomes increasingly dense towards the bottom, which is in agreement with gravitational drainage in drying foams seen in the literature. In the positive-negative cast bioreactor cores, this dense region will be removed before assembly of the reactor to ensure that the eventual core will resorb completely.

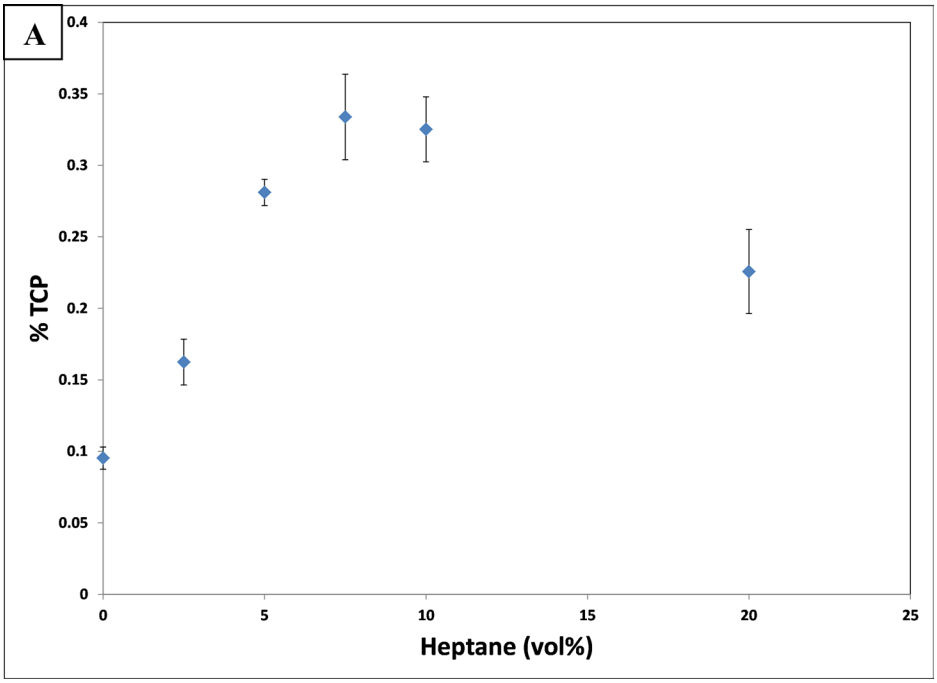

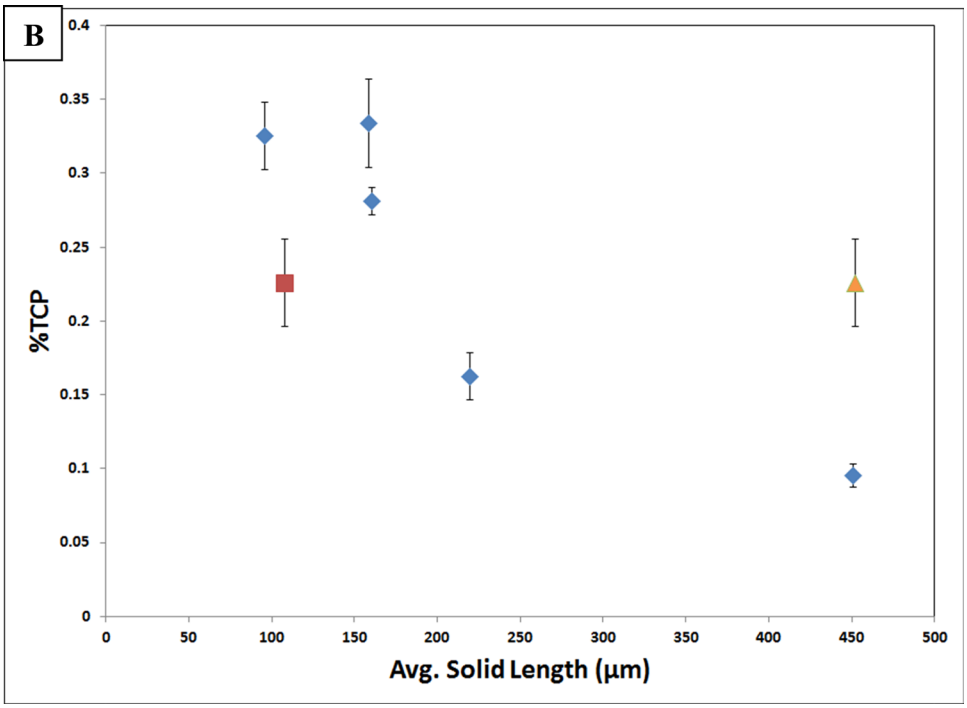

Figure 7.16. Graphs representing the effect of porosity on phase composition. A) %TCP graphed as a function of heptane content in the emulsion and B) %TCP graphed as a function of average solid length as calculated by equations in 7.1.2, red square represents 20 vol% heptane sample plotted as average solid length and orange triang represents 20 vol% plotted as average strut length.

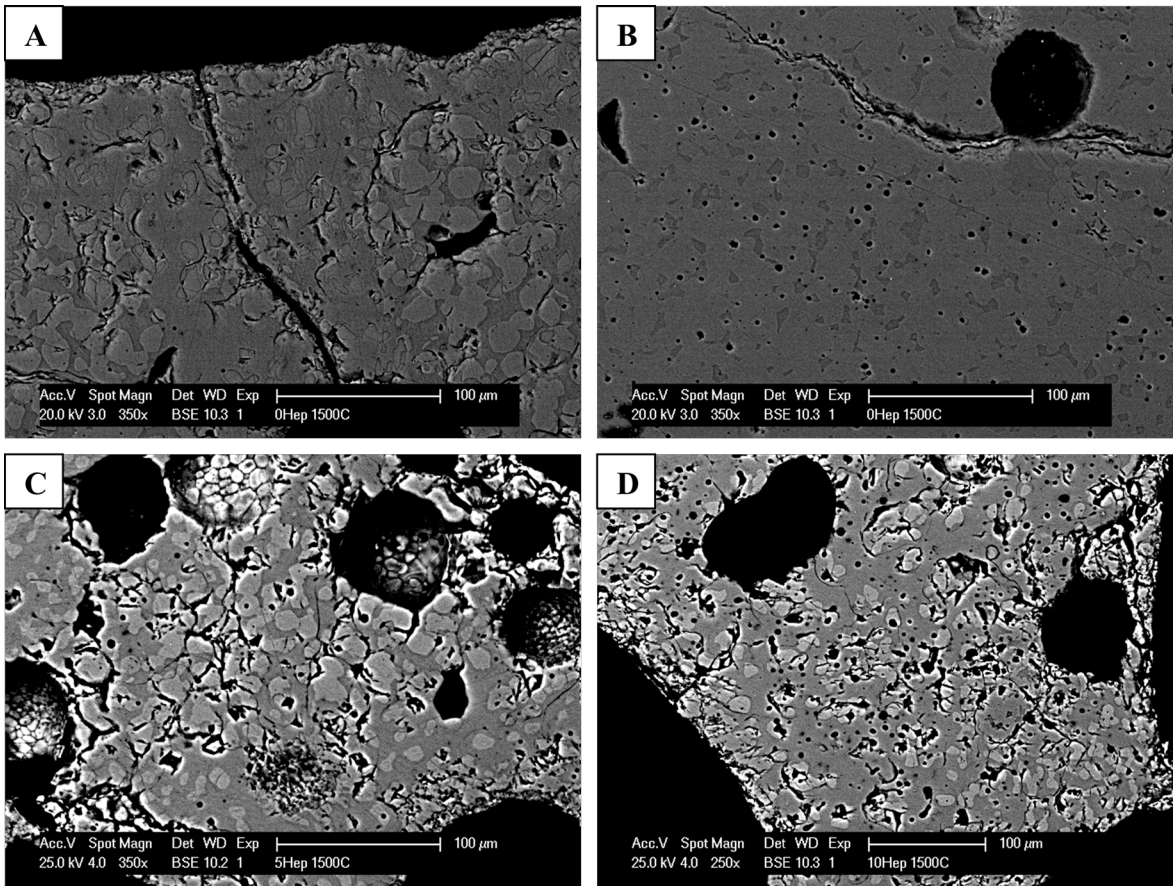

Figure 7.17. Cross-sectional micrographs taken with back-scattered electron imaging of samples produced with 0 vol% heptane at the A) surface and B) interior of the foam, C) 5 vol% heptane, and D) 10 vol% heptane. Lighter areas represent HAp while darker areas represent α-TCP.

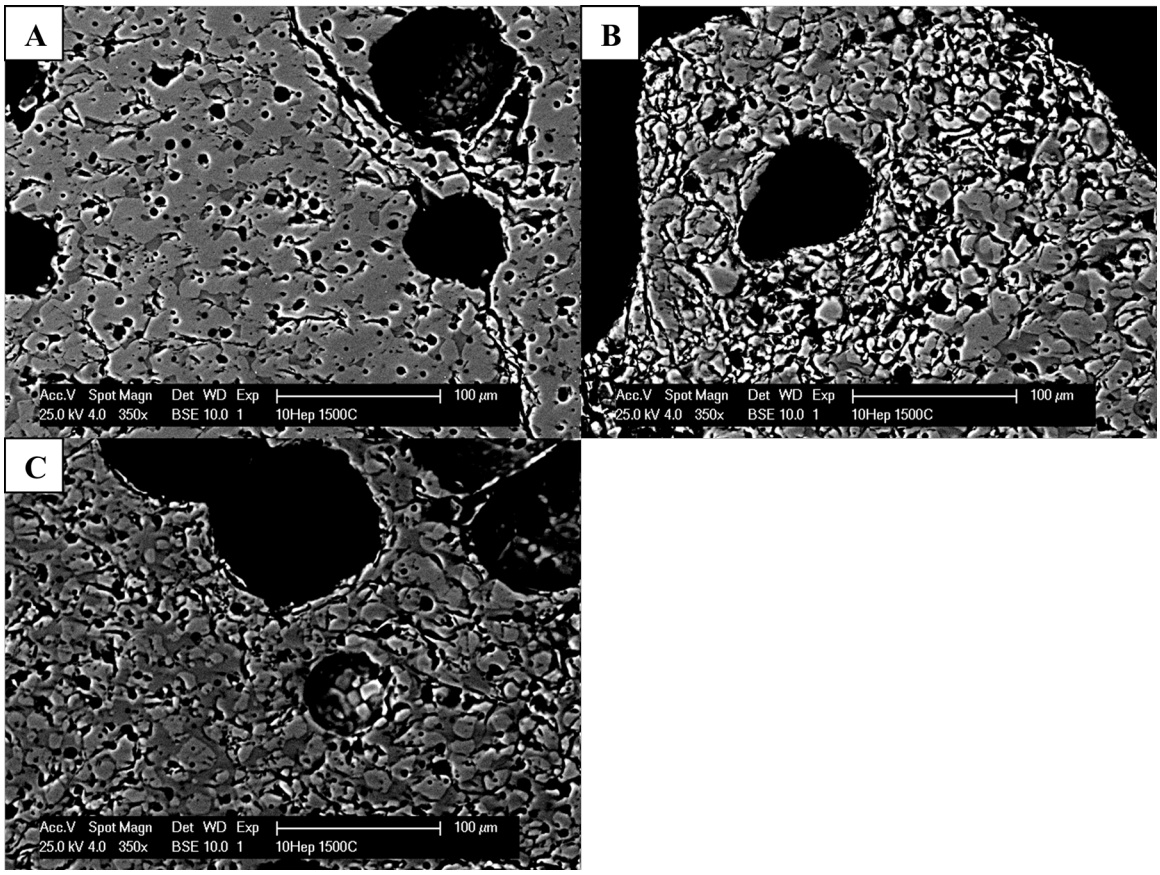

Figure 7.18. Vertical cross-sections of a foam made with 10 vol% heptane taken with back scattered electron imaging representing the a) bottom, b) middle, and c) top of the foam (350X).

7.3.5 Effect of α-TCP Content on Dissolution

As mentioned previously, the ceramic structure must degrade in the bioreactor core as the liver cells begin to form tissue (~4-8 weeks). The dissolution behavior of the biphasic CaP scaffolds created using high temperature heat treatment of HAp must be studied. Four α-TCP contents were created in foams by varying the sintering temperature from 1350°C to 1500°C: 2.16%, 4.71%, 49.79%, and 62.59%, which exhibited four distinct dissolution behaviors. Using the chemical formula in equation 2.2 the expected CaO contents in these samples are: 0.13 wt%, 0.25 wt%, 2.99 wt%, and 3.76 wt% respectively. Two different experimental conditions were

chosen to examine these behaviors. The static condition is where the ceramic is immersed in 1.5 mL of tris-buffered saline in an incubator and is examined as a comparison to experiments found in the literature. These experiments show small differences in dissolution similar to what is seen in dense samples in the literature [36,37]. At lower TCP contents, the porous CaP scaffolds release small amounts of Ca^{+2} ions in the saline, up to 11 ppm at 28 days, while scaffolds with higher TCP contents release large amounts, up to 375 ppm, as seen in Figure 7.19a. The microscopy and weight loss tell a different story. Figure 7.19c shows negligible weight loss in static samples over the course of 28 days, regardless of TCP content. Infrequent areas of pitting can be seen in the fracture surface of the 2.16 wt% TCP samples in SEM (Figure 7.20a). These 'pits' are voids on the surface formed by the dissolution of resorbable phases in the scaffold, and are distinguishable from initial porosity by their angular morphology [37]. This pitting is increasingly observed in samples with higher α-TCP contents, but in the two samples with high decomposition product a second dissolution mechanism is observed. Dissolution at the grain boundaries in the ceramic are observed, shown in Figure 7.20b, and are most likely due to CaO segregation at the grain boundary during sintering as described by Wang et al. [37]. The scaffolds with the two lowest α-TCP contents, which had less that 0.25 wt% CaO, showed no signs of grain boundary degradation. Additionally, the large amount of free Ca^{+2} ions in the saline at these high α-TCP contents can be prohibitive to the dissolution of the scaffolds. As seen in the literature, precipitation of CaP on the surface of the ceramic happens at high ion concentrations, leading to weight increases in certain samples as observed in microscopy in this study [13,37,93].

The second experimental condition used is perfusion to approximate the conditions seen in a bioreactor core. The problem of rising ion concentrations near the surface of the ceramic,

leading to reprecipitation and less mass loss, can be alleviated through the use of perfusion systems, in which fresh saline is constantly flowed into the chamber or recirculated through a large reservoir of fluid. Scaffolds with the same phase distributions used in the static experiments were placed in the chamber of a 3DKube bioreactor. This was then hooked up to a pump and 1L of TBS is constantly recirculated through the bioreactor. The first major observable difference between static dissolution and the perfusion experiments is in the Ca^{+2} ion concentration in the saline. The septum for extracting samples in the perfusion experiment is placed 1 mL downstream of the chamber so the volume of liquid associated with the scaffold in the sample chamber is the same as in the static case but of course the perfusion system recirculates the fluid at a rate of 5 mL/min. While the trends in ion release are similar, the amount of Ca^{+2} ions present after 28 days in the perfusion experiment is only 10% of what it was in the static case for 62.59 wt% α-TCP. This lower ion concentration correlates with significantly higher dissolution of the constructs. The same scaffolds in the static experiments showed no weight loss and small amounts of pitting at the surface; while over 30% weight loss was seen after 28 days in perfusion (Figure 7.19c). The microscopy showed not only large amounts of pitting at the surface, but large amounts of dissolution in the fracture surfaces in the interior of the scaffold as well (Figure 7.20c). If there was dissolution at the grain boundaries, it was indistinguishable in the microstructure after 4 weeks in perfusion. This is a promising result, since significant amount of dissolution of the scaffold can be seen in saline without cells present at physiological pH.

Samples containing 2.16 wt% α-TCP show similar levels of Ca^{+2} ions in the saline and weight lost as the static samples, but if the microscopy is examined, significantly more pitting is seen at the surface (Figure 7.20d). These similar numbers are due to the small amount of

resorbable phases in the scaffolds leading to little dissolution of the structure regardless of experimental conditions. As the α-TCP content is raised to 4.71 wt%, the Ca^{+2} ion concentration is 10% less than the static condition which is a continuing trend with the samples containing higher amounts of α-TCP. Some amount of pitting and precipitation is present in all scaffolds incubated in static conditions, but increased visible amounts of dissolution and few precipitates are seen under perfusion. Instead, precipitates are seen to form in the tubing outside of the cell chamber and are not found attached to the surface, with more precipitates observed as the α-TCP content is increased in the scaffold. This is consistent with perfusion washing away dissolved ions near the surface of the scaffold so dissolution is increased regardless of TCP content.

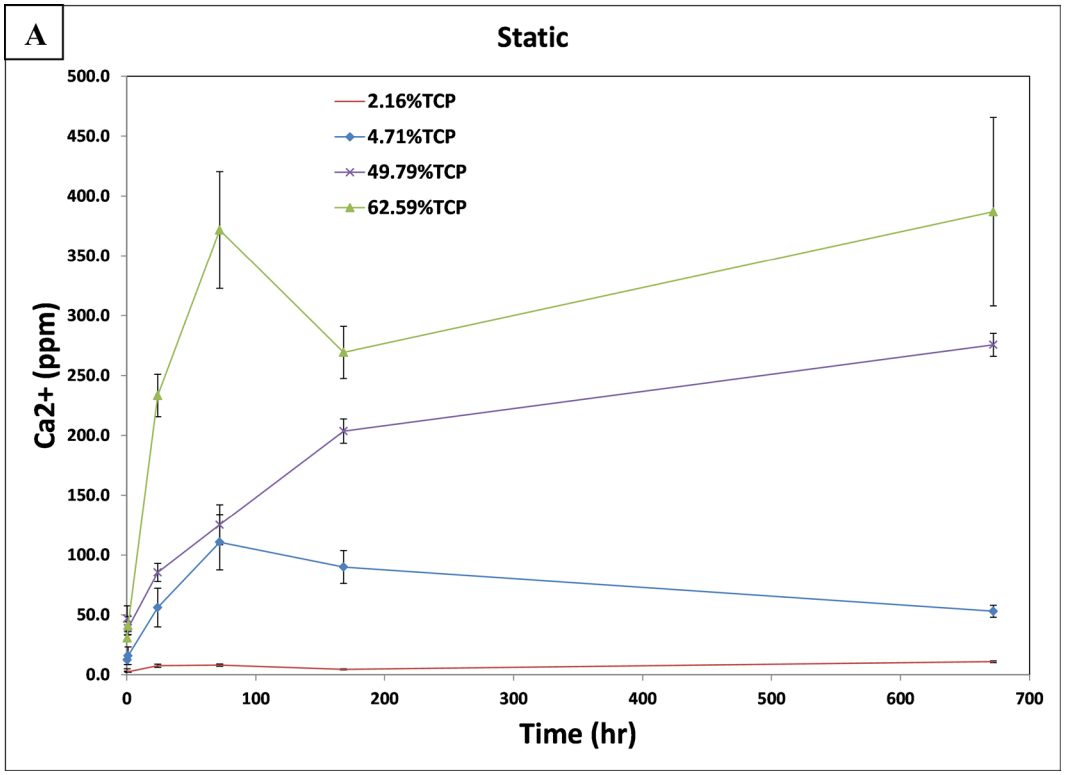

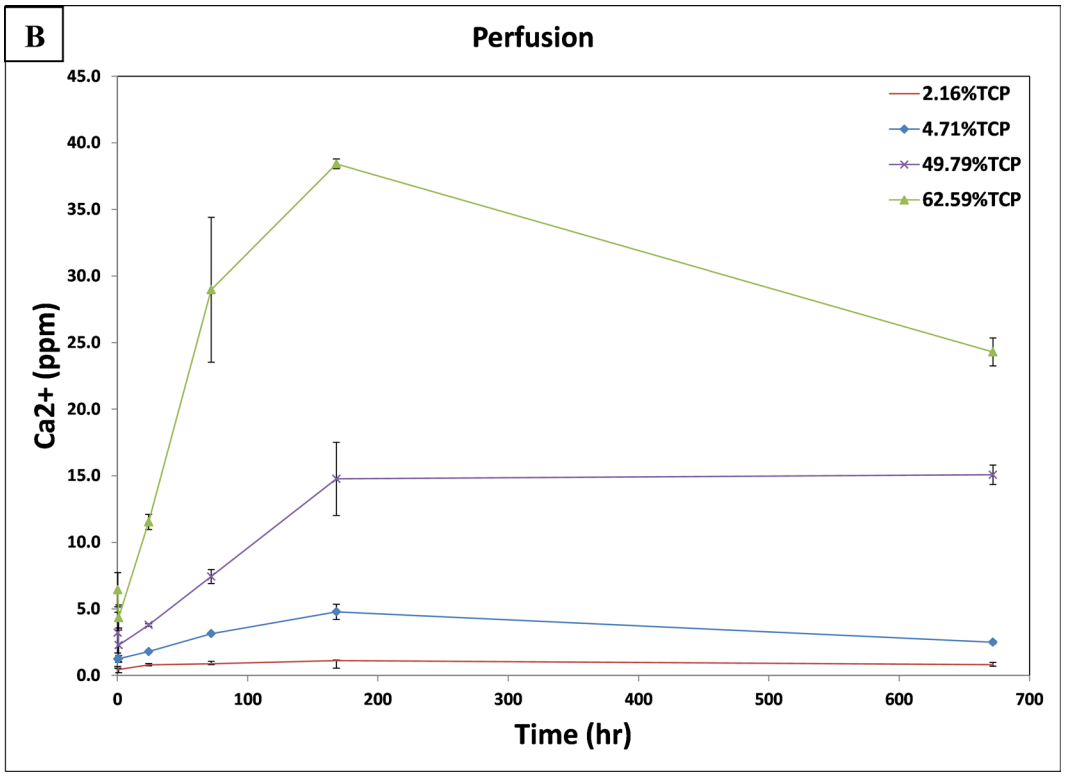
B
Perfusion
45.0
40.0
35.0
30.0
25.0
20.0
15.0
10.0
5.0
0.0
Ca2+ (ppm)
0
100
200
300
400
500
600
700
Time (hr)
2.16%TCP
4.71%TCP
49.79%TCP
62.59%TCP

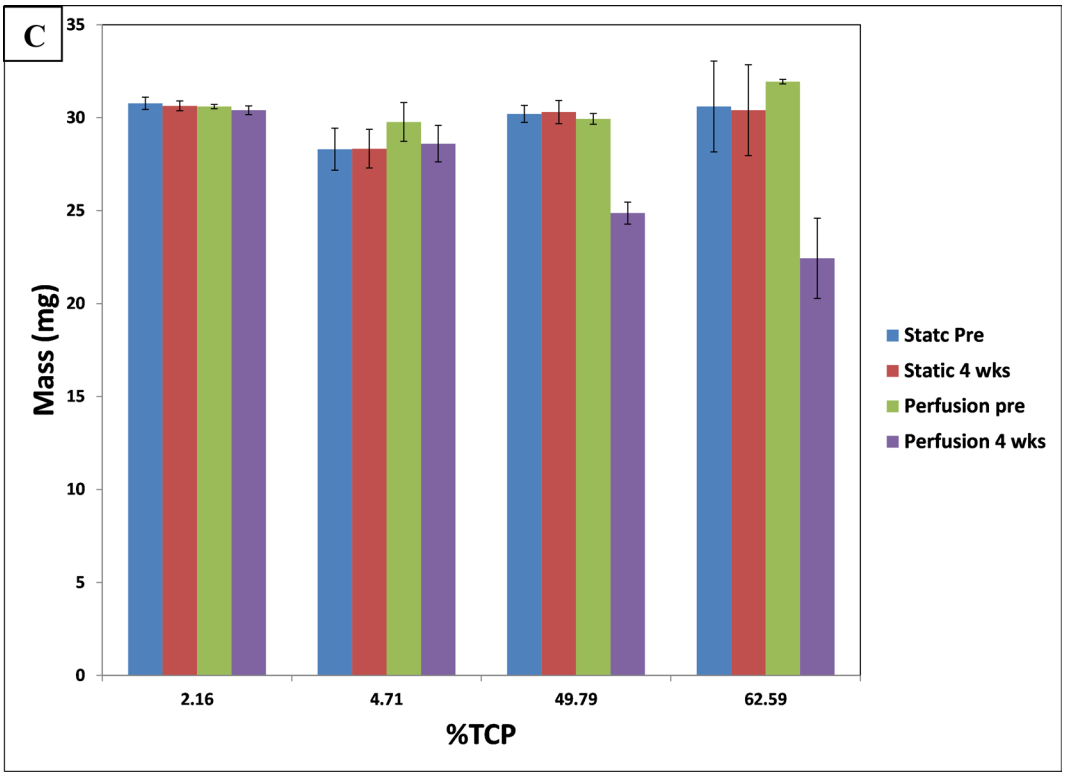

Figure 7.19. Ca^{+2} ion concentration in the tris-buffered saline was plotted as a function of time for all four α-TCP contents for A) static and B) perfusion experiments. C) The mass of the samples were also measured at day 0 and after 4 weeks in saline for both experiments and were graphed.

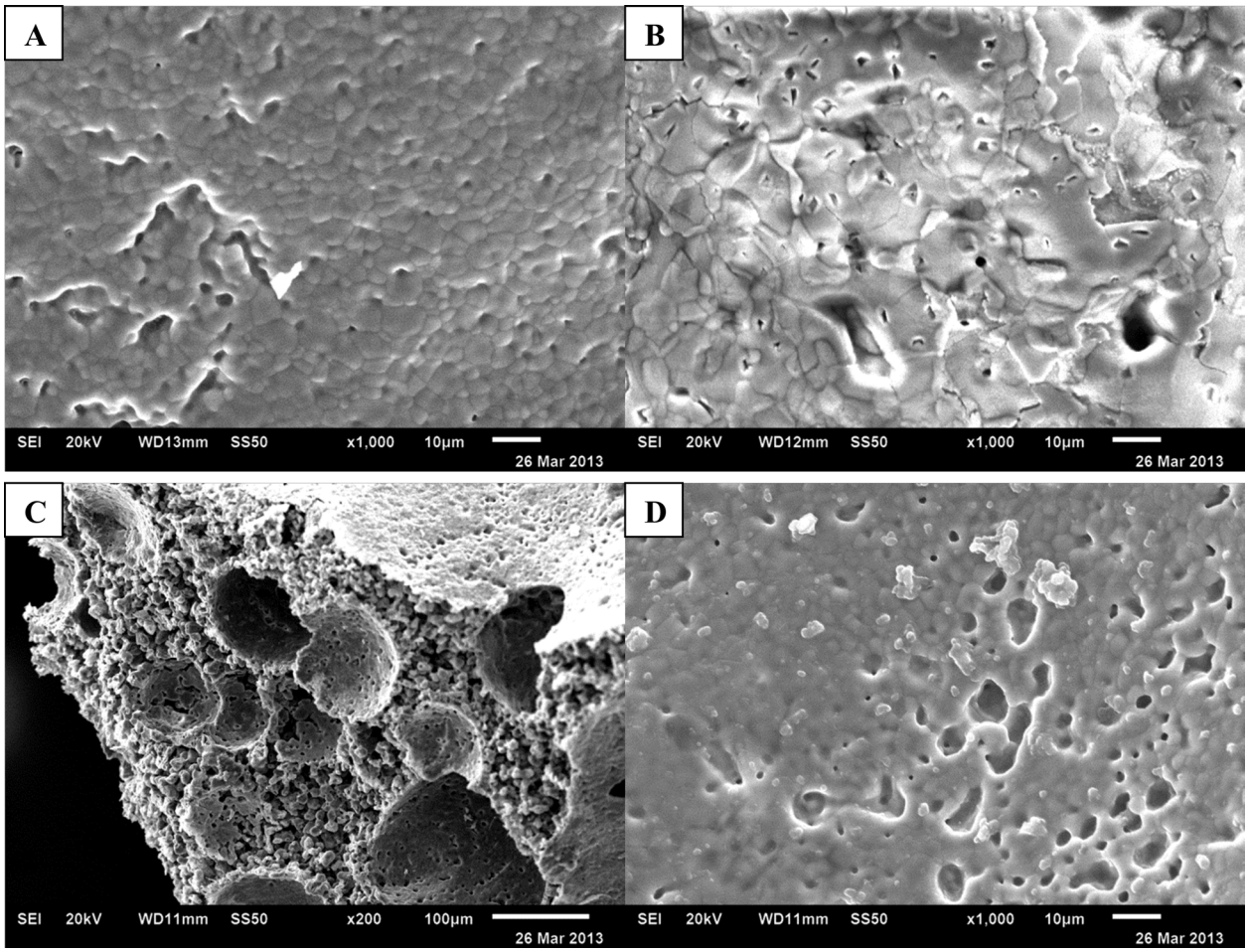

Figure 7.20. Micrographs of samples after four weeks in tris-buffered saline. A) is 2.16 wt% α-TCP in static condition (1000X), small amounts of pitting and precipitation seen on the surface, and B) is 49.79 wt% α-TCP in static condition (1000X), dissolution was seen at the grain boundaries. C) is a fracture surface of a 62.59 wt% α-TCP in perfusion condition (200X), large voids have formed in the struts due to dissolution and large amounts of pitting seen at the surface, and D) is the surface of a 2.16 wt% α-TCP in perfusion condition (1000X), significantly more pitting is seen compared to (A).

7.4 POSITIVE-NEGATIVE CASTING

7.4.1 Initial Positive-Negative Casting Experiments

Creating vascular-like channels in the bioreactor core is necessary to deliver cell culture medium to the liver cells in the pores of the ceramic and to provide a template for vascular tissue growth in the construct for future transplantation of the formed tissue. To create these channels, a positive-negative casting process was developed as described in previous sections. Polymeric vascular-like structures were placed in molds and an emulsion foam was formed around the template. During the sintering of the ceramic, the polymeric template was pyrolysed, leaving behind a macropore in the ceramic structure.

There was a significant effect of the macropore (created by embedding 3 mm diameter polystyrene tubes in the foam casting mold) spacing on the morphology of the foam in between the tubes. As the distance between macropores is decreased to the size of the pores formed in the expanded foam, the foam structure does not form in between the polymer tubes like it does throughout the bulk of the sample. As seen in Figure 7.21a, when the macropores (marked with arrow) are spaced at 5 macropore diameters from each other, the structure in between these features is similar to the 10 vol% heptane foams described in section 7.1.1. In addition, there is no observable effect on the microstructure for samples with a macropore spacing of 2.5 macropore diameters. When the spacing between the macropores is reduced to 1 macropore diameter, however, the foam region is not developed between the tubes, as shown by the blank space between macropores in Figure 7.21b. In this case, the size of the pores formed in the expanded foam is on the same order of the spacing between macropores. The foam is not able to expand to occupy the space between the tubes, forming a large void. This is most likely due to

the expanding heptane droplets in the emulsion wetting the polystyrene surface, effectively destroying the developing foam structure. These foams also have a discontinuous layer of dense ceramic that forms at the macropore interface that formed next to the surface of the polystyrene tube. This can be seen clearly in the fracture surface shown in Figure 7.21c. This layer is visible in all samples and is most likely due to electrostatic repulsion of the heptane bubble surface in the emulsion and the tube surface. In the bioreactor application, this layer can be used to keep the hydrogel containing the cells clear of the macropores during cell seeding, while still allowing for media to flow down the macropores and through the cracks in the surface layer and into the spaces occupied by the cells and hydrogel. This layer will also provide a surface for seeded vascular endothelial cells to attach and proliferate to form vascular tissue.

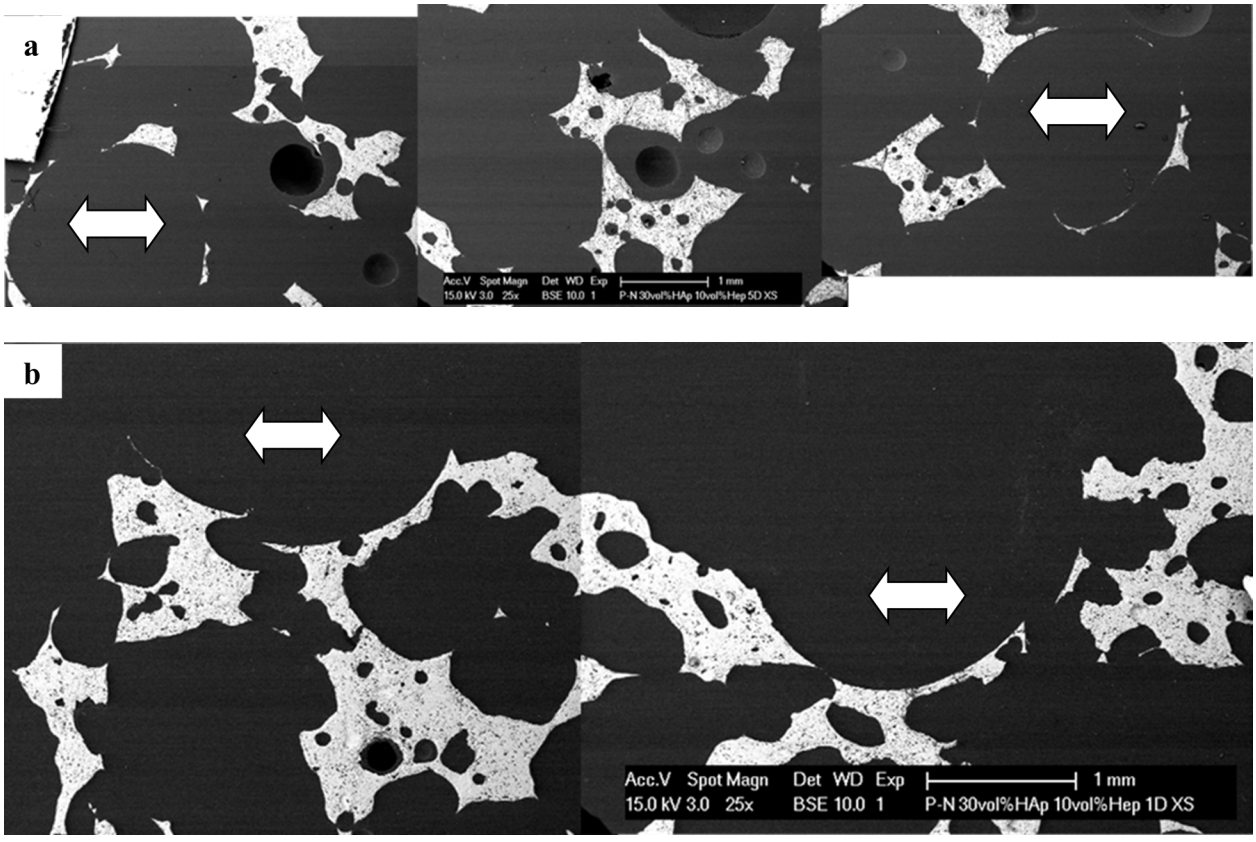

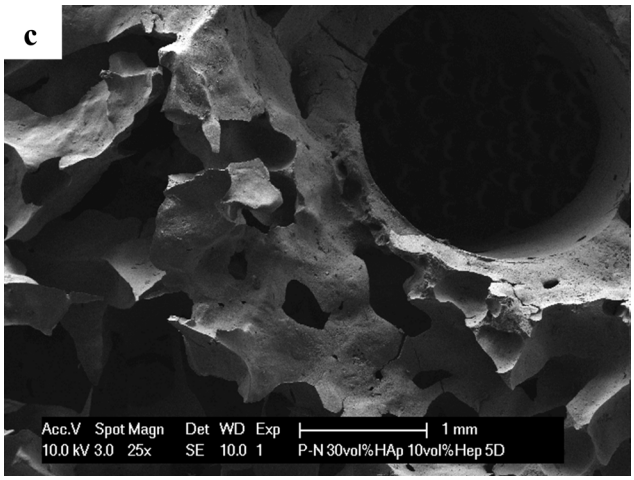

Figure 7.21. SEM image of a horizontal cross section of foam containing macropores (white arrows) at a spacing of distance equal to (a) 5 polystyrene tube diameters and (b) 1 polymer tube diameter. (c) SEM image of a fracture surface of a foam made with macropores spaced at 5 diameters showing the solid interface between the macropores and the foam.

7.4.2 Effect of Coatings on Polystyrene Tubes on Positive-Negative Casting

To address the problem of the foam structure collapsing between closely spaced channels the tube surface was coated to change it from hydrophobic to hydrophilic. As discussed in the previous section, the hydrophobic surface of the polystyrene tube was wetting for the coalescing heptane droplets leading to a collapse of the foam structure. This is imperative for eventually adding vascular-like channels into the scaffold, since the spacing of some of the macrochannels will be similar in length to the strut spacing in the foam. It was hypothesized that by altering the polystyrene to create a hydrophilic surface, the heptane droplets will not wet the surface and ideally pin the droplets to the surface to preserve the foam structure in between the macropores. The aqueous ceramic slurry phase in the emulsion should wet the surface, creating a thin layer of ceramic while the heptane droplets would remain intact preserving the foam structure.

Two coatings were examined in this study: Darvan C, an anionic polyelectrolyte, and benzethonium chloride, a cationic surfactant. While both coatings used in this study changed the wettability of the polymer surface, the effects on the foaming process were quite different, as seen in Figure 7.22. The foams created around tubes coated with the anionic polyelectrolyte did not appear to be any different from the uncoated tubes despite possessing a hydrophilic surface. The distance between the top of the foam and the region between the tubes (3.48mm) is actually slightly greater than if the tubes were untreated (2.76 mm). When the sample is coated in the cationic surfactant benzethonium chloride, a different result is seen, as the foam barely collapsed when compared to the first two conditions. Not only is the distance from the top of the foam to the region between the tubes 0.75 mm, smaller than casting with tubes without coating, the layer of ceramic formed at the surface of the tube is much thinner than both the Darvan C coated tubes and those without coating. This could be due to attractive forces between the HAp particles coated with anionic Darvan C and the cationic surfactant at the surface. Unfortunately, this ceramic layer is continuous due to the repulsive forces with the cationic surfactant used to stabilize the heptane droplets in the emulsion preventing pores to form at the interface. In contrast, the foams coated with Darvan C had a thicker, more discontinuous layer. In this case the Darvan C coated powder was repulsed by the surface and the positively charged heptane droplets were attracted to the surface. While both cases provide a surface for endothelial cells to attach, neither result is desirable. The first does not provide pathways for medium to reach the interior of the scaffold while the second creates a large barrier between the pores of the foam and the macropore which will cause inefficient medium delivery. This concept of interactions between the coated polymer surface and components of the emulsion will be further explored in the next section.

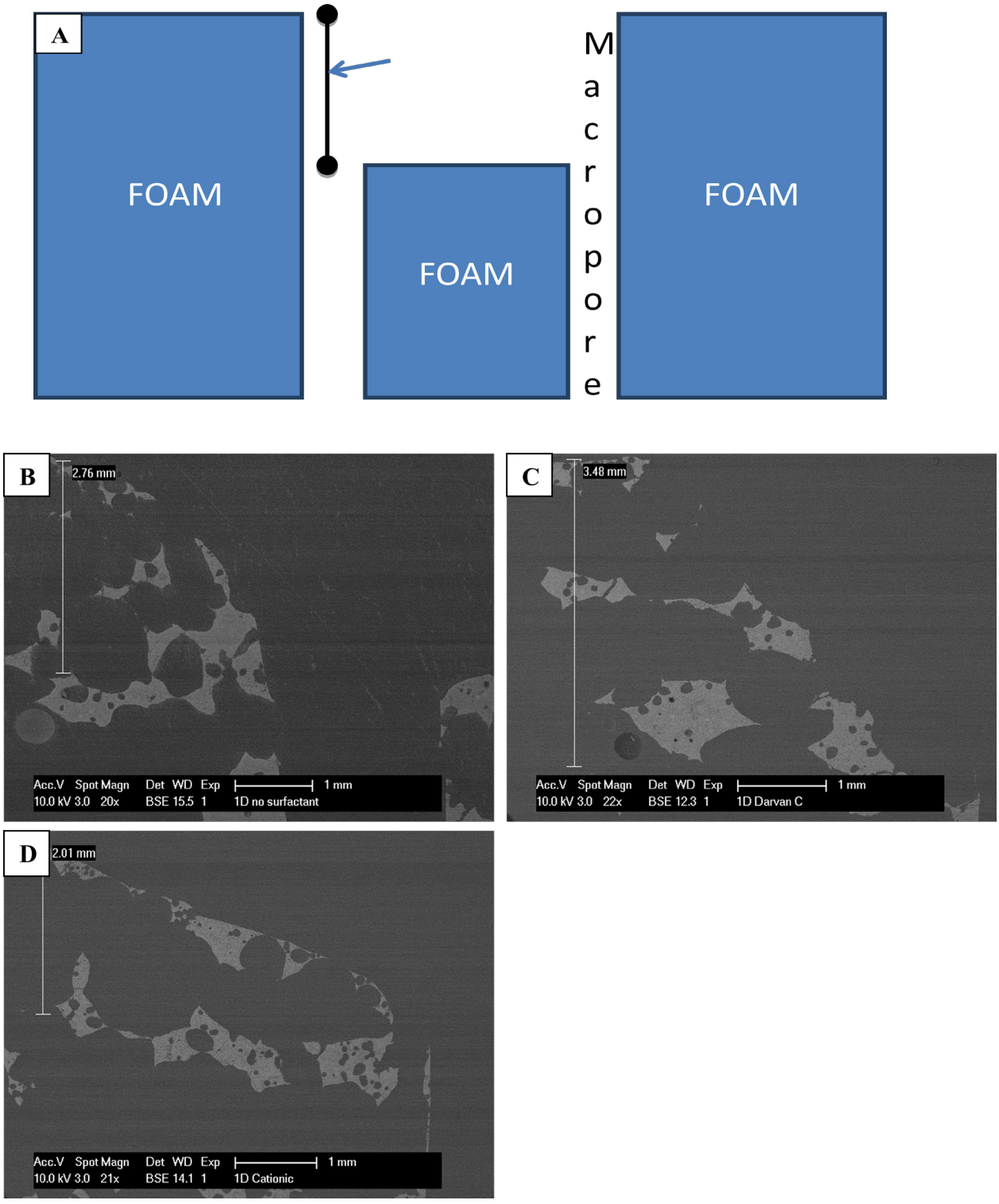

Figure 7.22. A) is a diagram illustrating the measurement taken (marked with an arrow), b-d are SEM image of a vertical cross section of foam showing collapse between macropores created with polystyrene tubes with (b) no coating, (c) coated with Darvan C, and (d) coated with benzethonium chloride.

7.4.3 Positive Negative Casting Around Closely Spaced Nylon Array

Changing the surface of the polymer preform was shown to affect the foaming of an emulsion. By further studying effects of the surfactant coating, a more ideal vascular-like network could be created. Also, as described in section 6.4.3, octane was used in the emulsion which created smaller pores in the resulting foam. This was deliberately altered so that the surfaces of the closely spaced macropores could be easily studied. The surfactant used to stabilize the emulsion was changed to sodium dodecyl sulfate, an anionic surfactant, so that the polyelectrolyte and surfactant in the emulsion were similarly charged. Similar to the previous section, three different coating conditions were used with differing results. Without a coating on the nylon arrays, the structure collapses, as seen in previous experiments (Figure 7.23a). This was expected due to the edge spacing of the nylon array being less than the foam bubble size examined in sections 7.4.1-7.4.2. When the nylon was coated with either surfactant, however, the resulting foam showed minimal structure collapse. The anionic surfactant produced a rather dense layer with some evidence of collapse seen in the macropores (Figure 7.23b). In this case, both the powder particles (Darvan C) and the alkane droplets (sodium lauryl sulfate) have repulsive forces towards the surface of the nylon. While the structure is not as collapsed as in the uncoated case, there is dense ceramic completely surrounding all surfaces that were in contact with the nylon preform. This is undesirable, as it leaves no pathways for medium to flow from the macrochannels into the interior of the scaffold. As seen in Figure 7.24a, there is a dense layer over 100 μm thick surrounding the macropore. While the structure did not collapse, the

repulsive forces between the octane droplet and the nylon surface were great enough to prevent pore formation near the macropore surface.

When a cationic surfactant is applied to the nylon surface, a more desirable structure is formed. With attractive forces for both, the powder particles and the octane droplets create a thin porous layer at the macropore interface (Figure 7.23c and Figure 7.24b), more than 10 times thinner than with an anionic surfactant coating (~10μm). Along with providing a surface for endothelial cells to attach, as the other coating conditions do, the porous layer allows for cell culture medium to flow into the interior of the scaffold. In these foams, the pores seem to be the same size no matter how close to the macropore channels they appear, which is desirable. This will provide a more uniform space for the cells to grow in the hydrogel within the future composite. While this could be a consequence of the smaller pores that are created when octane is used, the fact that the pores seem to be pinned to the interface suggests that a larger developing pore might be constricted to the space between the nylon array. The stability of the bubble should not be affected by its size as much as the charge and wetting behavior of the surface of the polymer template. The porosity of the foams used in this study is not ideal for cell culture; the principle seen here can be translated to future research, further discussed in section 9.3.

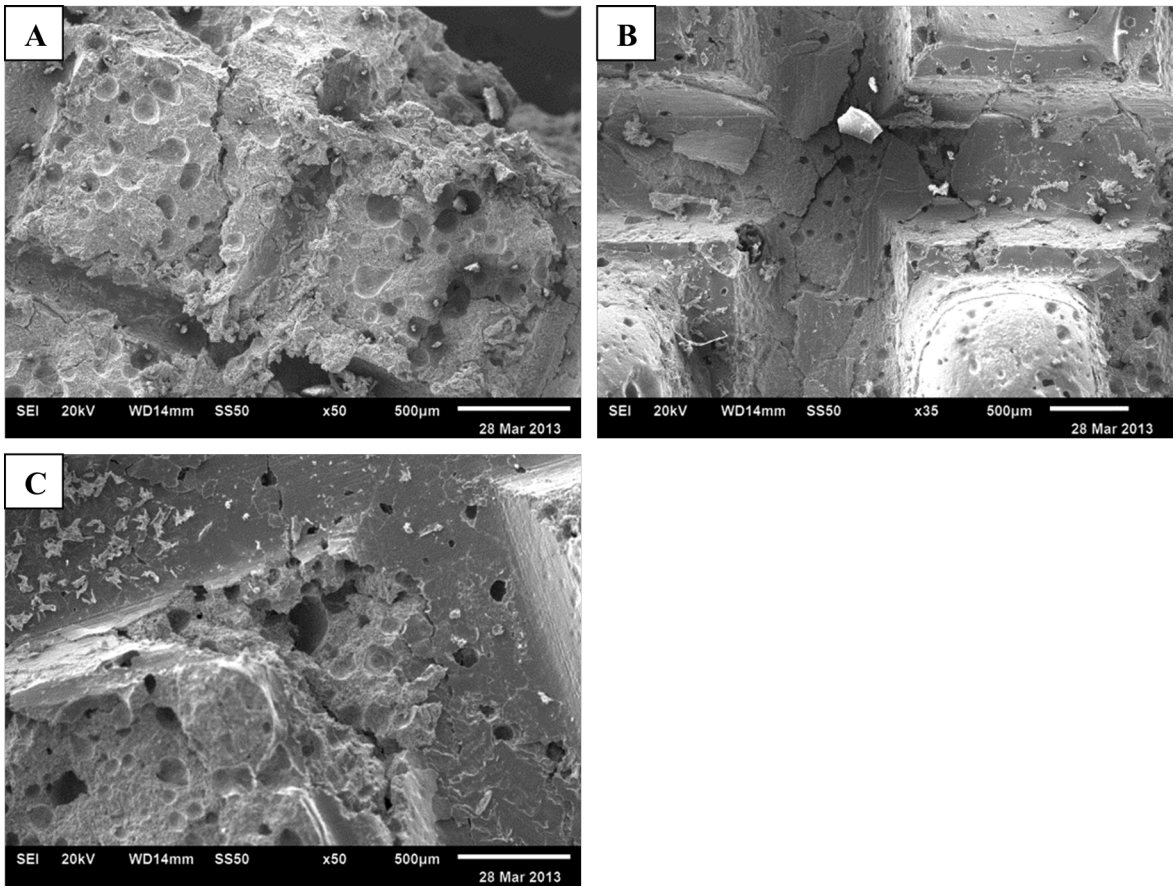

Figure 7.23. SEM image of a fracture surface of foam showing collapse between macropores created with nylon mesh with (a) no coating, (b) coated with sodium lauryl sulfate, and (c) coated with benzethonium chloride.

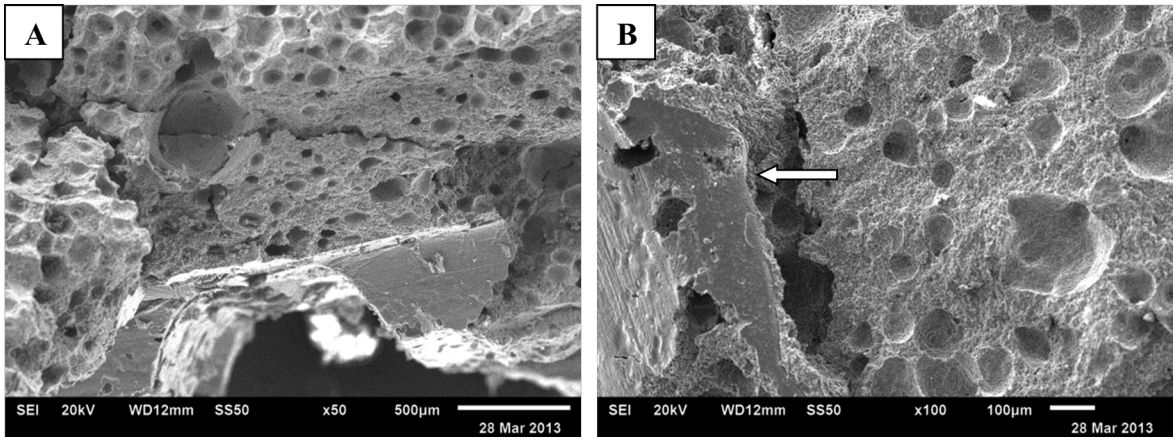

Figure 7.24. SEM image of a vertical fracture surface of foam along a macropore created with nylon mesh coated with (a) sodium lauryl sulfate and (b) benzethonium chloride.

8.0 CONCLUSIONS

8.1 PREPARATION OF A CERAMIC/HYDROGEL COMPOSITE STRUCTURE AND THE CULTURING OF LIVER CELLS

1) Open porous ceramic foams suitable for liver cell culturing can be created by using an emulsion foaming technique.

   An emulsion foaming technique can be used to create open porous hydroxyapatite suitable for cell culture. By changing emulsion variables such as amount of alkane, vapor pressure of alkane and solid loading of ceramic powder, the porosity and pore morphology can be altered. By creating an emulsion with a 30 vol% HAp suspension and 10 vol% heptane, a structure with porosity and pore size suitable for bioreactor cores can be made.

2) Human adult liver cells were successfully cultured in a collagen 1 hydrogel/hydroxyapatite composite.

   Cells were successfully cultured in a C1/HAp composite for 28 days with higher overall cell numbers and mature liver functions such as albumin secretion, liver plate like structures and evidence of bile duct formation over the other 5 conditions studied. Additionally, it was found that the presence of HAp increased the expression of vWF, a

mature endothelial cell marker, compared to a negative control, most likely due to the increase in Ca^{+2} ions near the surface of the scaffold.

8.2 EFFECT OF THE POROSITY ON THE HIGH TEMPERATURE TRANSFORMATION OF HAP AND CONSEQUENT EFFECTS ON DISSOLUTION

1) A coherent biphasic calcium phosphate scaffold can be created by heat treating porous hydroxyapatite at temperatures above 1350°C.

   Porous scaffolds have been created with as high as 62.59 wt% α-TCP, by heat treating HAp scaffolds at temperatures above 1350°C. These HAp scaffolds were partially decomposed to resorbable phases CaO and α-TCP (and to a lesser extent TeCP) without the damages seen in dense samples heated to the same temperatures.

2) Scaffolds with high amounts of α-TCP visibly degraded when they were perfused with tris-buffered saline over 28 days.

   Over 30% mass loss was seen in scaffolds created with 62.59 wt% α-TCP when perfused with tri-buffered saline for 28 days. It was seen that perfusion lead to much higher amounts of dissolution over the same scaffolds in static conditions in this study and those seen in the literature. This dissolution is necessary so that the ceramic structure degrades as liver tissue forms in the bioreactor core.

8.3 EFFECT OF A VASCULAR STRUCTURE ON THE PORE STRUCTURE OF THE FOAM

1) Vascular-like macropores can be created in a ceramic foam by foaming around surfactant coated polymer templates.

   By coating a polymeric vascular-like template in a surfactant that is of opposite charge of components in the emulsion, macropores can be created in a HAp foam. These surfactant coatings are necessary to preserve the foam structure between closely spaced macropores. These macropore channels are lined with a thin, discontinuous HAp layer. The pores in the layer will allow for cell culture medium to be delivered to cells injected into the pores of the ceramic foam. Endothelial cells can be injected and cultured on the HAp surface. Ca^{+2} ions that are dissociated from the CaP are beneficial to the proliferation of these cells and to formation of vascular tissue.

9.0 SUGGESTED FUTURE WORK

9.1 PREPARATION OF A CERAMIC/HYDROGEL COMPOSITE STRUCTURE AND THE CULTURING OF LIVER CELLS

1) Bioreactor experiments.

   After the success of static culturing of HAL cells in C1/HAp composites, perfusion conditions must be tested. Gerlach et al. has shown that tissue like structures will form when these cells are cultured in a bioreactor without any scaffold present [14]. This method can be used as a control to examine the effect of a composite scaffold in a bioreactor core. Bioreactors with a HAp core are already in production and used for bone marrow cell culturing. These bioreactors can be injected with HAL cells suspended in collagen and the hydrogel will crosslink inside of the cell compartment. Bioreactors can be run for 28 days and analyzed with RT-PCR, ELISA, and microscopy as the static experiments were.

9.2 EFFECT OF POROSITY ON THE HIGH TEMPERATURE TRANSFORMATION OF HAP AND CONSEQUENT EFFECTS ON DISSOLUTION

1) Test dissolution with WE complete medium.

   Dissolution test were already completed with tris-buffered saline at a physiologic pH. WE complete medium should be used in experiments similar to the TBS perfusion experiments to examine the dissolution behavior of CaP scaffolds in medium specific to liver cell culturing.

2) Test bioreactors with resorbable scaffolds.

   After the dissolution behavior in cell culture medium is tested, scaffolds with high α-TCP contents should be used in a bioreactor. This will not only give insight into the role of Ca^{+2} ions dissolving from the scaffold, but also the effect of cells on the degradation of the ceramic. CaP dissolution is frequently examined at low pH in the literature to more closely simulate the microenvironment the ceramic would experience in cell culture [37]. In the immediate area near the cell surface the pH can be much lower than what is seen in the bulk medium. Higher resorption rates are seen at this pH and can lead to a more complete dissolution of the ceramic. The same analysis techniques should be used to compare to the mostly HAp scaffolds used in 8.1. Additionally Ca^{+2} ion measurements can be taken from medium samples drawn from the cell chamber.

9.3 EFFECT OF A VASCULAR STRUCTURE ON THE PORE STRUCTURE OF THE FOAM

1) Create a positive-negative cast structure with complex structure and larger pores.

   A study will be done further expanding on the results found in section 7.4.3. The same polymer templates could be used with foams that have a larger pore size than those previously examined.

2) Create positive-negative cast structure with rat liver cast.

   It was found that by coating a polymer with a surfactant that was of opposite charge of the polyelectrolyte and surfactant in the emulsion, macropores with a thin porous ceramic layer could be created in a ceramic foam. This technique must also be applied to the rat liver vascular system copies described in section 6.4.3. Positive vascular copies must first be produced before these experiments can begin.

3) Develop bioreactor.

   Finally, after a positive-negative cast scaffold is created using a vascular system template, a bioreactor will be created using these scaffolds connected to a perfusion system. The inlet and outlet to the scaffold will be created by the portal vein and hepatic vein in the template.

   The ceramic will have to be coated with a polyurethane shell with cell injection ports added so that cells suspended in collagen can be injected into the interior of the scaffold. An injection port in the recirculation line must be added to inoculate vascular endothelial cells into the vascular-like channels.

   One final aspect that will be address is oxygenating the cell culture medium before it passes through the core. Because this reactor is designed to have a completely resorbable

core, there will be no oxygenation hollow fibers because they are not resorbable. Devices are on the market that accomplishes this task in other types of bioreactors, but they must be tested for the proposed systems.

BIBLIOGRAPHY

[1] K.D. Kochanek, M.A. Jiaquan Xu, S.L. Murphy, A.M. Miniño and H.C. Kung, "Deaths: Preliminary Data for 2009," *Natl. Vital Stat. Rep.*, **59** 1-51 (2011).

[2] T. Hoppo, J. Komori, R. Manohar, D. Beer-Stoltz and E. Lagasse "Rescue of Lethal Hepatic Failure by Hepatized Lymph Nodes in Mice," *Gastroenterology*, **140** 656-666 (2011).

[3] H. Yagi, B. Parekkadan, K. Suganuma, A. Soto-Gutierrez, R.G. Tompkins, A.W. Tilles and M.L. Yarmush, "Long-Term Superior Performance of a Stem Cell/Hepatocyte Device for the Treatment of Acute Liver Failure," *Tissue Engineering Part A*, **15**[11] 3377-3388 (2009).

[4] E. Schmelzer, F. Triolo, M.E. Turner, R.L. Thompson, K. Zeilinger, L.M. Reid, B. Gridelli and J.C. Gerlach, "Three-Dimensional Perfusion Bioreactor Culture Supports Differentiation of Human Fetal Liver Cells," *Tissue Engineering: Part A*, **16** 2007-2016 (2010).

[5] R. McClelland, E. Wauthier, J. Uronis and L. Reid, "Gradients in the Liver's Extracellular Matrix Chemistry from Periportal to Pericentral Zones: Influence on Human Hepatic Progenitors," *Tissue Engineering: Part A*, **14**[1] 59-70 (2008).

[6] W.S. Turner, E. Schmelzer, R. McClelland, E. Wauthier, W. Chen and L.M. Reid, "Human Heptoblast Phenotype Maintained by Hyaluronan Hydrogels," *Biomed. Mat Res B: Applied Biomaterials*, **82B** 156-167 (2007).

[7] C.W. Patrick, P.B. Chauvin, J. Hobley and G.P. Reece, "Preadipocyte Seeded PLGA Scaffolds for Adipose Tissue Engineering," *Tissue Engineering*, **5**[2] 139-151 (1999).

[8] F. Witte, H. Ulrich, M. Rudert and E. Willbold, "Biodegradable Magnesium Scaffolds: Part 1: Appropriate Inflammatory Response," *J. Biomed. Mater. Res.*, **81A**[3] 748-756 (2007).

[9] S. Higashiyama, M. Noda, S. Muraoka, M. Hirose, H. Ohgushi, M. Kawase and K. Yag, "Transplantation of Hepatocytes Cultures on Hydroxyapatite into Nagase Analbuminemia Rats", *J. BioSci and BioE*, **96** 83-85 (2003).

[10] R. Saito, Y. Ishii, R. Ito, K. Nagatsuma, K. Tanaka, M. Saito, H. Maehashi, H. Nomoto, K. Ohkawa, H. Mano, M. Aizawa, H. Hano, K. Yanaga and T. Matsuura, "Transplantation of Liver Organoids in the Omentum and Kidney," *Artificial Organs*, **35**[1] 80-83 (2011).

[11] J. Cihlar, A. Buchal and M. Trunec, "Kinetics of Thermal Decomposition of Hydroxyapatite Bioceramics," *J. Mater. Sci.*, **34** 6121-6131 (1999).

[12] P.N. Kumta, "Ceramic Biomaterials", in *An Introduction to Biomaterials*, eds S.A. Guelcher and J.O. Hollinger, CRC Press, 311-340 (2006).

[13] P. Ducheyne, S. Radin and L. King, "The Effect of Calcium Phosphate Ceramic Composition and Structure on in-vitro Behavior. I. Dissolution," *J. Biomed. Mater. Res.*, **39** 603-610 (1998).

[14] J.C. Gerlach, K Mutig, IM Sauer, P Schrade, E Efimova, T Mieder, G Naumann, A Grunwald, G Pless, A Mas, S Bachmann, P Neuhaus and K Zeilinger, "Use of Primary Human Liver Cells Originating from Discarded Grafts in a Bioreactor for Liver Support Therapy and the Prospects of Culturing Adult Liver Stem Cells in Bioreactors: a Morphologic Study," *Transplantation*, **76** 781-786 (2003).

[15] .L. Hench, "Bioceramics," *J. Am. Ceram. Soc.*, **81** [7] 1705-1728 (1998).

[16] A.R. Gazdag, J.M. Lane, D. Glaser and R.A. Forster, "Alternatives to Autogenous Bone Graft: Efficacy and Indications," *J. Am. Acad. Orthop. Surg.*, **3**[1] 1-8 (1995).

[17] M.I. Kay, R.A. Young and A.S. Posner, "Crystal Structure of Hydroxyapatite," *Nature*, **204** 1050–1052 (1964).

[18] S.D. Cook, K.A. Thomas, J.E. Delton, T.K. Volkman, T.S. Whitecloud III and J.F. Ke, "Hydroxylapatite Coating of Porous Implants Improves Bone Ingrowth and Interface Attachment Strength," *J. Biomed. Mater. Res.*, **26**[8] 989-1001 (1992).

[19] J.S. Thalgott, K. Fritts, J.M. Giuffre and M. Timlin, "Anterior Interbody Fusion of the Cervical Spine with Coralline Hydroxyapatite," *Spine*, **24**[13] 1295-1299 (1999).

[20] E.J. Evans, "Toxicity of Hydroxyapatite in-vitro: the Effect of Particle Size," *Biomaterials*, **12**[6] 574-576 (1991).

[21] A. El-Ghannam, P. Ducheyne and I.M. Shapiro, "Effect of Serum Proteins on Osteoblast Adhesion to Surface-Modified Bioactive Glass and Hydroxyapatite," *J Ortho. Res.*, **17[**3] 340–345 (1999).

[22] F.B. Bagambisa, and U. Joos, "Preliminary Studies on the Phenomenological Behaviour of Osteoblasts Cultured on Hydroxyapatite Ceramics," *Biomaterials*, **11**[1] 50-56 (1990).

[23] N. Adachi, M. Ochi, M. Deie and Y. Ito, "Transplant of Mesenchymal Stem Cells and Hydroxyapatite Ceramics to Treat Severe Osteochondral Damage After Septic Arthritis of the Knee," *J. Rheumatology*, **32**[8] 1615-1618 (2005).

[24] G.L. Darimonta, R. Clootsb, E. Heinenc, L. Seideld and R. Legrand, "In-vivo Behaviour of Hydroxyapatite Coatings on Titanium Implants: a Quantitative Study in the Rabbit," *Bioceramics*, **23**[12] 2569-2575 (2002).

[25] G. Daculsi, R. Z. Legeros, E. Nery, K. Lynch and B. Kerebel, "Transformation of Biphasic Calcium Phosphate Ceramics in-vivo: Ultrastructural and Physicochemical Characterization," *J. Biomed. Mater. Res.*, **23** 883-894 (1989).

[26] I.R. Gibson and W. Bonfield, "Novel Synthesis and Characterization of an AB-type Carbonate-Substituted Hydroxyapatite," *J. Biomed. Mater. Res.*, **59** 697-708 (2002).

[27] Y. Doi, T. Shibutani, Y. Moriqaki, T. Kajimoto and Y. Iwayama, "Sintered Carbonate Apatites as Bioresorbable Bone Substitutes," *J. Biomed. Mater. Res.*, **39** 603-610 (1998).

[28] I.R. Gibson, S.M. Best and W. Bonfield, "Chemical Characterization of Silicon-Substituted Hydroxyapatite," *J. Biomed. Mater. Res.*, **44** 422-428 (1999).

[29] A.E. Porter, N. Patel, J.N. Skepper, S.M. Best and W. Bonfield, "Comparison of in-vivo Dissolution Processes in Hydroxyapatite and Silicon-Substituted Hydroxyapatite Bioceramics," *Biomaterials*, **24** 4409-4620 (2003).

[30] N. Patel, S.M. Best, W. Bonfield, I.R. Gibson, K.A. Hing, E. Damien and P.A. Revell, "A Comparative Study on the in-vivo Behavior of Hydroxyapatite and Silicon Substituted Hydroxyapatite Granules," *J. Mater. Sci. Mater. Med.*, **13** 1199-1206 (2002).

[31] C. Ergun, T.J. Webster, R. Bizios and R.H. Doremus, "Hydrocylapatite with Substituted Magnesium, Zinc, Cadmium, and Yttrium. I. Structure and Microstructure," *J. Biomed. Mater. Res.*, **59** 305-311 (2002).

[32] C. Ergun, T.J. Webster, R. Bizios and R.H. Doremus, "Hydrocylapatite with Substituted Magnesium, Zinc, Cadmium, and Yttrium. II. Mechanisms of Osteoblast Adhesion," *J. Biomed. Mater. Res.*, **59** 312-317 (2002).

[33] C.M. Serre, M. Papillard, P. Chavassieux, J.C. Voegel and G. Boivin, "Influence of Magnesium Substitution on a Collagen-Apatite Biomaterial on the Production of a Calcifying Matrix by Human Osteoblasts," *J. Biomed. Mater. Res.*, **42** 626-633 (1998).

[34] A. Bandyopadhyay, S. Bernard, W. Xue and S. Bose, "Calcium Phosphate-Based Resorbable Ceramics: Influence of MgO, ZnO, and SiO_2 Dopants," *J. Am. Ceram. Soc.*, **89**[9] 2675-2688 (2006).

[35] Y.K. Jun and S.H. Hong, "Effect of Co-Precipitation on the Low-Temperature Sintering of Biphasic Calcium Phosphate," *J. Am. Ceram. Soc.*, **89**[7] 2295-2297 (2006).

[36] HY Yang, I Thompson, SF Yang, XP Chi, JRG Evans and RJ Cook, "Dissolution Characteristics of Extrusion Freeformed Hydroxyapatite–Tricalcium Phosphate Scaffolds," *J. Mater. Sci. Mater. Med.*, **19** 3345-3353 (2008).

[37] H Wang, JK Lee, A Moursi and JJ Lannutti, "Ca/P Ratio Effects on the Degradation of Hydroxyapatite In Vitro," *J. of Biomed. Mater. Res. A*, **67**[2] 599-608 (2003).

[38] J.C Trombe and G. Montel, "Some Features of the Incorporation of Oxygen in Different Oxygenation States in Apatitic Lattice," *J. Inorg. Nucl. Chem.*, **40** 15-21 (1972).

[39] C.J. Liao, F.H. Lin, K.S. Chen and J.S. Sun, "Thermal Decomposition and Reconstitution of Hydroxyapatite in Air Atmosphere," *Biomaterials*, **20** 1807-1813 (1999).

[40] J. Zhou, X. Zhang, J. Chen, S. Zeng and K. De Groot, "High Temperature Characteristics of Synthetic Hydroxyapatite," *J. Mater. Sci. Mater. Med.*, **4** 83-85 (1993).

[41] E.I. Dorozhkina and S.V. Dorozhkin, "Mechanism of the Solid-State Transformation of a Calcium-Deficient Hydroxyapatite (CDHA) into Biphasic Calcium Phosphate (BCP) at Elevated Temperatures," *Chem. Mater.*, **14**[10] 4267–4272 (2002).

[42] D.J. Green and P. Colombo, "Cellular Ceramics: Intriguing Structures, Novel Properties, and Innovative Applications," *Mater. Res. Bull.*, **28** 296-300 (2003).

[43] A. Royer, J.C. Viguie, M. Heughebaert and J.C. Heughebaert, "Stoichiometry of Hydroxyapatite: Influence on the Flexural Strength," *J. Mater. Sci. Mater. Med.*, **4** 76-82 (1993).

[44] A.J. Ruys, M. Wei, C.C. Sorrell, M.R. Dickson, A. Brandwood and B.K. Milthorpe, "Sintering Effects on the Strength of Hydroxyapatite," *Biomaterials*, **16** 409-415 (1995).

[45] E.C. Shors and R.E Holmes, An Introduction to Bioceramics, *eds* L L Hench and J Wilson, World Scientific Publishing Co., 181-190 (1993).

[46] P. Sepulveda, F.S. Ortega, M.D.M. Innocentini and V.C. Pandolfelli, "Properties of Highly Porous Hydroxyapatite Obtained by the Gelcasting of Foams," *J. Am. Ceram. Soc.*, **83** 3021-3024 (2000).

[47] J.G.P. Binner and J. Reichert, "Processing of Hydroxyapatite Ceramic Foams," *J. Mater. Sci.*, **31** 5717-5723 (1996).

[48] U.T. Gonzenbach, A.R. Studart, E. Tervoort and L.J. Gauckler, "Ultrastable Particle-Stabilized Foams," *Angew. Chem. Int. Ed.*, **45** 3526-3530 (2006).

[49] D. Weaire and S. Hutzler, The Physics of Foam, Claredon Press, (1999).

[50] D. Weaire, S. Cox and K. Brakke, "Liquid Foams – Precursors for Solid Foams," in Cellular Ceramics: Structure, Manufacturing, Properties and Applications, *eds*. M. Scheffler and P. Colombo, Wiley, 18-28 (2005).

[51] J.G.P. Binner, "Ceramic Foams," in Cellular Ceramics: Structure, Manufacturing, Properties and Applications, *eds*. M. Scheffler and P. Colombo, Wiley, 33-54 (2005).

[52] S. Barg, C. Soltmann, M, Andrade, D. Koch and G. Grathwohll. "Cellular Ceramics by Direct Foaming of Emulsified Ceramic Powder Suspensions." *J. Am. Ceram. Soc.*, **91** 2823-2829 (2008).

[53] I.D. Morrison and S. Ross, "Foams," in Colloidal Dispersions, Wiley, 456-493 (2002).

[54] J.S. Reed, Introduction to the Principles of Ceramic Processing, Wiley, (1988).

[55] N. Kristen and R. von Klitzing, "Effect of Polyelectrolyte/Surfactant Combinations on the Stability of Foam Films," *Soft Matter*, **6** 849-861 (2010).

[56] A.R. Studart, U.T. Gonzenbach, E. Tervoort and L.J. Gauckler, "Processing Routes to Macroporous Ceramics: A Review," *J. Am. Ceram. Soc.*, **89**[6] 1771–1789 (2006).

[57] A.R. Studart, V.C. Pandolfelli, E. Tervoort and L.J. Gauckler, "Gelling of Alumina Suspensions Using Alginic Acid Salt and Hydroxyaluminum Diacetate," *J. Am. Ceram. Soc.*, **85**[11] 2711–2718 (2002).

[58] H.X. Peng, Z. Fan and J.R.G. Evans, "Microstructure of Ceramic Foams", *J. Eur. Ceram. Soc.*, **20** 807-813 (2000).

[59] X.D. Zhanga, C.W. Macoskoa, H.T. Davisa, A.D. Nikolovb and D.T. Wasan, "Role of Silicone Surfactant in Flexible Polyurethane Foam," *J. Coll. Inter. Sci.*, **215**[2] 270-279 (1999).

[60] S. Barg, D. Koch and G. Grathwohl, "Processing and Properties of Graded Ceramic Filters," *J. Am. Ceram. Soc.*, **92**[12] 2854–2860 (2009).

[61] I.M. Arias, W.B. Jakoby, H. Popper, D. Schachter and D.A. Shafritz, The Liver: Biology and Pathobiology, Raven Press, (1988).

[62] A. Kamiya, T. Kinoshita, Y. Ito, T. Matsui, Y. Morikawa, E. Senba, K. Nakashima, T. Taga, K. Yoshida, T. Kishimoto and A. Miyajima, "Fetal Liver Development Requires a Paracrine Action of Oncostatin M Through the gp130 Signal Transducer," *EMBO J.*, **18**[8] 2127–2136 (1999).

[63] A. Martinez-Hernadez and P.S. Amenta, "The Extracellular Matrix in Hepatic Regeneration," *Faseb J.* **9** 1401-1410 (1995).

[64] B. Ohlstein, T. Kai, E. Decotto and A. Spradling, " The Stem Cell Niche: Theme and Variations," *Curr. Opin. Cell Biol.*, **16** 693-699 (2004).

[65] K.A. Moore and I.R. Lemischka, "Stem Cells and Their Niches," *Science*, **311** 1880-1885 (2006).

[66] D. Sadava, H.C. Heller, G.H. Orians, W.K. Purves and D.M. Hillis, "Differential Gene Expression in Development," in Life: The Science of Biology, Sinauer Associates, 426-447 (2008).

[67] J. Lee, M.J. Cuddihy and N.A. Kotov, "Three-Dimensional Cell Culture Matrices: State of the Art," *Tissue Engineering: Part B*, **14**[1] 61-87 (2008).

[68] K.Y. Lee and D.J. Mooney, "Hydrogels for Tissue Engineering," *Chem. Rev.*, **101**[7] 1869-1881 (2001).

[69] H.C. Ott, T.S. Matthiesen, S.K. Goh, L.D. Black, S.M. Kren, T.I. Netoff and D.A. Taylor, "Perfusion-Decellularized Matrix: Using Nature's Platform to engineer a Bioartificial Heart," *Nat. Med.*, **14** 213-221 (2008).

[70] B.E. Uygun, A. Soto-Gutierrez, H. Yagi, M.L. Izamis, M.A. Guzzardi, C. Shulman, J. Milwid, N. Kobayashi, A. Tilles, F. Berthiaume, M. Hertl, Y. Nahmias, M.L. Yarmush and K. Uygun, "Organ Reengineering Through Development of a Transplantable Recellularized Liver Graft Using Decellularized Liver Matrix," *Nat. Med.*, **16** 814–820 (2010).

[71] L.A. Estroff and A.D. Hamilton, "Water Gelation by Small Organic Molecules," *Chem. Rev.*, **104**[3] 1201-1217 (2004).

[72] T. Elkayam, S. Amitay-Shaprut, M. Dvir-Ginzberg, T. Harel and S. Cohen, "Enhancing the Drug Metabolism Activities of C3A - A Human Hepatocyte Cell Line - By Tissue Engineering Within Alginate Scaffolds," *Tissue Engineering*, **12** [5] 1357-1368 (2006).

[73] S. Even-Ram and K.M. Yamada, "Cell Migration in 3D Matrix," *Curr. Opin. Cell Biol.*, **17** 524–532 (2005).

[74] TS Weiss, B Jahn, M Cetto, KW Jauch and WE Thasler, "Collagen Sandwich Culture Affects Intracellular Polyamine Levels of Human Hepatocytes," *Cell Prolif.,* **35** 257-267 (2002).

[75] H. Tana, C.R. Chub, K.A. Payne and K.G. Marra, "Injectable in-situ Forming Biodegradable Chitosan–Hyaluronic Acid Based Hydrogels for Cartilage Tissue Engineering," *Biomaterials*, **30**[13] 2499-2506 (2009).

[76] LH Nguyen, N Annabi, M Nikkhah, H Bae, L Binan, S Park, Y Kang, Y Yang and A Khademhosseini, "Vascularized Bone Tissue Engineering: Approaches for Potential Improvement," *Tissue Engineering: Part B*, **18**[5] 363-382 (2012).

[77] MI Santos and RL Reis, "Vascularization in Bone Tissue Engineering: Physiology, Current Strategies, Major Hurdles and Future Challenges," *Macromol. Biosci.*, **10** 12-27 (2010).

[78] JS Miller, KR Stevens, MT Yang, BM Baker, DHT Nguyen, DM Cohen, E Toro, AA Chen, PA Galie, X Yu, R Chaturvedi, SN Bhatia and CS Chen, "Rapid Casting of Patterned Vascular Networks for Perfusable Engineered Three-Dimensional Tissues," *Nature Materials*, **11** 768–774 (2012).

[79] A Kiyota, T Matsushita and R. Ueoka, "Induction and High Density Culture of Human Hepatoblasts from Fetal Hepatocytes with Suppressing Transformation," *Biol. Pharm. Bull.* **30**[12] 2308-2311 (2007).

[80] B Nilius and G. Droogmans, "Ion Channels and Their Functional Role in Vascular Endothelium," *Physiol. Rev.*, **81**[4] 1415-1459 (2001).

[81] PM Eckl, WR Whitcomb, G Michalopoulos and RL Jirtle, "Effects of EGF and Calcium on Adult Parenchymal Hepatocyte Proliferation," *J. Cell Physol.*, **132**[2] 363-366 (1987).

[82] C. Fenge and E. Lullau, "Cell Culture Bioreactors," in Cell Culture Technology for Pharmaceutical and Cell-Based Therapies, *eds.* S.S. Ozturk and W.S. Hu, CRC Press, 155-197 (2006).

[83] H.R. Kariminiaae-Hamedaani, K. Kanda and F. Kato, "Wastewater Treatment with Bacteria Immobilized onto a Ceramic Carrier in an Aerated System," *J. Biosci. BioE.*, **95**[2] 128-132 (2003).

[84] J.M.S. Cabral, "Ex-vivo Expansion of Hematopoietic Stem Cells in Bioreactors," *Biotech. Let.*, **23** 731-741 (2001).

[85] M. Saito, T. Matsuura, T. Masaki, H. Maehashi, K. Shimizu, Y. Hataba, T. Iwahori, T. Suzuki, F. Braet, "Reconstruction of Liver Organoid Using a Bioreactor," *World J. Gastroenterol.*, **12**[12] 1881-1888 (2006).

[86] Y. Xie, P. Hardouin, Z. Zhu, T. Tang, K. Dai and J. Lu, "Three-Dimensional Flow Perfusion Culture System for Stem Cell Proliferation Inside the Critical-Size β-Tricalcium Phosphate Scaffold," *Tissue Engineering*, **12**[12] 3535-3543 (2006).

[87] B.A. Laishes and G.M. Williams, "Conditions Affecting Primary Cell Cultures of Functional Adult Rat Hepatocytes 1. The Effect of Insulin," *In vitro*, **12**[7] 521-532 (1976).

[88] J.H. Marciano, M.M. Reboredo, A.J. Rojas and R.J.J. Williams, "Integral-Skin Polyurethane Foams," *Poly. Eng. & Sci.*, **26** 717-724 (1986).

[89] HF Lu, KN Chua, PC Zhang, WS Lim, S Ramakrishna, KW Leong and HQ Mao, "Three-Dimensional Co-culture of Rat Hepatocyte Spheroids and NIH/3T3 Fibroblasts Enhances Hepatocyte Functional Maintenance," *Acta Biomaterialia,* **1** 399-410 (2005).

[90] C Rodríguez, MT Donato, A Boobis, RJ Edwards, PS Watts, J Vicente Castell and MJ Gómez-Lechón, "Cytochrome P450 Expression in Human Hepatocytes and Hepatoma Cell Lines: Molecular Mechanisms That Determine Lower Expression in Cultured Cells," *Xenobiotica*, **32**[6] 505-520 (2002).

[91] A Pietrangelo, A Panduro, JR Chowdhury and DA Shafritz, "Albumin Gene Expression is Down-regulated by Albumin or Macromolecule Infusion in the Rat," *J. Clin. Invest.,* **89** 1755-1760 (1992).

[92] Y Shapira and D Lichtman, "Properties of Materials Used in Vacuum Technology," in Methods of Experimental Physics: Vacuum Physics and Technology, *eds.* GL Weissler and RW Carlson, Academic Press, 348-350 (1980).

[93] PW Brown and RI Martin, “An Analysis of Hydroxyapatite Surface Layer Formation,” *J. Phys. Chem. B,* **103** 1671-1675 (1999).